

Analytical and experimental study of the wettability of silicon against different substrates.

by:

Almudena Casado Chacón

in partial fulfillment of the requirements for the degree of Doctor in
Materials Science and Engineering

Universidad Carlos III de Madrid

Supervisors:

Dr. Srdjan Milenkovic

Dr. José Manuel Torralba

Tutor:

Dr. Srdjan Milenkovic

Leganés, 7 de Junio de 2019

Esta tesis se distribuye bajo licencia “Creative Commons **Reconocimiento – No Comercial – Sin Obra Derivada**”



A Papilindo y a Mamuchita.

*“Acepta la dificultad de edificarte a ti mismo y el valor
de empezar corrigiéndote. El triunfo del verdadero
hombre surge de las cenizas de su error”*

Pablo Neruda

Agradecimientos

Esta tesis es el fruto del trabajo de muchas personas que han colaborado científicamente durante estos cinco años, pero también pertenece a todas aquellas personas que me han apoyado para llegar a buen término.

En primer lugar, quería agradecer a mis supervisores Srdjan Milenkovic y José Manuel Torralba que me dieran esta oportunidad y toda la confianza depositada en mí y en mi trabajo. Gracias por toda la ayuda, la paciencia y por mostrarme como amar a la ciencia.

Estoy muy agradecida a Imdea Materiales y a todos los que formamos parte de esta familia. Especialmente a Marcos Angulo, Miguel Castillo y Antón Jormescu y al resto de técnicos por su disponibilidad, sus ganas de ayudar y por su paciencia para enseñarme a usar los equipos. También quiero destacar al grupo de informáticos, por su inestimable ayuda, Raúl Merchán, Daniel González y Max Steward.

Me gustaría agradecer al departamento de Departamento de Ciencia e Ingeniería de Materiales e Ingeniería Química, el tiempo invertido en mi investigación, el uso de sus instalaciones y toda la ayuda que he recibido. Gracias al Dr. Ignacio Jimenez del Instituto de ciencias materiales de Madrid (ICMM-CSIC) por su colaboración con los recubrimientos. Thanks very much to High-temperature research group of the Foundry research institute of Krakow, particularly, Natalia Sobczak and Wojciech Polkowski, because of the good welcome and the friendliness.

Me encantaría mencionar a todos mis compañeros porque tanto a nivel personal como laboral han colaborado a que mis años de investigación se convierta en una muy buena experiencia. Especialmente a Anna, Alex, Andrea F, Andrea G, Elena, Joseba, Laura, Marta, Miguel, Paqui, Alfonso, Ángel, Bárbara, Dani, Gustavo, Hugo, Jaime, Juan Carlos, Luis, Miguel, Marcos, Marcos, al equipo coche, a los del comunio, y a todos con los que he compartido excelentes viajes, ya que les considero más amigos que compañeros de trabajo. Muchas gracias por todo su cariño y su atención a Juana, Paco y Gema. También tengo que acordarme de todos aquellos amigos, ajenos al trabajo, que tanto se han preocupado por mis avances y mis dificultades Angel, Borru, Lau, Nancy, Judith, Vicen, Palo, Judi y a

tantísimas más personas que no entran en estas hojas.

Por ultimo quiero agradecer todo su apoyo a mi familia que son los que verdaderamente han sufrido mis cambios de humor y mis preocupaciones. Gracias a mis padres por tantísimo esfuerzo para darme una buena educación, y por todas sus renunciaciones para que yo pueda llegar a donde estoy ahora. Gracias a mis hermanos por su apoyo incondicional y por creer más en mí que yo misma, aunque lo expresen a su estilo y forma. Gracias a Abue a tiuchita y al resto de la familia, por todo su cariño y su comprensión porque gracias a ellos, siento que nunca caminaré sola.

Resumen

A causa de la crisis del petróleo se produjo un auge en la industrial fotovoltaica y, por tanto, del silicio solar. La obtención del silicio mediante vías metalúrgicas está marcada por su alta reactividad y, el relativo, alto punto de fusión del silicio (1414°C). Por tanto, en la producción de silicio se necesitan materiales que soporten altas temperaturas, pero que al tiempo no contaminen el silicio. Además, para evitar la pérdida de material y la posible rotura de los crisoles, se necesitan materiales con los que el silicio no interactúe ni infiltre. El material más usado es el grafito porque las impurezas no afectan a la efectividad de las placas solares. Sin embargo, la reactividad entre el silicio y el grafito facilita la mojabilidad y la infiltración del silicio, aumentando el coste del proceso. Por otro lado, el control de los procesos de mojado e infiltración es importante para otras aplicaciones como la fabricación de materiales cerámicos o incluso en soldadura. Por todo ello, esta tesis se centra en la búsqueda de un material que pueda ser usado como crisol en un proceso de purificación de silicio y en obtener información útil sobre la interacción con el silicio tanto para aplicaciones fotovoltaicas como para soldadura o la fabricación de refractarios. La investigación está dividida en materiales alternativos al grafito como crisoles, un estudio exhaustivo de substratos grafiticos y finalmente posibles recubrimientos para evitar o reducir la mojabilidad y la infiltración.


En este trabajo se ha comprobado que a pesar de su buen comportamiento frente al silicio la alúmina reacciona con el silicio, por lo que no puede ser utilizada como crisol, al igual que los recubrimientos de TiO_2 y B_4C , aunque en el caso de B_4C se lograra reducir la infiltración significativamente. También, se demuestra que material compuesto carbón-carbón podría ser usado como crisol. Por otro lado, el mejor comportamiento frente al silicio se obtuvo por un grafito con granos y poros muy pequeños.

Abstract

Due to the oil crisis, there has been an increase in interest in the photovoltaic industry, as well as in the demand for solar silicon. The key parameters for the purification of solar silicon through metallurgical routes are the relatively high melting point of Si (1414°C) and its high reactivity. Therefore, materials should withstand high temperatures and do not get polluted in contact with silicon. Moreover, materials, which are not wetted and infiltrated by silicon in order to avoid the loss of material and the possible break of the crucible, are sought. Graphite substrates are largely used because the effect of its impurities is negligible on the efficiency of solar cells. However, the reactivity between silicon and graphite boosts the wetting and infiltration of the molten silicon, increasing the cost. On the other hand, the phenomena of wetting and infiltration are also a key factor in other applications such as the fabrication of refractories or brazing. As a result, this thesis is focused on finding a material which can be used in any process of silicon purification and on obtaining useful information about wetting and infiltration. The research is divided into the search for alternative materials for the crucibles, apart from graphite for photovoltaic applications, an accurate analysis of the behavior of molten silicon against graphite substrates and finally, the use of coatings in order to avoid wetting and infiltration. In this work it has been proved that despite its good behavior against silicon, alumina reacts with silicon, so it can not be used as a crucible. Similarly, is with the TiO₂ and B₄C coatings, although in the case of B₄C it is possible to reduce the infiltration significantly. Also, it is shown that carbon-carbon composite material could be used as a crucible. On the other hand, the best behavior against silicon was obtained by a graphite with very small grains and pores.

Published and submitted content

- Casado, A., Torralba, J. & Milenkovic, S. Wettability and Infiltration of Liquid Silicon on Graphite Substrates. *Metals (Basel)*. **9**, 300 (2019). doi:10.3390/met9030300.

My role is co-author. This article is included in its entirety in chapter 4.  The material from this source included in this thesis is not singled out with typographic means and references.

- Casado A., Milenkovic S., Torralba J.M. Behavior of liquid Silicon on several substrates. 55th National Congress of the Spanish Society of Ceramics and Glass; Sevilla Spain (2016)
- Casado A., Milenkovic S., Torralba J.M. Materials for the purification of solar silicon. 6th International Congress on Ceramics; Dresden, Germany (2016)
- Casado A., Milenkovic S., Torralba J.M. Infiltration of liquid Silicon on several substrates. 14th International Conference European Ceramic Society; Toledo Spain (2015)

Preface

This thesis has been carried out at IMDEA Materials Institute under the supervision of Dr. Srdjan Milenkovic and Dr. Jose Manuel Torralba, with the strong collaboration of the Department of Material Science and Engineering and Chemical Engineering of the Carlos III University of Madrid, Materials Science Institute of Madrid (ICMM-CSIC) and the High-temperature research group of the Foundry Research Institute of Krakow, funded by Ferrosolar by the industrial project entitled “Sicasol”.

Some of the obtained results have been published in journal papers in publications and conference presentations at international level:

- Casado, A., Torralba, J. & Milenkovic, S. Wettability and Infiltration of Liquid Silicon on Graphite Substrates. *Metals (Basel)*. 9, 300 (2019). doi:10.3390/met9030300.
- Casado A., Milenkovic S., Torralba J.M. Behavior of liquid Silicon on several substrates. 55th National Congress of the Spanish Society of Ceramics and Glass; Sevilla Spain (2016)
- Casado A., Milenkovic S., Torralba J.M. Materials for the purification of solar silicon. 6th International Congress on Ceramics; Dresden, Germany (2016)
- Casado A., Milenkovic S., Torralba J.M. Infiltration of liquid Silicon on several substrates. 14th International Conference European Ceramic Society; Toledo Spain (2015)

Table of contents

1. Introduction and state of art.....	32
1.1 Introduction	32
1.2 Literature Review	36
• Reactivity.....	36
• Wettability	38
• Infiltration and spreading.....	39
1.2.1 Oxides substrates	40
1.2.2 Graphite substrates.....	42
1.2.3 Covalent ceramics	48
1.3 Summary	51
2. Motivation and objectives	52
2.1 Motivation	52
2.1.1 Oxides substrates	52
2.1.2 Graphite Substrates.....	53
2.1.3 Covalent ceramics	55
2.2 Objectives.....	56
3. Materials and experimental methods.....	58
3.1 Materials.....	58
3.1.1 Graphite materials	58
3.1.2 Coatings on graphite substrates.....	59
3.1.3 Alumina.....	59
3.1.4 C/C Composites.....	60
3.2 Characterization and preparation of materials before the experiments.....	61
3.2.1 Density	61
3.2.2 Preparation of substrates	61
3.2.3 Rugosity	62
3.2.4 X-ray computed tomography (XCT)	62
3.2.5 Ramman micro-spectroscopy.....	63
3.3 Wettability and infiltration experiments.....	64

3.3.1	Induction Furnace	64
3.3.2	Sessile drop method	65
3.4	Characterization and analysis after the experiments	69
3.4.1	X-ray diffraction (XRD)	69
3.4.2	Light Optical Microscopy (LOM)	70
3.4.3	Scanning electron microscopy (SEM) and Energy Dispersive X-ray (EDX)	70
3.4.4	Focused ion beam (FIB) and Transmission electron microscopy (TEM)	71
4.	Alumina and carbon composites	72
4.1	Refractory substrates	73
4.1.1	Substrates characterisation.....	73
•	Porosity analysis	73
•	Crystallinity analysis	74
•	Rugosity analysis	74
4.1.2	Image observation Sessile drop test	75
•	Analysis of the drop parameters.....	78
•	Optical microscopy analysis of Sessile drop samples	80
•	X-Ray analysis of the Sessile drop samples.....	85
4.1.3	Discussion	87
	CONCLUSIONS.....	91
5.	Graphite substrates.....	92
5.1	Graphite from Tokai Carbon Co, LTD	92
5.1.1	Characterisation of material.....	92
•	Porosity analysis	92
•	Crystallinity analysis	94
•	Rugosity analysis	94
5.1.2	Sessile drop test.....	95
5.1.2.1	Classic method.....	95
•	Analysis of the Sessile drop test	96
•	Optical microscopy analysis of Sessile drop samples.	99
•	X-Ray and Raman analysis of the Sessile drop samples.....	103
5.1.2.2	Dispensed drop	104

•	Analysis of the Dispensed drop test.....	105
•	Optical microscopy analysis of the Sessile drop samples	108
•	SEM analysis of the Sessile drop samples.....	110
•	X-Ray and Raman analysis of the Sessile drop sample	111
5.1.3	Induction furnace test.....	112
•	Optical microscopy analysis of the induction furnace samples.....	113
•	SEM analysis after induction furnace test	114
•	X-Ray analysis after the induction furnace test	115
5.2	Graphite from Sigrafine and Carbon-lorraine	116
5.2.1	Characterization of material	116
•	Porosity analysis	116
•	Crystallinity analysis	117
•	Rugosity results	118
5.2.2	Sessile drop test	118
•	Analysis of the Sessile drop test	118
•	Optical microscopy analysis of the Sessile drop samples	123
•	SEM analysis of the Sessile drop samples.....	124
•	X-Ray and Raman analysis of the Sessile drop samples.....	126
5.3	Discussion	128
	CONCLUSIONS.....	131
6.	Coated graphite substrates	132
6.1	Boron carbide (B ₄ C).....	132
6.1.1	Characterisation of material.....	132
•	Optical microscopy analysis of Sessile drop samples.	132
6.1.2	Sessile drop test.....	133
•	Analysis of the Sessile drop test	134
•	Optical microscopy analysis of Sessile drop samples.	136
•	SEM analysis of the Sessile drop samples.....	138
•	X-Ray and Raman analysis of the Sessile drop samples.....	141
6.2	TiO ₂ Coatings	143
6.2.1.	Characterisation of materials.....	143

•	Analysis of the Sessile drop test	144
•	Optical microscopy analysis of Sessile drop samples.	145
•	SEM analysis of the Sessile drop samples.....	146
•	X-Ray and Raman analysis of the Sessile drop samples.....	147
	CONCLUSIONS.....	149
7.	Study of the surface.....	150
7.1	Introduction	150
7.2	Induction furnace test and characterisation of the material.....	151
7.3	Analysis of results.....	152
•	Optical microscopy analysis of Sessile drop samples.	152
•	SEM analysis of the Sessile drop samples.....	155
•	X-Ray and Raman analysis of the Sessile drop samples.....	158
•	TEM analysis of the surface from the induction furnace test	159
	CONCLUSIONS.....	161
8.	Discussion.....	162
8.1	Oxides substrates.....	163
8.1.1	Alumina.....	163
8.1.2	TiO ₂	164
8.2	Graphite Substrates	165
8.2.1	Analysis for photovoltaic applications.....	165
8.2.2	Reaction	166
•	SiC layer on the interfaces	167
8.2.3	Relation between spreading and infiltration rate.	168
8.2.4	Other parameters.....	169
•	Influence of rugosity	169
•	Influence of crystallinity	170
•	Influence of the atmosphere	170
•	Differences between Classic and dispensed Sessile drop test.....	171
•	Influence of the type of porosity	172
•	Graphite substrates	172
8.3	Covalent ceramics.....	174

9. Conclusions	176
9.1 Oxides substrates.....	177
9.2 Graphite Substrates	178
9.3 Covalent ceramics.....	180
10. Futures lines	182
11. Bibliography	184

Table of abbreviations and symbols

Table of abbreviations

BSE	Back-scattered electron	LSI	Liquid silicon infiltration
CCD	Charge-couple device	MGS	Metallurgical grade silicon
CVD	Chemical vapour deposition	PV	Photovoltaic
DSAHT	Drop Shape Analysis for High Temperatures	RBCS	Reaction bonding of silicon carbide
DP	Diffraction patterns	RPC	Reaction product control
EDX	Energy Dispersive X-ray spectroscopy	SE	Secondary electron
EGS	Electronic grade silicon	SEM	Scanning electron microscopy
FIB	Focused ion beam	SGS	Solar grade silicon
HREM	High-resolution transmission electron microscopy	TEM	Transmission electron microscopy
LMIS	Liquid-Metal Ion sources	XCT	X-ray computed tomography
LOM	Light optical microscopy	XRD	X-ray diffractometer

List of symbols

A	Area	ξ	Tortuosity
α	Volume of fraction	$P_{O_2}^f$	Partial pressure of oxygen
D	Spreading distance	ρ	Density
D1, D2	Bands structural disorder from Ramman Analysis	R	Radius of the drop
e	Thickness	R_a	Average rugosity
E_{2g}	Vibrational mode	r_{eff}	Effective radius
G	Bands grade of cristallynity from Ramman Analysis	ρ_{SiC}	Silicon carbide density
η	Liquid viscosity	σ	Liquid surface tension
H	Infiltration distance	U_{inf}	Infiltration rate
Θ	Contact angle	U_{spr}	Spreading rate
M_{SiC}	SiC molecular weight.	W_a	Adhesion work

Table of figures

Figure 1. 1. Limits of impurity concentrations in p-type silicon for impurities determining degradation threshold of solar cells: 1 EGS; 2 SGS; 3 MGS.....	33
Figure 1. 2. Scheme of how the surface of silicon depends on the conditions. a) initial silicon piece, b) oxide-free containing adsorbed oxygen (b1) or clean (b2), and c) oxidized surfaces ¹⁷	37
Figure 1. 3. Definition of contact angle.....	38
Figure 1. 4. Cross section schematic of the silicon-graphite interface.	39
Figure 1. 5. Curve fitting of the first-order region of the Raman spectrum.....	46
Figure 2. 1. General scheme of the outline of the thesis	57
Figure 3. 1. Example of results of rugosity from Hommel tester T1500.	62
Figure 3. 2. Curve fitting of the first-order region of Raman spectrum	63
Figure 3. 3 Scheme for argon testing (a) and for vacuum testing (b).	65
Figure 3. 4. Sessile drop testing methods and procedures ⁵²	65
Figure 3. 5. Scheme of the equipment used for wetting and infiltration experiments. A detail of the drop-substrate disposition is adapted from ⁵³	67
Figure 3. 6 Schematic of the camber of experiment of the experimental complex device.	68
Figure 4. 1. Schematic of the blocks: studied substrates and used techniques.....	72
Figure 4.1. 1 Image of the distribution of pores in different materials, being a), b), c) and d) graphite, alumina, composite 1 and composite 3, respectively.	73
Figure 4.1. 2. Images of sessile drop test, a) on graphite, b) on alumina c) on composite 1 and d) on composite 2.....	75
Figure 4.1. 3. Contact angle and parameters of silicon drop with time of graphite, alumina and composite 1 and 2 substrates.	76
Figure 4.1. 4. Comparison of variation of a. contact angle and b. relative drop height (mm/mm) of substrate with the time.....	79
Figure 4.1. 5. a. Top view and b. cross section images of substrates after sessile drop test.....	81
Figure 4.1. 6. Micrographs of a. Graphite, b. Alumina, c. Composite 1 and d. Composite 2 after sessile drop test.....	84
Figure 4.1. 7. . X- ray results of graphite before and after sessile drop test (cross section and surface).....	85
Figure 4.1. 8. X- ray results of alumina before and after sessile drop test (cross section and surface).....	85
Figure 4.1. 9. . X- ray results of composite 1 before and after sessile drop test (cross section and surface).....	86
Figure 4.1. 10. X- ray results of composite 2 before and after sessile drop test (cross section and surface).....	86

Figure 5.1. 1. Image of the distribution of pores in different graphite, being a) G330, b) G347, c) G348 and d) G550.	93
Figure 5.1. 2. Image of the interconnectivity of pores in different materials, being a) G330, b) G347, c) G348 and d) G550.....	93
Figure 5.1. 3. Images of sessile drop test, a) on G330, b) on G347 c) on G348 and d) on G350.....	95
Figure 5.1. 4. Contact angle and parameters of silicon drop with time a) on G330, b) on G347 c) on G348 and d) on G350.	96
Figure 5.1. 5. Comparison of variation of a. contact angles and b. relative drop height (mm/mm) of substrates with the time	98
Figure 5.1. 6. a. Top view and b. side view images of substrates after sessile drop test.	100
Figure 5.1. 7. Top and cross side micrographs of a. G330, b. G347, c. G348 and d. G550 after sessile drop test.....	102
Figure 5.1. 8. X-Ray results of graphite substrates after Sessile drop test.	104
Figure 5.1. 9. Raman shift results of graphite substrates after Sessile drop test.	104
Figure 5.1. 10, Images of sessile drop test, a) on G330, b) on G347 c) on G348 and d) on G350... ..	105
Figure 5.1. 11. Contact angle and parameters of silicon drop with time on G347 and G348 during dispensed test	105
Figure 5.1. 12. Comparison of variation of a. contact angles and b. relative drop height (mm/mm) of substrates with time	106
Figure 5.1. 13 a. top and cross section images of substrates after sessile drop test.....	108
Figure 5.1. 14 top and cross section micrographs of a. G347 and b. G348 after dispensed sessile drop test.....	110
Figure 5.1. 15. X-Ray results of graphite substrates after Sessile drop test	111
Figure 5.1. 16. Raman shift results of graphite substrates after Sessile drop test.	112
Figure 5.1. 17. a. top and cross section images of substrates after high vacuum test.	113
Figure 5.1. 18. Cross-section micrographs of G330, G347, G348 and G530 after induction furnace test.	114
Figure 5.1. 19. X-ray results of graphite substrate after induction furnace test.	115
Figure 5.2. 1. Image of the distribution of pores in different graphite substrates, being R6650, R6710 and Lorraine	116
Figure 5.2. 2. Image of the interconnectivity of pores in different materials, R6650, R6710 and Lorraine	117
Figure 5.2. 3. Images of classic sessile drop test, a) on Carbon-Lorraine b) on R6650 and c) on R6710.	118
Figure 5.2. 4 Contact angle and parameters of silicon drop with time of a) on Lorraine, b) on R6650 and c) on R6710.....	120
Figure 5.2. 5. Comparison of variation of a. contact angles and b. relative drop height (mm/mm) of substrates with the time	121
Figure 5.2. 6. a. Top view and b. cross side images of substrates after sessile drop test.....	123
Figure 5.2. 7. Micrographs of a. Lorraine, b. R6650 and c. R6710 after sessile drop test	125

Figure 5.2. 8. X-Ray results of graphite substrates after Sessile drop test.	126
Figure 5.2. 9. Raman shift results after the Sessile drop.....	127
Figure 6.1. 1. Images of B ₄ C coatings a. 2 μm and b. 4 μm	133
Figure 6.1. 2 Images of sessile drop test of B ₄ C coatings a. 2 μm and b. 4 μm.....	133
Figure 6.1. 3. Contact angle and parameters of silicon drop with time a) on B ₄ C (2 μm), b) B ₄ C (4 μm).	134
Figure 6.1. 4. Comparison of variation of a. contact angles and b. relative drop height (mm/mm) of substrates with the time	135
Figure 6.1. 5. a. Top view and b. side view images of substrates after sessile drop test.	136
Figure 6.1. 6. Top view micrographs of a. B ₄ C (2 μm) and b. B ₄ C (4 μm).	138
Figure 6.1. 7. Cross section micrographs of a. B ₄ C (2 μm) and b. B ₄ C (4 μm).....	140
Figure 6.1. 8. X-Ray results of coating graphite substrates after Sessile drop test.....	141
Figure 6.1. 9. Raman shift results of graphite substrates after Sessile drop test.	141
Figure 6.2. 1. Images of sessile drop test on TiO ₂ coating substrate.	143
Figure 6.2. 2. Contact angle and parameters of silicon drop with time on substrate coated by TiO ₂	144
Figure 6.2. 3. a. Top view and b. side view images of TiO ₂ coating substrates after sessile drop test.	145
Figure 6.2. 4. Micrographs of TiO ₂ coating substrate a. top view and b. cross section.	146
Figure 6.2. 5. X-Ray results of TiO ₂ substrates after Sessile drop test.	147
Figure 6.2. 6. Raman shift results of TiO ₂ substrates after Sessile drop test.	147
Figure 7. 1. a. Top view and b. side view images of substrates after induction furnace test.....	152
Figure 7. 2. Relation between radius maximum (R _{max}) and the infiltration distance maximum (H _{max})	154
Figure 7. 3. Top view micrographs of the samples after induction furnace test.	155
Figure 7. 4. Cross section micrographs of the samples after induction furnace test.	156
Figure 7. 5. X-Ray results of coating graphite substrates after induction furnace test.	158
Figure 7. 6. Raman shift results of graphite substrates after induction furnace test of sample 1.	159
Figure 7. 7. Scheme of the lamella obtain by the Fib from the interface Silicon- Carbide	160
Figure 7. 8. Result of the TEM, a. micrographs and atomic map. b. Lines scan of content of silicon and carbon atoms	160
Figure 8. 1. Schema about the blocks: materials studied and techniques used.	162

List of Tables

Table 1. 1 Contact angles of silicon on substrates close the melting point.	41
Table 1. 2. Values of the contact angle according to the properties of graphite	48
Table 1. 3. Equilibrium contact angle according the main factors reported by several authors.....	50
Table 3. 1. Comparison of typical properties commercial graphite materials.....	59
Table 3. 2. Properties of alumina material.....	59
Table 4.1. 1. Density results	73
Table 4.1. 2 Ratio to quantify the grade of crystallinity.....	74
Table 4.1. 3. Values of average rugosity	74
Table 4.1. 4. Spreading and infiltration rate measured on several substrates in the different stages.	80
Table 4.1. 5. Infiltration and spreading rates, values of effective radius and maximum infiltrated length according properties of graphite and work condition	82
Table 4.1. 6. Values of silicon-graphite substrate, silicon-composite 1 and silicon-composite2.....	87
Table 4.1. 7.Values of contact angle according properties of graphite	88
Table 5.1. 1 Density results	92
Table 5.1. 2. Ratio to quantify the grade of crystallinity.....	94
Table 5.1. 3.Values of average rugosity	94
Table 5.1. 4. Spreading measured on several graphite substrates before and after drop formation	99
Table 5.1. 5. Values of effective radius and maximum infiltrated length according properties of graphite substrates and work condition	101
Table 5.1. 6. Values of the SiC layer thickness (e) and the thickness of the SiC crystals formed around the silicon droplet (e_d)	103
Table 5.1. 7. Spreading and infiltration rate measured on G347 and G348 substrates during dispensed sessile drop method.....	107
Table 5.1. 8. Values of effective radius and maximum infiltrated length according properties of graphite and work condition.....	109
Table 5.1. 9. Values of the SiC layer thickness (e) and the thickness of the SiC crystals formed around the silicon droplet (e_d)	110
Table 5.1. 10. Values of effective radius and maximum infiltrated length according properties of graphite substrates and work condition	114
Table 5.2. 1 Density results	116
Table 5.2. 2. Ratio to quantify the grade of crystallinity.....	117
Table 5.2. 3. Values of average rugosity	118

Table 5.2. 4. Spreading and infiltration rate measured on several graphite substrates before and after drop formation	122
Table 5.2. 5. Infiltration and spreading rates, values of effective radius and maximum infiltrated length according properties of graphite substrates and work condition	124
Table 5.2. 6. Values of the SiC layer thickness (e) and the thickness of the SiC crystals formed around the silicon droplet (e_d)	126
Table 6.1. 1. Spreading and infiltration rate measured on several graphite substrates before and after drop formation	135
Table 6.1. 2. Values of effective radius and maximum infiltrated length according properties of graphite substrates and work condition.	137
Table 6.1. 3. The values of the SiC layer thickness (e).	140
Table 6.2. 1. Spreading rate of TiO ₂ coating after Sessile drop test.....	145
Table 6.2. 2. Values of effective radius and maximum infiltrated length according properties of graphite substrates and work condition.	146
Table 7. 1. Values of maximum width spread (W_{max}) and maximum infiltrated length (h_{inf}), and the diameter of D) from the optical images.....	153
Table 7. 2. The values of the SiC layer thickness (e) and the size of the SiC crystals formed around the silicon droplet (e_d).....	158
Table 8. 1. The main results obtained by different substrates.	165
Table 8. 2. Values of thickness of SiC layer and size of SiC crystals around the droplet in comparison other parameters at 1450°.....	167
Table 8. 3. Value of the tortuosity in comparison with the porosity parameters	168
Table 8. 4. Analysis of the rugosity against the main results	169
Table 8. 5. Values of crystallinity against of main parameters of the contact angle	170
Table 8. 6. Effect of the atmosphere in the main parameters of the reaction, the wetting and the infiltration.....	170
Table 8. 7. The main results from the classic and dispensed Sessile drop test	171
Table 8. 8. Images of the distribution of pores in different graphite and parameters of the porosity in comparison with the maximum infiltration distance (h_{max}).....	172
Table 8. 9. Main parameters obtained for carbonaceous materials.....	172
Table 8. 10. The main results after the sessile drop test of the G348 and the B ₄ C coatings.	174

1. Introduction and state of art

1.1 Introduction

Nowadays, silicon is a very important part of the world economy. This is because it is being the main raw material in the semiconductor's industry, and as a consequence, Silicon is largely used in metallurgy, photovoltaic and electronic industries.

It is the eighth most common element in the universe by mass. Although, it is the most abundant element in the earth's crust after oxygen, it appears less frequently as a pure free element in nature. The main problem of silicon is its high reactivity, in fact, it is such corrosive that it is called "universal solvent"¹.

Depending on the degree of purity, we can classify silicon in three main groups: electronic grade silicon (EGS), solar grade silicon (SGS) and metallurgical grade silicon (MGS). The photovoltaic properties of silicon depend on the concentrations of individual impurities, so the maximum acceptable concentrations define the conversion efficiency of solar cells. In Figure 1 it is shown the relationship between the cell efficiency and impurity concentration for different silicon grades².

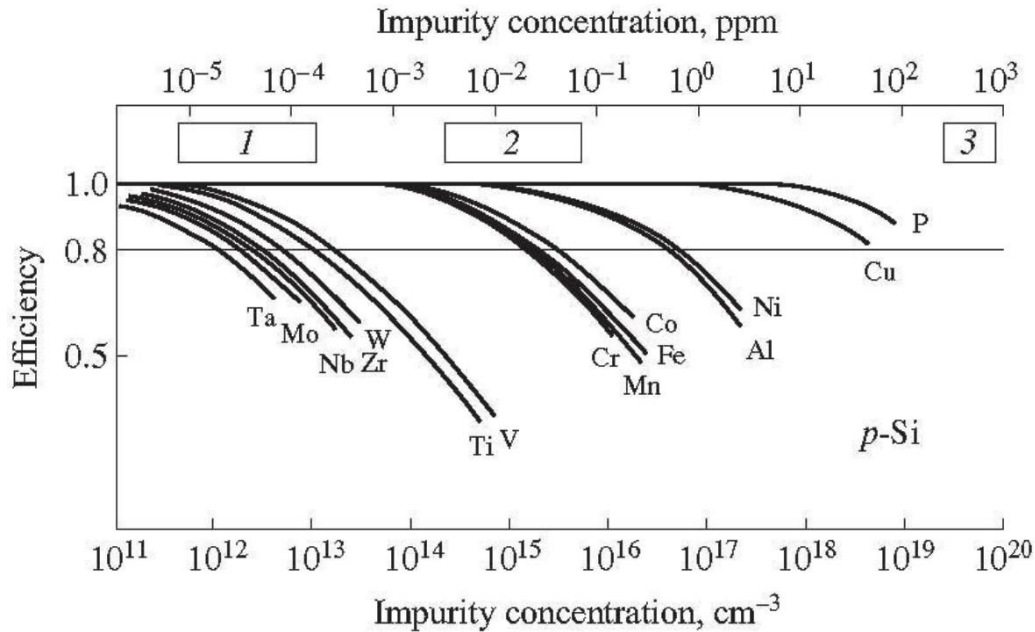


Figure 1. 1. Limits of impurity concentrations in p-type silicon for impurities determining degradation threshold of solar cells: 1 EGS; 2 SGS; 3 MGS.

Although most free silicon is used in the metallurgical industry, the most interesting application is the highly pure silicon used in the electronic industry. In recent years, there has been a rapid growth in the development of the photovoltaic industry because of the oil crisis.

Photovoltaic energy is considered mainly as a renewable electric source, and silicon is considered the dominant material for the fabrication of solar cells, so that, low-cost solar-grade silicon feedstock is needed^{3,4}. In order to produce solar-grade silicon (SGS), metallurgical-grade silicon (MGS) is purified because it is a direct and cost-effective way. There are several methods of purification, being the Siemens chemical route, but this process is still the main production method. However, the Siemens process has high cost and it is a source of environmental pollution.

Therefore, different metallurgical routes have been developed in recent years. These methods include several stages, for example, the Photosil process⁵ includes melting, plasma treatment and directional solidification in a crucible. The vacuum refining of molten silicon

is used to eliminate volatile elements from liquid silicon such as P, Al, Ca, and Mn⁶, while boron and other metallic impurities are removed by directional solidification and plasma treatment⁷.

Besides the elimination of the impurities from metallurgical silicon, during the purification is important to avoid the contamination of silicon with elements from the furnace. Refractory oxide-based materials (usually used in melting furnaces) contain electrically active metallic elements so that they are not used for silicon melting. Graphite is often used for crucibles, substrates and dies for the purification of silicon in the processing of low-cost solar cells⁸.

Graphite has advantages such as good electrical and thermal conductivity, good thermal shock resistance, and relatively low cost. In addition, the dissolved carbon is not an electrically active impurity in the PV cells. However, graphite is an oxidizing material in air and it reacts with silicon. Moreover, its open porosity increases these disadvantages. The reactivity between Si and graphite can be a determining factor of the lifetime of graphite crucibles⁶⁻¹⁰. Molten silicon initially does not wet carbon materials. However, owing to the reactivity between Si and C, a SiC layer is formed which enhances strongly the wettability¹¹. In order to avoid the impurities, inert materials not-wetted by silicon are required. Nevertheless, such materials have not been found yet because molten silicon is very reactive. Hence, wetting and infiltration of molten silicon into the refractories should be minimized¹. In addition to silicon purification or crystal growth, knowledge about wetting and infiltration of silicon in graphite is relevant for techniques such as reaction bonding of silicon carbide (RBSC)⁸ and liquid silicon infiltration (LSI)¹².

For porous graphite substrates, wettability and infiltration are managed by the reactions along the triple line (vapour, liquid and solid)¹³. It is known that the reaction between silicon and graphite allows the phenomena of wetting and infiltration. Wettability depends on the rugosity¹⁴, temperature¹⁵, atmosphere¹⁶, open porosity and type of substrate¹. Since the exact influence of each factor is still not known, there is a large scatter of results⁸⁻¹⁵. Molten silicon initially does not wet carbonaceous materials. However, owing to the reactivity between Si and C, a SiC layer is formed that strongly enhances the wettability¹. Perfect

wettability (angle contact equals zero) is found in substrates with both high surface rugosity and a large average pore size¹. Moreover, silicon sticking is due to the good wetting and the infiltration and leads to several defects which reduce the electrical properties¹⁷. Nevertheless, there is no accurate knowledge about the key factors governing infiltration kinetics¹⁸. It is known that infiltration does not vary according to Washburn's equation because it is controlled by the formation of a SiC layer at the triple line of the infiltration front and not by viscous resistance. However, there is no theoretical model that describes this process, despite the existence of several studies⁸⁻¹³.

1.2 Literature Review

During the purification of silicon, besides the elimination of impurities from the molten silicon, phenomena as the reaction, wetting or infiltration should be avoided. It should be taken into account that Si melting point is at 1414°C.

The reaction between silicon and crucible or dies material could pollute the silicon leading to a decrease in the electrical properties. On the other hand, silicon will stick to the crucible if the liquid wet the crucible. Moreover, spontaneous infiltration takes place when the liquid shows good wetting on the substrates. Both infiltration and wetting decrease dramatically the lifetime of the crucible. To sum up, materials that do not react and are not wet by silicon are need¹⁹. Therefore, wettability, infiltration and reaction between silicon and different materials are key factors in this dissertation.

In this section, a brief explanation of the mentioned phenomena is presented and then, a literature review of the behaviour of molten silicon against oxides substrates, graphite substrates and covalent materials²⁰.

- **Reactivity**

The high melting temperature of silicon (1414°C) boost the reactivity with materials from the crucibles and moulds. The likely reaction can propitiate the contamination of the silicon, and also, the decrease the crucible lifetime. Thus, materials with negligible reactivity are needed²¹.

On the other hand, it should be taken into account that the SiO₂ passive layer is formed when fresh silicon is in contact with the air. Hence, the interaction between silicon and oxygen can occur on during the test:



Equation 1 represents the passive oxidation of silicon and equation 2 provides the active oxidation of silicon, the main difference is that the oxide formed in the first equation is solid while in the second it is gas.

During the heating in the furnace, the elimination of the SiO_2 layer which covers the fresh silicon is due to the formation volatile SiO thanks to the reaction between the passive layer and the fresh silicon (Equation 3).



According to Drevet²¹, a piece of silicon heated in a furnace can be oxidized or de-oxidized depending on the partial pressure of oxygen $P_{\text{O}_2}^f$ (see Figure 1. 2)

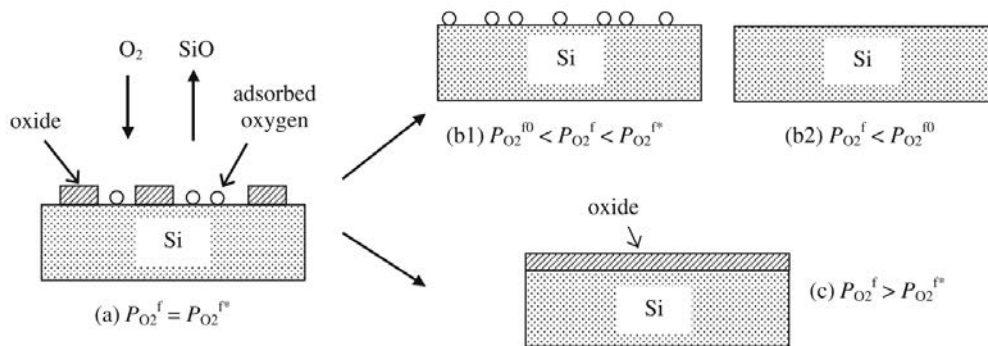


Figure 1. 2. Scheme of how the surface of silicon depends on the conditions. a) initial silicon piece, b) oxide-free containing adsorbed oxygen (b1) or clean (b2), and c) oxidized surfaces¹⁷.

Where $P_{\text{O}_2}^{f*}$ is a critical partial pressure of oxygen, that is related to the equilibrium pressure of SiO . If the partial pressure of oxygen is higher than the critical value, the passive layer will be formed c) (equation 1). If it is lower, the surface obtained will be oxide-free but likely it will contain adsorbed oxygen (equation 2). However, the dissolution of the SiO_2 layer due to the reaction with the fresher silicon (equation 3) provides another threshold value $P_{\text{O}_2}^{f0}$. This parameter is related to the surface tension of Si. The surface, obtained for $P_{\text{O}_2}^f < P_{\text{O}_2}^{f0}$, are clean, namely, oxide-free and adsorption-free¹⁷.

According to Camel¹⁷, the surface of the silicon will be clean during the experiments under industrial argon or high vacuum. But the high affinity between silicon and oxide is a key factor when the substrate has oxides.

- **Wettability**

The wettability of a liquid is measured through the contact angle, noted by θ in Figure 1.3¹. A substrate is wetted by a liquid if the value of the contact angle is lower than 90 degrees and non-wetted if it is higher.

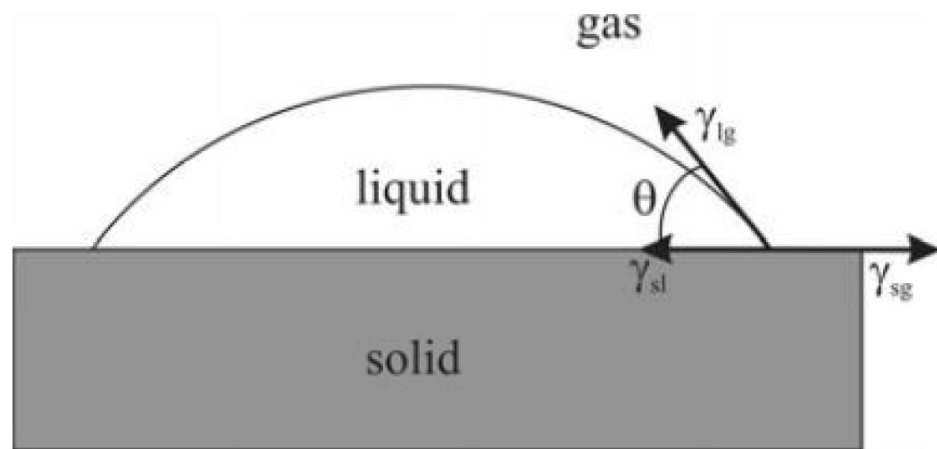


Figure 1. 3. Definition of contact angle.

A good wettability behaviour entails a large point of contact between the liquid and the substrate, hindering the later detachment. If the silicon sticks to the substrates, the cracks can be developed, reducing the crucible lifetime as well as the loss of the silicon. Thus, non-wetting behaviour is required²¹.

According to the Young equations:

$$\cos \theta = \left(\frac{\sigma_{SV} - \sigma_{SL}}{\sigma_{LV}} \right) \quad \text{Equation 4}$$

$$\cos \theta = (W_a / \sigma_{LV}) - 1 \quad \text{Equation 5}$$

Being θ , the contact angle; W_a , the adhesion work; σ_{LV} , the surface energy of liquid; σ_{SV} , the surface energy of solid; and σ_{SL} the solid/liquid interface energy. As the liquid silicon at the

melting point has surface energy around to 800 mJ/m^2 , the good wetting of silicon is obtained if the adhesion work is also high, namely, the interfacial bonds are strong, for example, the chemical in nature²¹

- **Infiltration and spreading**

There are two kinds of phenomena in liquid silicon – solid graphite system: the depth infiltration of silicon liquid through the pores inside of substrate (it is denominated H in figure 6) and the spreading (noted D), that is the zone measured from the solid-liquid-vapor three phase line¹⁴. Both phenomena are linked to wettability; good wettability implies large spreading distances and the spontaneous infiltration²¹.

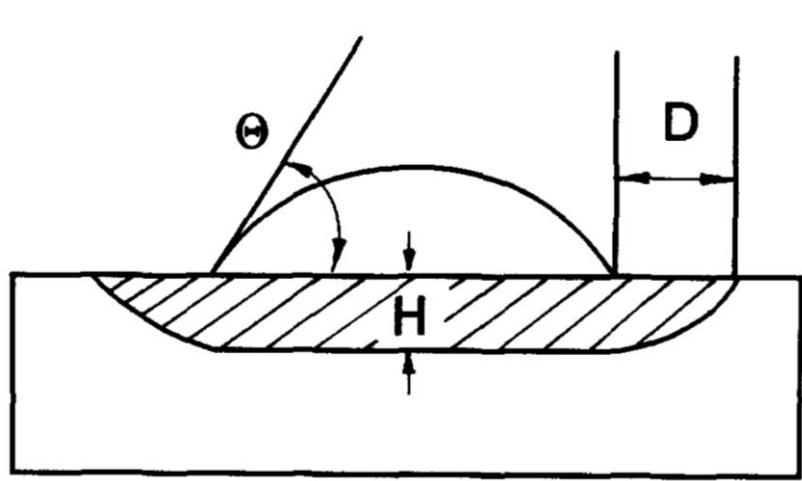


Figure 1. 4. Cross section schematic of the silicon-graphite interface.

For a non-reactive system, the infiltration is controlled by viscous resistance and the infiltration depth agrees with the Washburn's equation²²:

$$h^2 = r_{\text{eff}} \frac{\sigma \cos \theta}{2\eta} t = Kt \quad \text{Equation 6}$$

Where r_{eff} is the effective radius, σ is the liquid surface tension, Θ is the contact angle, η is the liquid viscosity. In the theory, contact angles lower than 90° can infiltrate without external pressure, but in the practice contact angles lower than 60° are need²³.

1.2.1 Oxides substrates

The oxides have high thermodynamic stability, electric insulators and whose bonding characteristic is between mainly ionic as MgO (Pauling ionicity: 71%) and more covalent as SiO₂ (Pauling ionicity: 51%)²⁴.

The main oxides used as substrates during Si wetting experiment are SiO₂, AlO₂ and MgO₂. As it is commented in section 1.2, generally, the surfaces obtained are totally clean due to the use of atmosphere with low oxide contain. However, for this kind of substrates, the dissolution of the oxides from the substrates can affect the behaviour of molten silicon in spite of the protective atmosphere.

The initial contact angle between silicon and oxides is close to 90°. However, higher values were found for non-reactive liquid (115°-135°), indicating, chemical interaction contribute significantly in this case. The dissolved oxygen in silicon, the high affinity for O or the formation of volatile SiO (equation 3) can be key factors in the behaviour of the molten silicon.

According to the literature, corrosion rings are formed during the experiments. Champion et al²⁵ affirms they are produced by the dissolution in the triple line and by the evaporation of the liquid metal, meanwhile, Saiz et al²⁶ say the corrosion rings are linked to the evaporation and the pinning of the drop due to the triple line ridges.

Currently, crucibles made of Si₃N₄ and coated by SiO₂ are used during the growth of solar silicon ingots. The porous SiO₂ coating is used as a mechanical fuse in order to improve the detachment, owing to the fact the work adhesion between silicon and silicon oxide is low. Besides, the infiltration is hindered due to the fact it is controlled by the deoxidation of Si₃N₄.

Table 1. 1 shows the values of the contact angle of silicon on oxides substrates around the Si melting point. It is significant that every value tends to 90°, likely, due to the fact that the final interface is Si/SiO₂.

Particularly for Si/Al₂O₃ system, thermodynamic calculation shows molten silicon dissolves the alumina, leading to the saturation of the molten silicon and the precipitation of SiO₂ on the interface. Hence, the system is reactive and the wetting is managed by the reaction¹⁷.

Currently, crucibles made of Si₃N₄ and coated by SiO₂ are used during the growth of solar silicon ingots. The porous SiO₂ coating is used as a mechanical fuse in order to improve the detachment, owing to the fact the work adhesion between silicon and silicon oxide is low. Besides, the infiltration is hindered due to the fact it is controlled by the deoxidation of Si₃N₄¹⁹.

Table 1. 1 Contact angles of silicon on substrates close the melting point.

Substrates	Contact Angle	
	Yuan ²⁷	Maeda ²⁸
Graphite	2.07	1.72
Alumina	4.23	3.07
Composite 1	2.24	1.52
Composite 2	1.72	1.38

On the other hand, it is known that the addition of Ti to a metal whose melting point is moderate decrease dramatically the contact angle, but there are no studies for silicon. The formation of Ti-oxides on the interface indicates contact angles close to 90°, although the Si-Ti interaction is very strong²⁹.

1.2.2 Graphite substrates

Previous studies^{6–10} have shown that the reaction between silicon and graphite on the triple line manage the behaviour of molten silicon against graphite.



Some researchers suggest that reactive wetting is managed by adsorption, namely, spreading kinetics are controlled by the migration of a ridge in the triple line³⁰. In contrast, other authors suggest a model called “reaction product control” (RPC) where wetting and spreading rate is managed by the formation of the new compound²⁰. However, the experimental data agree more with RPC. Initially, the contact angle corresponds to the contact angle of the liquid and unreacted solid. Then the reaction occurs along the triple line, the liquid advance over non-wettable substrate, the movement is allowed thanks to the formation of the new compound layer and until the contact angle reach the equilibrium. So, the final contact angle is equal to liquid/new compound system³¹.

According to several authors, the spreading time (t_{spr}) is around 10-10⁴s and linear with the time²¹. The values are much higher in comparison with the non-reactive system ($t_{spr}=10^{-2}$)²³. Regarding the contact angle, several studies have revealed that initially the system is Si/C, whose contact angle $\Theta_o \approx 145^\circ$ (for vitreous carbon) and finally, after the formation of SiC layer, the contact angle is $\Theta_f \approx 40^\circ$ as the system is Si/SiC.

As the wetting is managed by the reaction (equation 5), the interesting area is the triple line, where the liquid is in contact with the substrate and the reaction allows the movement. After this area, the SiC layer is getting thickness due to diffusion of the silicon and the dissolution of the graphite. In a few seconds, the reaction products cover the interface. The reactivity on the interface is considered as bilayer by many authors^{32–35}. The layer I is formed by submicronic SiC particles close to the graphite area thanks to the previous carbon dissolution. On the other hand, the layer II is formed by SiC crystal (-5-10 μm) on the layer I due to the dissolution of the submicronic SiC particles from the layer I. However, differences were found in the literature, for example, Favre et al³⁶ considered as an only one layer. Besides, Zhou et al³⁷ believe the SiC crystals are formed in the liquid, instead of the layer I.

On the other hand, Li and Hausner³⁸ affirm layer II is forming during the cooling phase. Moreover, Deike et al³⁹ suggest that layer I is a mix of unreacted silicon and SiC. The thickness of these layers, e , is likely managed by the diffusion of the carbon through the SiC. According to that, the thickness can be expressed as $e \sim t^n$, being $n=1/2$ ⁴⁰ or $n=1/4$ ³⁷. In addition to Deike et al³⁹ affirm for vitreous carbon the maximum thickness is reached at 10 min while for polycrystalline the thickness increase with the time. In contrast, Voytovych et al¹⁰ suggest that the thicker of the layer increase until a certain time when the layer reaches a maximum, then, the growth of the layer remains almost constant in every carbonaceous case: vitreous graphite ($e_{\max} \sim 10-12 \mu\text{m}$) and polycrystalline graphite ($e_{\max} \sim 15-20 \mu\text{m}$). In fact, Voytovych¹⁰ suggested the SiC carbide layer is formed in the interface. Firstly, a thin and reactive layer is formed by nucleation, then, there is a rapid growth until the maximum thickness is obtained and finally, only the microstructure homogenization took place. According to Kumar⁴¹

$$e = \sqrt{\left(\frac{2D}{\rho} C_{Si,l}\right)} \sqrt{t} = 2.843 \times 10^{-7} \sqrt{t} \quad \text{Equation 8}$$

Being e , thickness of silicon carbide layer; D , diffusion coefficient of silicon through silicon carbide layer; ρ , the density of silicon carbide; $C_{Si,l}$, the density of silicon in liquid phase and t , reaction time.

In order to evaluate the reactivity, Caccia et al¹⁸ suggest the following method:

$$n_{SiC}[\text{mol}] = \frac{\rho_{SiC} \times e \times A}{M_{SiC}} \quad \text{Equation 9}$$

Being ρ_{SiC} silicon carbide density; e , the thickness of the SiC layer formed on the interface; A the base of the area of the drop; and M_{SiC} the SiC molecular weight.

Einset et al²² considered the infiltration was controlled by viscous resistance and the infiltration depth agrees with the Washburn's equation (equation 5). The remarkable difference between the theoretical constant (K_{theor}) and calculated constant (K) is explained by the authors because the pores are closed during the experiment. However, recent studies suggest the infiltration is controlled by the reaction, in the same way than wetting,

due to fact that the infiltration rate is linear with the time, not parabolic as Wasburn's equation. Besides, the active energy is higher than in viscous flow. In fact, the closure of pores can be the reason why infiltration stops⁴². An accurate study about reactive information²⁹ propose to calculate the infiltration depth $h(t)$ using the radius R , the volume V , obtained during the experiments assuming that the infiltration flow is vertical,

$$\mathbf{h(t)} = \frac{1}{\alpha_{\text{eff}}} \left(\frac{3V_{\text{inf}}}{\pi(R^2 + R_0^2 + RR_0)} \right) \quad \text{Equation 10}$$

Where the subscript o indicates at time zero, namely, when the drop is formed and melted. The infiltration volume (V_{inf}) is the variation between initial volume V_0 and volume $V(t)$. The volume fraction of liquid which infiltrates, α_{eff} , usually in non-reactive infiltration has used the percentage of open porosity, but owing to the variation of the molar volume (V^m) in this case is not accepted, being $V_C^m = 5.5 \text{ cm}^3$ for carbon, $V_{\text{Si}}^m = 11.6 \text{ cm}^3$ for silicon and $V_{\text{SiC}}^m = 12.5 \text{ cm}^3$ for silicon carbide. α_{eff} is calculated by equation 8.

$$\alpha_{\text{eff}} = \alpha_{\text{Si}} + \alpha_{\text{SiC}} \frac{V_{\text{Si}}^m}{V_{\text{SiC}}^m} \quad \text{Equation 11}$$

During cooling, stress owing to volume change and the difference in the thermal expansion rate lead to developing cracks in the graphite crucible¹⁷.

Besides, the infiltration rate is calculated by ($U_{\text{inf}} = h_f^*/t_{\text{inf}}$), being h_f^* the infiltration distance measure from the micrographs after experiments and t_{inf} , the time of infiltration measured in situ²⁹.

For the reactive system, several studies suggest wetting and infiltration are managed by the reaction (equation 1). Then, the kinetics rates are constants. Spreading rate ($U_{\text{spr}} = dR/dt$) is the variation of the radius of the drop with the time and infiltration rate ($U_{\text{inf}} = dh/dt$) the variation of the infiltration depth. In fact, some authors⁸ have reported that

$$\frac{dh}{dt} = \frac{dR/dt}{\xi} \quad \text{Equation 12}$$

Being ξ , the tortuosity is a factor of the substrate, which is the ratio of actual flow path length to the straight distance between the ends of the flow path. Besides, the value of the tortuosity is inversely proportional to the porosity percentage and the pore size⁸.

Camel et al¹⁷. proposed values of the spreading rate U_{spr} (dR/dt) around $10 \mu\text{m/s}$, which is several orders of magnitude lower than the spreading rate measured in non-reactive system²⁴. Moreover, if the infiltration rate has similar value, so that $U_{inf}/U_{spr} = (0.65-0.95)$, then it is a reactive system, hence, the reaction at the triple line manages the wetting, where the growth of the SiC layer is parallel to the Si/C interface⁸.

The most relevant values of contact angle depend on the different parameters:

- Influence of rugosity

The rugosity is measured by average rugosity (R_a), namely the arithmetic average of the absolute distance between peaks and valleys¹. The rugosity can affect the contact angle owing to the fact that as rugosity increases the surface area and the drop can be pinned by the defects²³. For the well-wetted system the rugosity enhances the wetting while for a poorly wetted system, the wetting is hindered by the rugosity⁴³. According to Li et al¹⁴, the substrates with a higher value of rugosity will obtain a smaller contact angle. Regarding the results of Ciftja¹, perfect wettability (contact angle equal zero) is found in substrates with both high surface rugosity and large average pore size. In spite of this, results showed that density does not have a high influence on the wettability of silicon on graphite. In addition, the preparation of the substrates influences the rugosity due to the fact the pores are closed by the graphite particles formed during the polishing²⁹.

- Influence of crystallinity

According to Beyssac et al., the crystallinity of carbonaceous materials can be analysed and even quantified by Raman microspectroscopy. Figure 3 shows the typical Raman spectrum of a carbonaceous material⁴⁴.

The G band indicates the vibrational mode E_{2g} . A narrow and high intensity G peak is characteristic for a material with a high degree of crystallinity, while a wide and low intensity G peak indicates amorphous materials. The D band indicates the structural disorder. The D1 band has a high intensity and width in disordered materials; D2 in amorphous materials are not distinguishable from the G band, and D3 is present in amorphous material as a wide band.

To quantify the grade of crystallinity, Beyssac et al. proposed the ratio $D1/(D1+D2+G)$, where the parameters represent the area of the bands. The lower the value of this ratio, the higher is the grade of crystallinity.

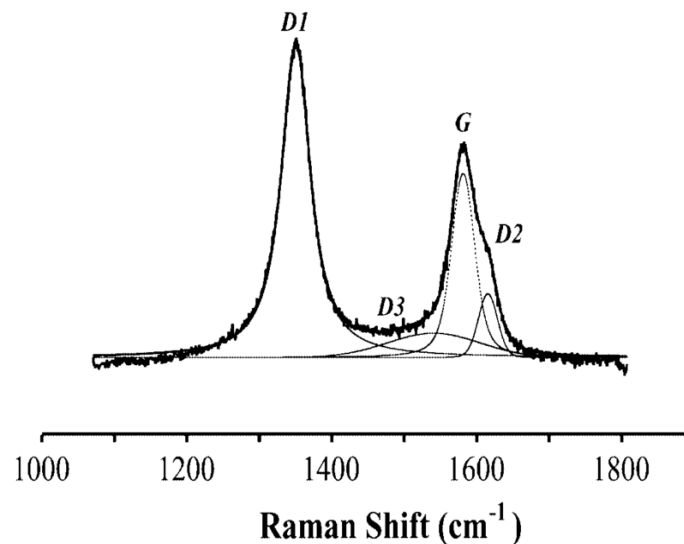


Figure 1. 5. Curve fitting of the first-order region of the Raman spectrum.

According to Eustathopoulos et al²⁰, the wettability on carbonaceous materials depends on the grade of crystallinity. Amorphous materials lead to a difficult the reaction between silicon and graphite due to the interruption by impurities; thus, the wettability becomes worse.

- Influence of the atmosphere

The atmosphere is another key factor of silicon purification, owing to the effect of the silicon evaporation. Under Argon atmosphere these effects are neglected. In contrast, under

vacuum, a SiC layer is likely formed by silicon transport through the vapour phase, at the temperature near to the melting point⁸. Consequently, the initial angle contact is lower and the infiltration rate is higher than those obtained with other atmospheres such as Helium or Argon⁸. These findings agree with the previous formation of silicon carbide due to the evaporation and condensation of the silicon under high vacuum.

Besides, the atmosphere is a key factor in the de-oxidation of the surface, a formation of the volatile SiO is higher in argon than in vacuum²¹.

- Influence of the temperature

Caccia et al¹⁸ analyzed the wetting behavior of the silicon alloy against glassy carbon at a different temperature. According to the results obtained when the temperature increases the spreading rate increases too. In addition, the carbon dissolution also increases, the SiC layer formed is more compact and the size of SiC crystals decrease. Nevertheless, the SiC layer thickness remains constant.

- Influence of the type of graphite

Vitreous carbon showed higher values of initial and final contact angle than polycrystalline graphite substrate^{14,15,38}. Meanwhile, the infiltration distances were deeper for polycrystalline graphite than vitreous carbon³⁷.

- Influence of the type of porosity

The small size of pore leads to reduce stress during the cooling as well as boosts the closure of pore and thus, minimize the infiltration depth¹⁷. High porosity could lead to the creation of cracks during the infiltration due to the stress⁴⁵. Besides, according to Li et al, if the open porosity increase, the infiltration distance increase¹⁴, this agrees with capillary forces.

Table 1. 2. Values of the contact angle according to the properties of graphite

Authors	Substrate	Final angle (°)	contact	Temperature	Atmosphere	Ra (µm)
Li and Hausner ^{14,38}	Graphite	3° 35°		1430°C	Argon	3.18 0.005
	Vitreous carbon	10° -40°		1430°C	Argon	<0.005
Dezellus ¹²	Graphite	35° -40°		1430°C	Vacuum	0.002- 0.004
	Vitreous carbon	36°		1430°C	Vacuum	0.005
Whalen and Anderson ¹⁵	Graphite	5° -15°		1502°C	Vacuum	
	Vitreous carbon	40° -50°		1502°C	Vacuum	
Ciftja ¹	Graphite	6° ~30°		1600°C	Argon	0.93 0.06
Israel ⁸	Graphite	~12°		1460°C	Argon	0.77

1.2.3 Covalent ceramics

Carbides and nitrides of silicon, aluminium and boron are considered predominantly covalent ceramics. These materials are interesting because of the stable oxide that can form and their effect on the wetting.

- Si on SiC

During the test of silicon against SiC substrate, the silicon reacts and dissolves the silicon carbide, and the deoxidation of silicon carbide occurs. As in the Si case, a very thin oxide layer is formed over the SiC when the substrates are in contact with air at room temperature, but during the experiments under argon, at melting point, the surface is free of oxides and the final contact angle is around 40°²⁰. On the other hand, under high vacuum, the graphite layer is formed thanks to the loss of silicon by evaporation, then, molten silicon reacts with this layer forming again SiC. Thus, the wetting is reactive⁴⁶.

- Si on Si₃N₄

The main characteristics of Si₃N₄ are the low solubility of nitrogen in molten silicon and the formation of stable oxide in contact with the air at room temperature. Unlike SiC, at Si melting point under argon, the substrate surface keeps oxidizing for a while. The initial contact angle is around 85°, as Si/SiO₂ system. However, the final contact angle is around 49°, as Si/ Si₃N₄ system. The variation of the contact angle and the kinetics is due to the de-oxidation of the surface against molten silicon²¹.

In the industry, Si₃N₄ is used as a coating for the crucibles⁴⁷. Owing to the fact Si₃N₄ layer works as a barrier to avoid wetting and infiltration as well as bad mechanical properties.

- Si on BN and B₄C

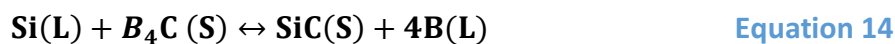
The main property of the BN is that is not wetted by silicon. The contact angles obtained⁴⁸ are 105°-145°. These values are usually linked to a non-reactive system, but according to Drevet et al, the Si/BN is a reactive system. Where the parenthesis indicate the boron is dissolved in the liquid.



Regarding equation 13, the final contact angle should be the contact angle of the product, namely, of the Si₃N₄ (~50°). According to Drevet et al, the reactivity is very weak, thus, the equilibrium is reached before to Si₃N₄ layer was formed. Hence, the final contact angle does not have to be the contact angle of the product.

BN cannot be used by photovoltaic applications because of the boron dissolution which deteriorate the electrical properties of the silicon. However, it can be used as a crucible to small quantities of silicon. Likely, the infiltration is negligible and the detachment is easy due to the weak adhesion²³.

B₄C also presents a reactive wetting, according to equation 14



In contrast to BN, the Gibbs energy value standard is positive but lower than for SiC, so a SiC layer will be formed when the system reaches the equilibrium. This theory agrees with the low contact angle obtained in the literature⁴⁹

Table 1. 3. Equilibrium contact angle according the main factors reported by several authors

Authors	Substrate	Contact angle	Temperature	Atmosphere
	SiC	8°	1693 K	Argon
Yuan, Huang and Mukai ²⁷	Si ₃ N ₄	89°	1697 K	Argon
	p-BN	144°	1698 K	Argon
	BN	145°	1699 K	Argon
	SiC(self-bonded)	30°	1775 K	Vacuum
Whalen and Anderson ¹⁵	SiC(hot-pressed)	41°	1775 K	Vacuum
	Si ₃ N ₄	43°	1699 K	Vacuum
	Si ₃ N ₄	10°	1775 K	Vacuum
Drevet ⁴⁸	BN	105° -145°	1703 K	Argon
Naidich ⁴⁹	B ₄ C	<<90	-	-

1.3 Summary

Due to the oil crisis, stock of solar silicon is needed for the photovoltaic industry. The obtaining process of solar silicon from the purification of metallurgical silicon has been developed nowadays. In order to avoid the contamination and the sticking of the silicon, materials which do not react or is are not wetted by silicon are sought. In spite of the large literature data, there is not accurately knowledge about reactive, wetting and infiltration.

The possible substrates are divided into three groups: oxides substrates, graphitic substrates and covalent materials.

- Oxides substrates show a high contact angle, but the molten silicon can be polluted by the oxide leading to a deterioration in the electric properties.
- Graphitic substrates are wetted by the silicon, but the impurities from the dissolved carbon do not affect the efficiency of the solar cells.
- Covalent materials have an adequate wettability but of dissolution the some of the material is not acceptable for PV applications.

The behaviour of molten silicon against several substrates are analysed in this dissertation in order to obtain information which material is the most suitable for the photovoltaic, and others applications such as the brazing, reaction bonding of silicon carbide (RBSC) and liquid silicon infiltration (LSI).

2. Motivation and objectives

2.1 Motivation

The study of the behaviour of molten silicon against several substrates is a highlighted topic for different industrial areas, for example, the solar silicon obtained through the purification of metallurgic silicon or the production of refractory materials through reaction bonding of silicon carbide (RBSC) and liquid silicon infiltration (LSI)¹². Even, for brazing applications²³.

Due to the fact that the melting point of silicon is 1414°C and it is considered as “universal dissolvent”¹, the main parameters to be considered in these applications are the reactivity, the wettability and the infiltration. On one hand, inert materials not-wetted by silicon are required for photovoltaic applications while for reaction bonding of silicon carbide (RBSC), are required materials with good wetting in order to obtain a spontaneous infiltration which is needed.

As in Drevet et al²⁴, the behaviour of molten silicon will be analysed against oxides substrates, graphite substrates and covalent ceramics.

2.1.1 Oxides substrates

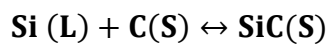
The oxides substrates show a high value of contact angle, but due to its oxygen content, the silicon could be polluted during the experiments. Several authors^{27,28} reported the contact angles obtained for oxides substrates were close to 90°. Although these results are usually linked to non-reactive systems, recent studies suggested the system is reactive²¹. This theory should be supported by more detailed chemical studies.

Particularly, in the case of the alumina, corrosion rings were found. According to Champion²⁵, this rings are linked to the substrate dissolution in the triple line and the evaporation of the liquid metal. In contrast, Saiz et al⁵⁰ asserted that the rings are produced by the evaporation of the liquid and the pinning of the drop. . However, it is still not clear the exact mechanism of their formation.

On the other hand, the titanium is largely used to decrease the contact angle in non-reactive systems, but there are no similar results reported for the silicon. On one hand, the reactivity between titanium and silicon is strong (according to the phase diagram), and on the other hand Ti-oxides can obtain contact angle close to 90°. Therefore, further studies are needed to reveal the influence of Ti on the wettability

2.1.2 Graphite Substrates

Previous researches⁶⁻¹⁰ have shown Si/C that is a reactive system managed by the reaction on the triple line:



Equation 15

Regarding the data, the model which better fit is the reaction product control (RPC) where wetting and the spreading rate is managed by the formation of the new compound²⁰. In the Si/C system, firstly, the contact angle is high because silicon does not wet to carbon but finally the contact angle drop like in the Si/SiC³¹ system.

Due to the reaction on the interface, a SiC layer is formed, and according to several authors³²⁻³⁵ is a bilayer one. The layer I is formed by a thin layer formed instantaneously and the layer II is formed by SiC crystals. However, there are some differences between the formation and the thickness of this layer. For example, Li and Hausner³⁸ affirm layer II is forming during the cooling phase. Even, Deike et al³⁹ affirm for vitreous carbon than the maximum thickness is reached at 10 min while for polycrystalline carbon the thickness increases with the time while Voytovych et al¹⁰ suggest than in every graphite substrate, the thickness increases until a certain layer reaches a maximum.

On the other hand, there is a lack of information about silicon infiltration. Firstly, the way to measure the infiltration distance or the kinetics rates. Einset et al²² considered that infiltration was controlled by viscous resistance and the infiltration depth agrees with the Washburn's equation, but the results showed that infiltration depth is linear, hence the infiltration is managed by the reaction in the triple line. For that reason, Voytovich et al²⁹ proposed a model based on the fact than infiltration flow is vertical and through the volume and the radius of the drop. In contrast, the infiltration rate is measured by $U_{inf}=h_f^*/t_{inf}$, where h_f^* is the infiltration distance measured from the micrographs instead to use their model because of the accuracy of the model.

As wetting and infiltration are controlled by the reaction between silicon and graphite, Camel et al¹⁷ suggested the kinetics rates, spreading and infiltration, should have the same order although the value of the infiltration rate should be smaller due to the tortuosity, which is the ratio between the way followed by a liquid and the distance between two points in a straight line. Israel et al⁸ affirmed that the tortuosity is inversely proportional to the porosity percentage and the pore size.

In spite of the fact of the system is reactive, a scatter of results is obtained for Si/C system, according to literature the most relevant parameters are:

- Influence of rugosity

In general, the rugosity enhances the wetting. In order to decrease the rugosity, the sample usually are previously prepared. Although it is known the polishing of the substrates influences due to the fact that the pores are closed by the graphite particles²⁹, and there is not any study about how to affect at the same time infiltration and wetting.

- Influence of crystallinity

According to Eustathopoulos et al²⁰, the wettability on carbonaceous materials depends on the grade of crystallinity. The reaction in amorphous materials is hindered by the impurities, hence wetting and infiltration. Although these results should be supported for more studies.

- Influence of the atmosphere

The atmosphere is another highlighted parameter for Silicon experiments, because of the silicon evaporation. Particularly under vacuum, it is probable the previous formation of silicon carbide due to the evaporation and condensation of the silicon⁸. Decreasing the initial angle contact in comparison with other atmospheres such as Helium or Argon⁸. More results to support this theory are needed.

- Influence of the type of porosity

The porosity has been analyzed by the mean size of pores and by the percentage of porosity. For example, Camel et al affirmed that the small size of pores leads to reduce stress during the cooling as well as boosts the closure of pores and thus, minimize the infiltration depth¹⁷. However, the influence of the interconnectivity of pores with the infiltration has not been studied.

2.1.3 Covalent ceramics

Besides the oxygen, silicon has high affinity with carbides, nitrides and borides. These compounds have been analysed, showing a high contact angle owing to the formation of a stable oxide.

This thesis is focused on the borides, due to the fact that BN is not wetted by silicon. Although BN is not valid for photovoltaic applications because it is a reactive system and the silicon can be polluted by boron. On the other hand, B₄C showed values of contact angles smaller than 90°, and the results suggested the system is reactive, thus, the liquid silicon can be polluted but it should be supported by further researches.

2.2 Objectives

The general objective of this thesis is to look for inert materials and not wetted by molten silicon for photovoltaic applications as well as to analyse and understand the reaction, wetting and infiltration and their main parameters. In order to get this information, specific partial objectives have been established for each kind of materials.

- Oxides substrates
 - To analysis the influence of the oxides on the reaction, wetting and infiltration of molten silicon.
 - To reveal the mechanism of formation of the corrosion rings
 - To determine the influence of the titanium on the wetting.
- Graphite substrates
 - To study the availability of different carbonaceous materials, such as carbon-carbon composites, as crucibles for photovoltaic applications.
 - To investigate the formation of the silicon carbide layer and the modelling of infiltration in order to obtain the kinetics for graphite substrates.
 - To identify of the highlighted parameters as rugosity, crystallinity, atmosphere and porosity.
- Covalent ceramics
 - To study the behaviour of B_4C against molten silicon, identifying the nature of the system and the main parameters controlling.

Nowadays, several studies about coatings are being developed, for example, Si_3N_4 is used as a mechanical fusile⁴⁷. Hence, this thesis includes a “coating” chapter where the graphite has been coated by B_4C and TiO_2 . On the other hand, in the chapter 4 is studied alumina, C-C composites or graphite substrates. In Figure 2. 1 , there is a schematic explanation of the outline of the thesis including the analysed materials in each chapter in order to clarify where the results can be found.

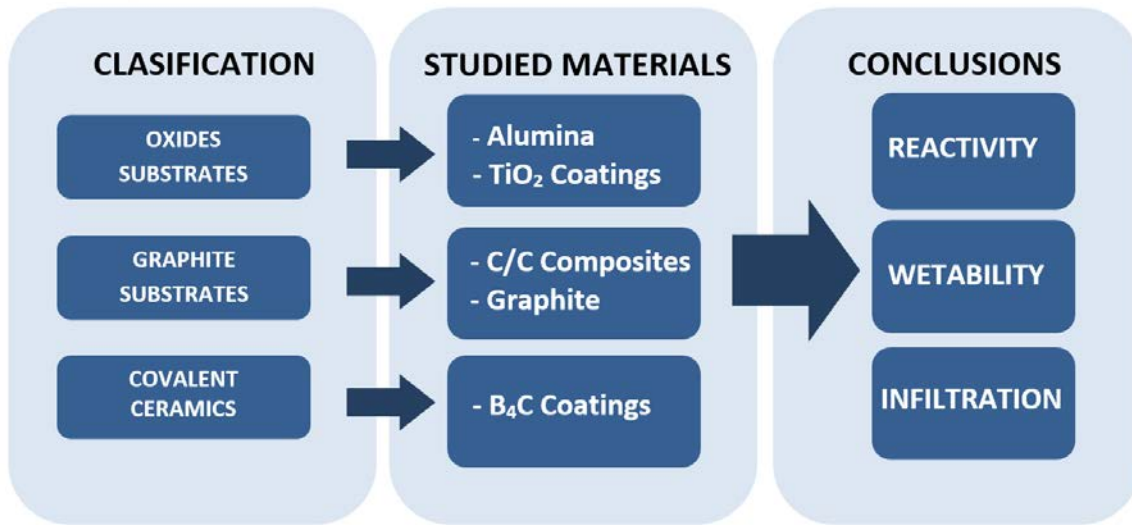


Figure 2. 1. General scheme of the outline of the thesis

3. Materials and experimental methods

3.1 Materials

3.1.1 Graphite materials

In order to study the relationship between the characteristics of commercial graphite substrates and their behaviour against molten silicon several kinds of graphite were studied.

- Tokai Carbon Co, LTD

CIP (Cold Isostatic Pressing) is the method used to obtain the graphite grades G330, G347, G348 and G530 used as substrates. This method consists of introducing powder in a rubber bag (moulding with little transformation resistance), sealing and then, applying pressure through a liquid, usually water. Thanks to that the compressive force is the same in all the directions, so that, the compressing and moulding is isotropically and the obtained material has a homogeneous density.

The results of this method are graphite materials with fine grain, high density and homogenous structure.

- Sigrafine

R6650 and R6710 were provided by Sigrafine. The method of fabrication of this kind of graphite materials was isostatic and vibration moulding. These materials show fine-grain, high purity and high corrosion resistance.

- Carbon Lorraine

Carbon Lorraine was provided by Ferroatlantica.

Table 3. 1. Comparison of typical properties commercial graphite materials

	G330	G347	G348	G530	R6650	R6710	Lorraine
Average grain size (μm)	13	11	8	7	7	3	15
Bulk density (g/cm^3)	1.79	1.85	1.92	1.82	1.84	1.88	1.75
Open porosity % Vol	15	12	8	14	10	10	12
Pore size (μm)	2.2	2.5	-	-	1.1	0.6	-

3.1.2 Coatings on graphite substrates

- B_4C coatings

B_4C^1 coating was made using CVD method, previously there was a study to get homogenous and thicker coatings. This method consists of a wafer, in our case made of boron, is got in touch to volatile precursors in order to react or decompose on the surface of the substrate, producing the desired coating.

- TiO_2 coatings

TiO_2 coatings were made using a sputtering Quorum Q150T ES in spite to use pure titanium as a wafer, a passive layer TiO_2 was formed instantaneously due to the oxygen of the air and the coating thickness was $0.5 \mu\text{m}$ to obtain a homogenous lawyer.

3.1.3 Alumina

Alumina substrates were provided by Magnesita, particularly ALUDUR 96. And the specifications are:

Table 3. 2. Properties of alumina material

Composition	Bulk density (g/cm^3)	Open porosity % Vol
96% Al_2O_3 , 3% SiO_2 and 0.2 Fe_2O_3	3.05	16

¹ B_4C coating was made by the professor Ignacio Jimenez in Science Materials Institute of Madrid (ICMM-CSIC).

3.1.4 C/C Composites

Two kinds of carbon-carbon composites (C/C composites) were provided by Ferroatlantica. Composite 1 is formed by fibers in different directions made of Graphite 3R and composite 2 is made of graphite 2H.

3.2 Characterization and preparation of materials before the experiments

3.2.1 Density

The apparent density is the ratio between the mass of the material and volume of material plus volume closed pores and it was measured with a pycnometer. On the other hand, total density takes into account the volume of material close pores and also open porosity and it was measured by the Archimedes method.

· Pycnometer method:

This method is based on gas displacement techniques and Boyle's law. Helium is used as an inert gas that penetrates into fine pores (up to 2 Angstroms), allowing a very precise measure of the apparent volume (material and closed porosity volume). The model used is Helio Accupyc picnometer. Thanks to this technique the apparent density of the sample can be obtained, because the helium is introduced into all communicating pores but not in the isolated ones.

· Archimedes method

This method measures total porosity and is based on the Archimedes principle. First, the weight of the sample m_1 is measured in air, then is covered by paint m_2 and finally is immersed in ethanol while is also measured the weight $-m_3-$ when displace a certain volume of water.

$$\rho_{\text{total}} = \frac{m_1}{\frac{m_2 - m_3}{\rho_{\text{ethanol}}} - \frac{m_2 - m_1}{\rho_{\text{paint}}}} \quad \text{Equation 3. 1}$$

Being ρ , the density.

3.2.2 Preparation of substrates

The substrates were slices of dimensions 15x15x5 mm while silicon was cut in cubes of 3x3x3 mm. After that, the substrates were grounded and polished in order to get a flat and smooth surface, except for composite materials as these substrates had already a treated

surface. In the case of coated materials, sputtering and CVD methods were applied after polishing.

3.2.3 Rugosity

The rugosity was measured by a contact profilometer Hommel tester t1500. The contact profilometer has a cantilever that is moved in contact with the sample vertically, and also laterally a certain distance. The displacement of the cantilever can be measured and converted into a digital signal, obtaining surface characteristics according to DIN 4768 and ISO 4287/1. The most used parameter is the rugosity arithmetic average R_a , that it is the average height of irregularities on the surface.

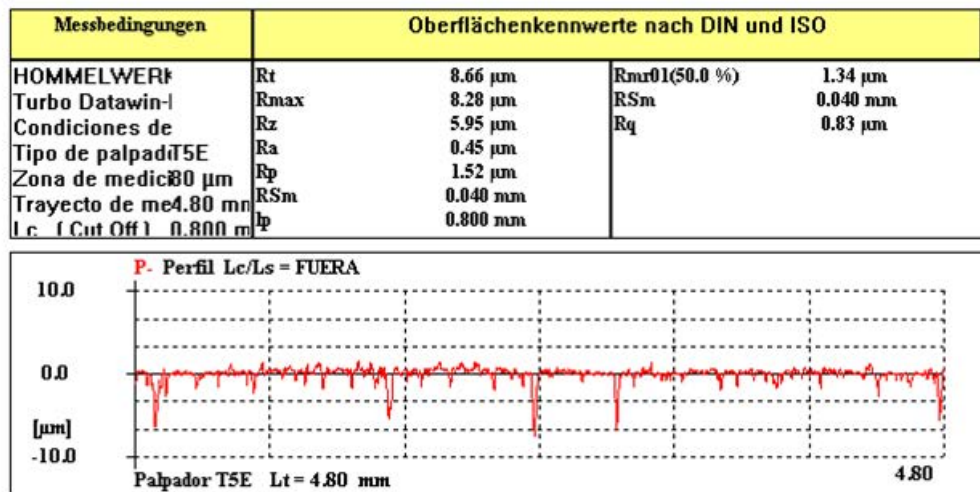


Figure 3. 1. Example of results of rugosity from Hommel tester T1500.

3.2.4 X-ray computed tomography (XCT)

The X-ray computed tomography (XCT)⁵¹ is a non-destructive technique which obtains three dimensional (3D) information about the structures of the samples. The material is placed between an X-ray source and a detector. The intensity of the X-rays which arrives on the detector depends on the absorption coefficient of the studied material and the energy of the incident X-ray. Due to the difference in intensity, the detector can record radiographs. The material is rotated a certain angle and a radiography is taken. This process is repeated

many times until obtaining a full 3D reconstruction of the material where we can distinguish pores, cracks, different chemical phases and elements, etc.

The substrates were analysed in an X-ray computer-assisted 3D nanotomography scanner (Nanotom, Phoenix) to know the size and distribution of the pores. The tomographies were taken from 0° to 360°, every five grades in order to obtain a good 3-d reconstruction. Then, the results were analysed by the softwares FIJI and Avizo.

3.2.5 Raman micro-spectroscopy

Raman micro-spectroscopy system (Renishaw PLC) was used in order to the study of crystallinity. According to Beyssac et al⁴⁴, the crystallinity of carbonaceous materials can be analysed by Raman microspectroscopy, even quantify it. Figure 3. 2 shows typical Raman spectra of carbonaceous material.

The G band indicates the vibrational mode E_{2g} , a material whose peak G is narrow and has high intensity, corresponds with materials with a high grade of crystallinity, while amorphous materials have G peak wide and very low intensity. On the other hand, the D band indicates the structural disorder, for amorphous materials, D1 band has high intensity, D2 is not distinguishable from G band and D3 is a wide band.

In order to quantify the degree of crystallinity, Beyssac et al proposed a ratio $D1/(D1+D2+G)$, the parameter represents the area of the bands. The lower value of this ratio, the higher grade of crystallinity.

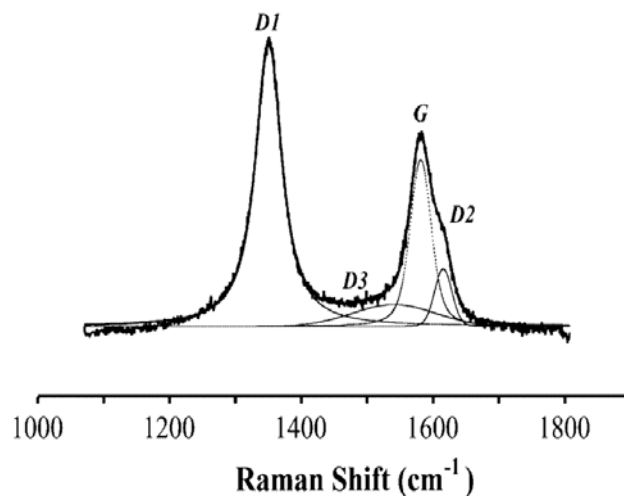


Figure 3. 2. Curve fitting of the first-order region of Raman spectrum

3.3 Wettability and infiltration experiments

3.3.1 Induction Furnace

Induction melting technique was used in order to do wettability and infiltration experiments. This consists of heating the silicon piece on the substrate through a magnetic field generated by the electric current which it is flowing through the coil.

Eddy currents are induced by this magnetic field and allow the heating of the sample. For this reason, the sample must be conductive. This technique reaches high temperatures and depends fundamentally on the power supply. Others advantages are: it is no necessary an external source of heat neither heat conduction, and besides, only the sample is heated. This means energies savings, due to energy used for the heating is exactly what you need, there is no loss of energy to heat up another part of the furnace. However, the sample has to be contained in a crucible. Ceramics are usually used as the crucible, the material is the limiting factor to maximum temperature and heating rate in order to avoid the thermal shock.

The wettability and infiltration experiment were done in a VSG 002 DS from PVA TePla AG. The working conditions were the maximum capacitor, a coil of 80 mm and the power of 3 kW. The crucible chosen was made of graphite from Schunk and to avoid electric arc, the crucible was covered by graphite foam and by an electrical insulating paper. Thermocouples types R from Omega were used to control of the temperature under vacuum or argon. Small silicon pebbles (around 80 mg) were put on the substrates inside of the graphite crucible (see Figure 3. 3). Depending on the experiments different periods of time and atmospheres (vacuum and argon) were used. Particularly under the high vacuum atmosphere, a cover of graphite foam was used because of silicon evaporation.

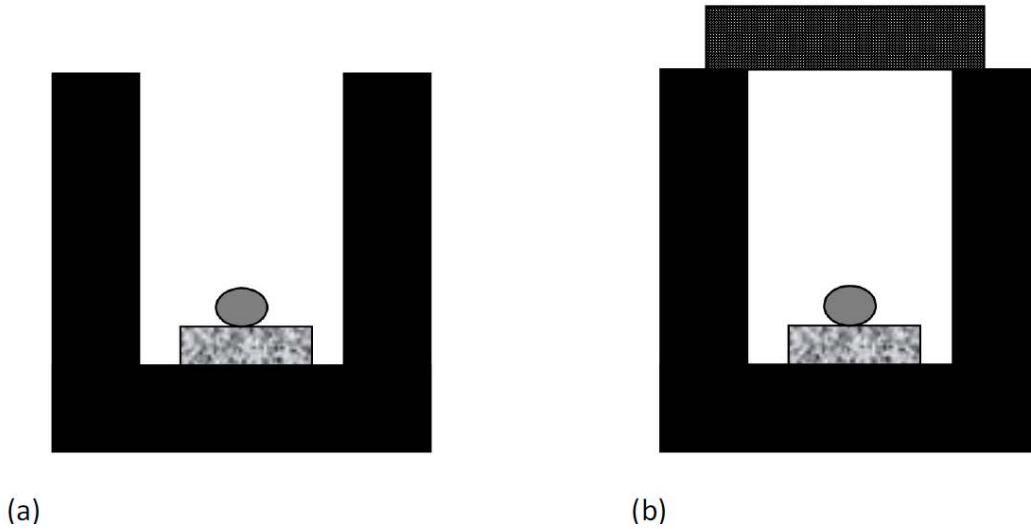


Figure 3. 3 Scheme for argon testing (a) and for vacuum testing (b).

3.3.2 Sessile drop method

The sessile drop test is largely used because the analysis of the wetting behaviour is measured in situ. There are several ways to measure of the contact angle⁵² (see Figure 3. 4)

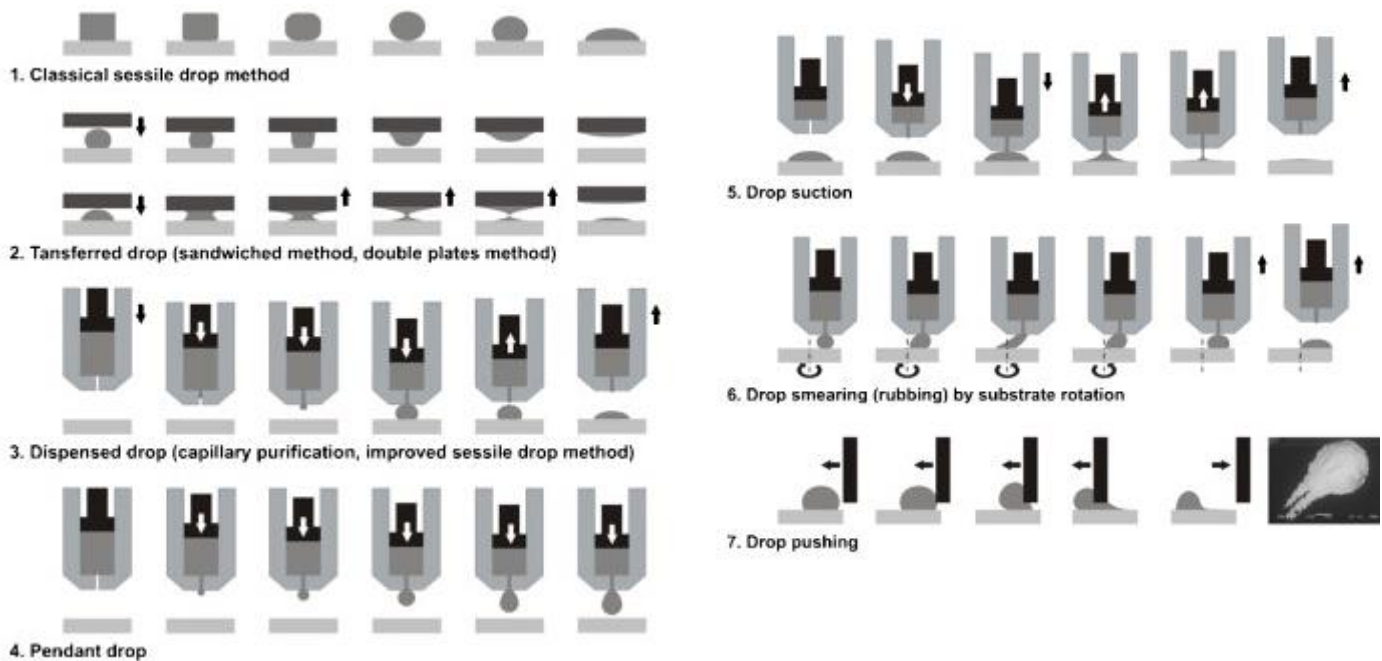


Figure 3. 4. Sessile drop testing methods and procedures⁵².

The most used methods are the classic and the dispensed drop. The classic method consists of melting a piece of the material under study on the substrate, recording the process by a computer and then analyzing it by specific software in order to measure the contact angle and the kinetic rates. In contrast, the dispensed drop consists of melting the silicon inside of a plunger and once, the piece is melted is deposited on the substrate by capillarity. The main advantages of dispensed drop are the drop is free of oxide, the temperature is uniform in whole the drop and the wetting behavior is not affected by the melting³¹.

Wettability and infiltration were measured using sessile drop methods: classic and dispensed drop. The classic sessile drop method consists of melting a Silicon drop (about 80 mg of mass) directly on a substrate while dispensed drop sessile drop method, silicon was melted inside a capillary and then the drop was dispensed on the substrate. In both cases, the experiments were recorded by a high-speed video camera. Then, main parameters such as contact angle, height, and width of the drop are measured by using specific software.

The types of equipment used are:

- DSAHT (Drop Shape Analysis for High Temperatures) Krüss

The equipment² used was DSAHT (Drop Shape Analysis for High Temperatures) Krüss, which is represented in

Figure 3. 5, consist of a tubular furnace with a lighting system and high resolution camera which allow a real time analysis of the drop formation and the spreading of the liquid on the solid surface through the systematic taking of photos. The good control of temperature is due to a thermocouple situated inside of the holder. To avoid oxidation, cycles of vacuum were performed before to introduce argon, that it is the atmosphere used during the experiments.

² Equipment from the Department of Engineering and science Material of university of Carlo III of Madrid

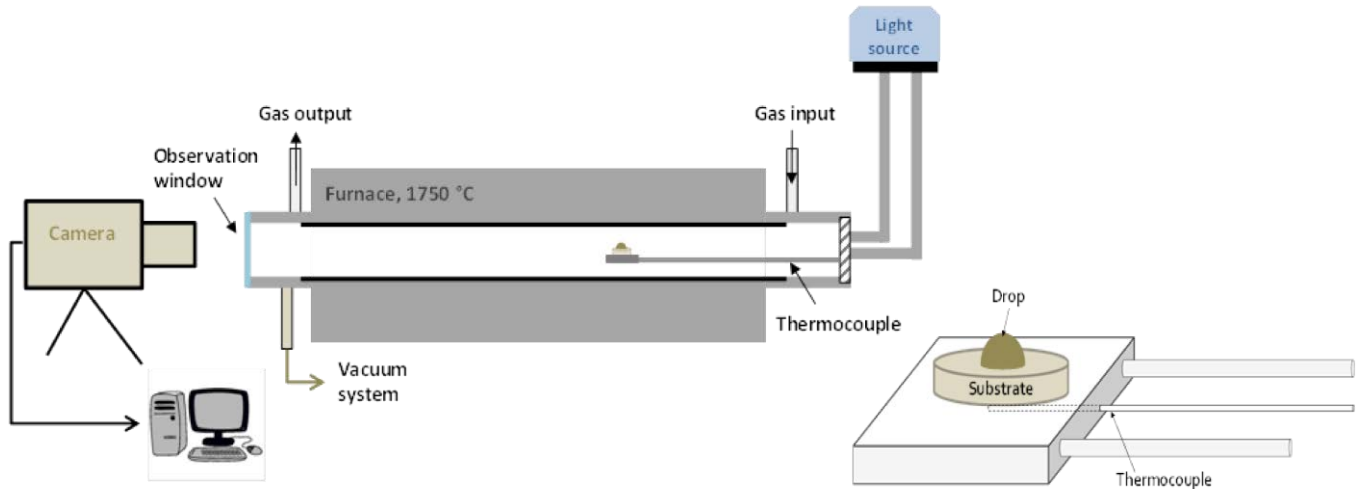


Figure 3. 5. Scheme of the equipment used for wetting and infiltration experiments. A detail of the drop-substrate disposition is adapted from ⁵³.

The images obtained during the test were analyzed by the software Drop Shape Analysis DSA100, which permit analyses of the contact angle and parameter of the drop such as height and width, through mathematical calculations for example Young-Laplace, height method.

- Experimental complex device for investigation of high temperatures

The analysis at high temperature was made in a lab experimental setup³, which consists (see Figure 3. 6) horizontally and rotary with windows in order to record the process through a high-resolution digital camera. Besides, a capillary with vertical movement allows dispensing the drop. The temperature is measured in real time by four thermocouples and the atmosphere is controlled by devices to keep static or flowing gas depending on the level of the pressure⁵².

³ Equipment from the high temperature research group of the foundry research institute of Cracow.

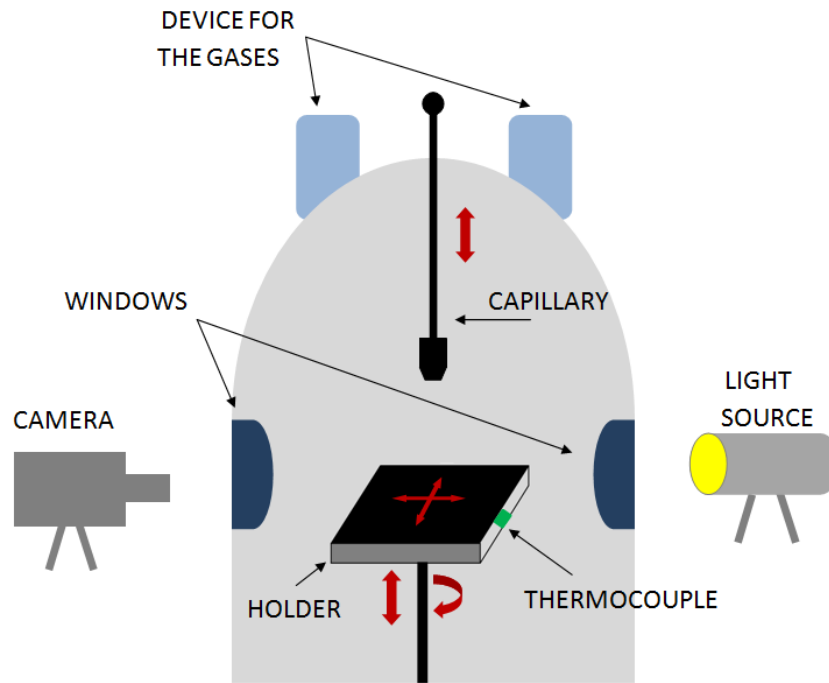


Figure 3. 6 Schematic of the camber of experiment of the experimental complex device.

Classic and dispensed sessile drop methods were made for silicon and several substrates. The images obtained during the test were analysed by the software Matlab, the contact angle and the height and width of the drop were calculated by image analysis through mathematical calculations for example adjustment of the circle and method of the tangent.

3.4 Characterization and analysis after the experiments

The microstructural characterization of top side and cross section of the samples after the experiments was a key point in this dissertation. The reactions of silicon with the substrates surface and pores were analysed by X-ray diffractometion (XRD), Light optical microscopy (LOM), Scanning electron microscopy (SEM) and Energy Dispersive X-ray spectroscopy (EDX), transmission and scanning electron microscopy with the field emission gun (FEG S/TEM).

In order not to modify the surface, firstly, the samples were analysed by X-ray diffractometion (XRD), and then, were prepared for microscopy. The preparation of the samples consisted of cutting them with a wire cutting machine, then the samples were cold-mounted with a resin. After, they were ground by SiC abrasive paper and finally polished with diamond past. It is noteworthy there were parts of the sample very soft as graphite and other really hard as silicon carbide so that the mirror-like surface was not got it in order to avoid loss of the material.

3.4.1 X-ray diffraction (XRD)

X-ray diffraction (XRD) is a technique to characterize the crystalline phases presents on the surface of the samples. X-rays are generated by X-ray tubes, through a focused electron beam which is accelerated by high voltage field. If the lengths of the wave of X-Rays generated are the same order of magnitude as the atomic radios of the target atoms, electrons can diffract the X-Rays beam. The scattered X-rays keep information about the position and type of found atoms. In addition, if the samples show crystalline structures, the collision is elastic and amplified thanks to its periodic distribution. Obtaining a diffraction pattern where the distribution of atoms in the material can be deduced.

In this thesis, the formed phases were examined by a Philips X-ray diffractometer X'Pert⁴ from University Carlos III and an X-ray diffractometer Analytical Empeyrean. In both cases, the work conditions were 40kV/40mA and it was used a copper anode.

⁴ Equipment from the Department of Engineering and science Material of university of Carlo sll of Madrid

3.4.2 Light Optical Microscopy (LOM)

Light optical microscopy was used to do a primary characterization of the sample, to check the symmetry and length of spreading on the top side and the infiltration length in the cross section. The device used was a BX51 optical microscope which is equipped with the software AnalySIS auto where areas and lengths were measured by image processing.

3.4.3 Scanning electron microscopy (SEM) and Energy Dispersive X-ray (EDX)

After a previous characterization with Light Optical Microscopy (LOM), Scanning Electron Microscopy (SEM) was used to obtain higher magnifications and through Energy Dispersive X-ray (EDX), a chemical analysis was made.

SEM consists of using an electron beam to scan the material, obtaining images with better resolution and higher magnification of LOM. The Electron beam is focused and accelerated by a magnetic field, then, the signal emitted by the material becoming in images on different detectors. In fact, the versatility of this technique is due to the possibility to get different information about the material thanks to these detectors. The detectors used in this study were secondary electron (SE) and back-scattered electron (BSE). SE offers information about the topography of the sample while BSE obtains images with high contrast between the different compositions of the materials.

In addition, the atoms of the material, which are excited by the electron beam, emit X-rays with specific energy for each element. The quantity and the energy of X-ray emitted can be measured by the energy dispersive X-ray spectrometer (EDX), obtaining a pattern. Each element has his own pattern, so that, the elements present in the sample can be analyzed and therefore, the composition of the material.

EVO MA 15 scanning electron microscope from Zeiss was used and the working conditions were: 15 to 20 kV as acceleration voltage, 550 μm as spot size and 8mm as working distance. On the other hand, EDS Oxford INCA 350 was used for chemical microanalysis.

3.4.4 Focused ion beam (FIB) and Transmission electron microscopy (TEM)

For a more accurate study of the interface formed by the reaction between silicon and the substrate, a transmission electron microscopy (TEM) was used and a dual beam FIB-SEM device for the preparation of the samples.

The focused ion beam (FIB) is included in certain SEM. As the name indicates, the images are obtained by an ion beam, besides, the FIB is a really good machining tool to scan samples. The source used is Liquid-Metal Ion sources (LMIS) from where the ions are emitted. The ion beam, commonly Ga^+ , is accelerated by a potential difference and focused by electrostatic lenses. FIB can scan or remove material from the sample depending on the current of the ion beam. Low current allows excite the atoms of the material and to emit secondary electrons to obtain the images achieving 5 nm resolution. In contrast, high current allows removing material with high accuracy by sputtering. In this study, FEI Helios Nanolab 600i FIB FEG-SEM dual-beam microscope was used to prepare the sample for Transmission electron microscopy (TEM).

Transmission electron microscopy (TEM) is used for cases a high resolution is needed, such as dislocations, grain boundaries or interfaces. High energy electrons are transmitted through the sample and the formed image are collected in a photographic film, fluorescent screen or a charge-couple device (CCD). Part of the electrons are inelastically scattered, it means, their direction keeps paralleled to the incident beam, but the rest of the electrons, diffracted electrons, collide elastically and change their direction. Thanks to the different modes, useful information is obtained by the modification of the emitted electron beam. For example, diffraction contrast allows distinguishing defects structures due to Bragg scattering. On the other hand, phase contrast or high-resolution transmission electron microscopy (HREM) give information about crystal structure at atomic resolution and also diffraction patterns (DP). For this study, FEG S/TEM microscope Talos F200X, FEI was used.

4. Alumina and carbon composites

The main aim of this thesis was to analyse the behaviour of several types of substrates against molten silicon. This study is focused on wettability, infiltration and reactivity of the interface between molten silicon and the substrates.

In order to clarify, the results of this dissertation are divided into three large blocks depending on the material the substrate is made the of: alumina and carbon composites materials, graphite substrates and coated graphite substrate (B_4C and TiO_2). Figure 4. 1 shows a schema linking which block has been studied with which material and through which techniques were used in order to obtain information about reactivity, wettability and infiltration.

Each large block will be explained in different chapters and then there will be a general discussion in order to obtain global conclusions.

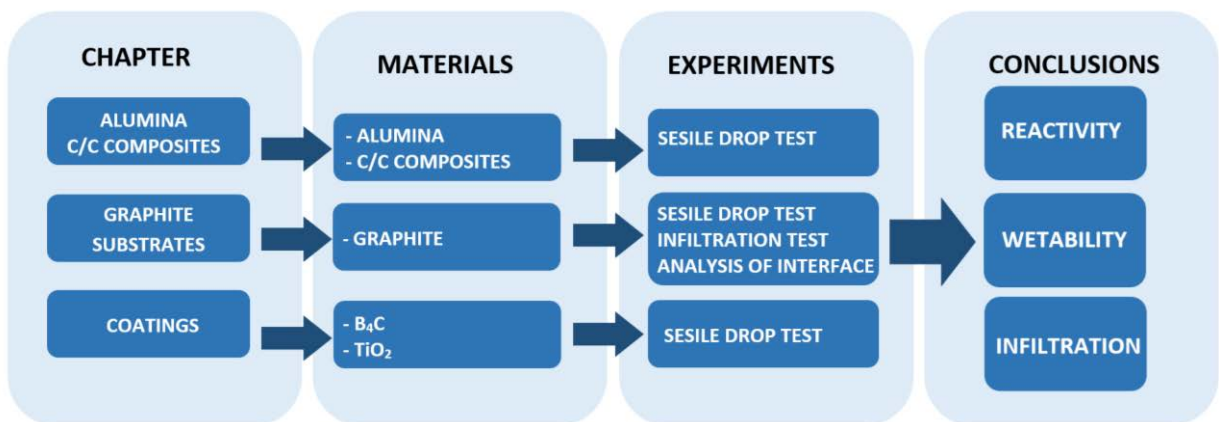


Figure 4. 1. Schematic of the blocks: studied substrates and used techniques.

4.1 Refractory substrates

4.1.1 Substrates characterisation

- Porosity analysis

Open porosity and total density were measured by Archimedes method and the results are shown in Table 4.1. 1

Table 4.1. 1. Density results

Material	Apparent Density	Total Density	Archimedes porosity %	Tomography porosity %	Pore mean size (μm)
Graphite Lorraine	2.07	1.72	17	22.3	9.32
Alumina	4.23	3.07	27.43	27.92	14.66
Composite 1	2.24	1.52	32.33	32.3	26.25
Composite 2	1.72	1.38	19.51	23.89	11.62

Every material has open porosity and the maximum is in composite 1 and the minimum in graphite. Similarly, composite 1 has the largest pore mean size meanwhile graphite substrate shows the smallest.

Porosity has been also measured by image analysis and the results are rather similar to results of the Archimedes method. The difference can be due to the error of each method.

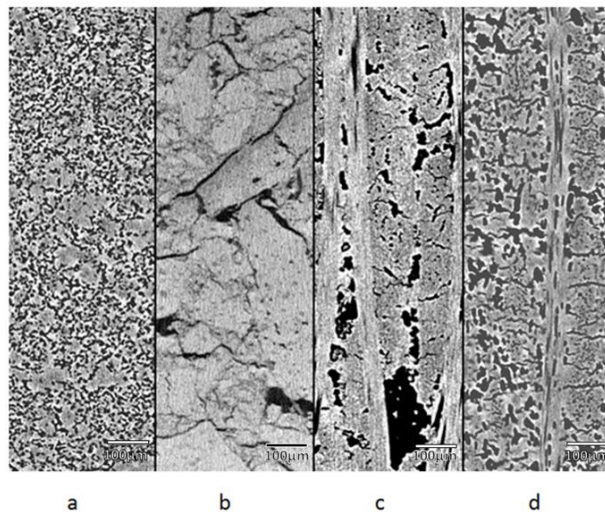


Figure 4.1. 1 Image of the distribution of pores in different materials, being a), b), c) and d) graphite, alumina, composite 1 and composite 3, respectively.

In addition, the distribution of pores obtained by tomography is shown in Figure 4.1. 1. Regarding the distribution, porosity in the graphite is distributed homogeneously throughout the material. However, in the case of alumina, mostly the porosity has been found at the grain boundaries. On the other hand, the distribution of porosity in composite materials depends on the packing direction of the fibers.

- **Crystallinity analysis**

According to Beyssac et al, the crystallinity of carbonaceous substrate can be analysed and also quantified by Raman microspectroscopy⁴⁴, through the ratio $D1/(D1+D2+G)$, where the parameters represent the area of the bands, being the G band indicates the vibrational mode E_{2g} and the D bands indicate the structural disorder.

Table 4.1. 2 Ratio to quantify the grade of crystallinity

	Graphite	Composite 1	Composite 2
$D1/(D1+D2+G)$	0.36	0.55	0.39

The lower value of this ratio, the higher grade of crystallinity. As a result, Composite 1 shows less crystallinity than graphite and composite 2.

- **Rugosity analysis**

The results of average rugosity (R_a) are shown in Table 4.1. 3

Table 4.1. 3. Values of average rugosity

	Graphite	Alumina	Composite 1	Composite 2
R_a (μm)	4.83	3.29	4.48	7.02

Composite 2 has the highest value of average rugosity in the meantime alumina has the lowest. These values are affected by the open porosity which increases the average rugosity.

4.1.2 Image observation Sessile drop test

Figure 4.1. 2 shows images captured during the sessile drop tests. The images of the most relevant moments were isolated from the video sequence recorded.

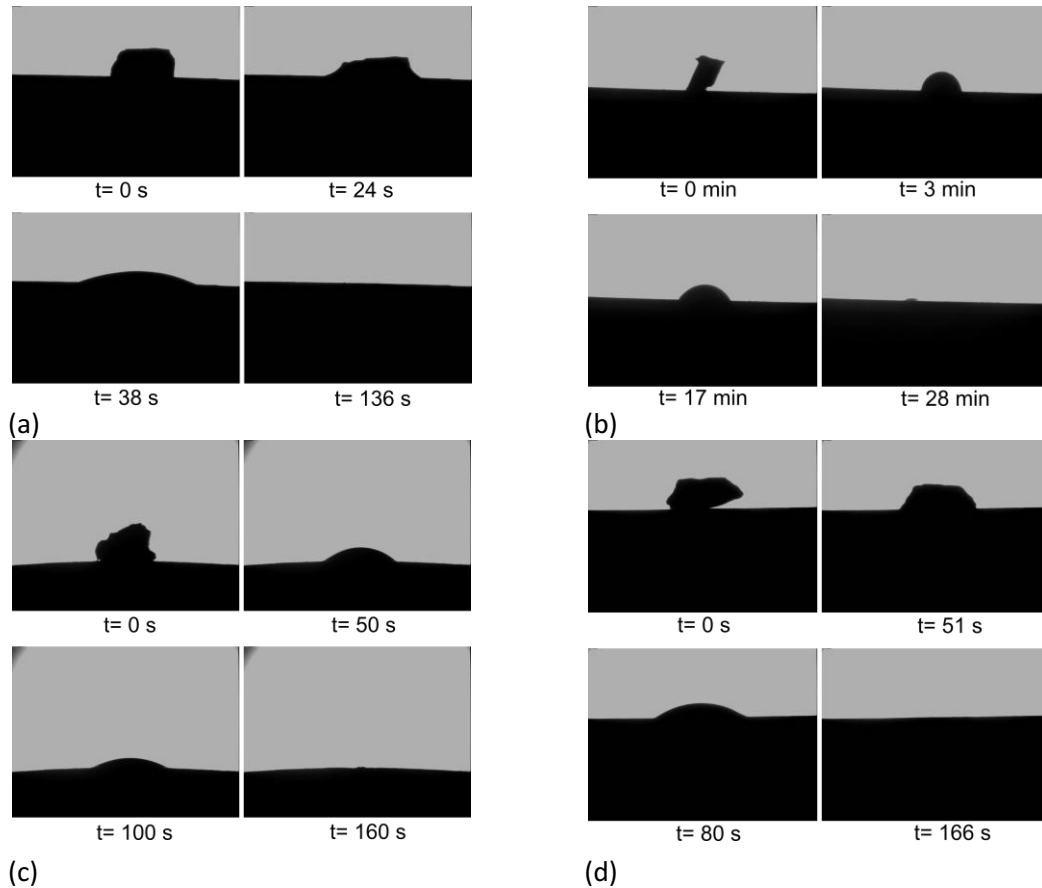


Figure 4.1. 2. Images of sessile drop test, a) on graphite, b) on alumina c) on composite 1 and d) on composite 2.

Silicon melting starts at the bottom of the sample, that is the area in contact with the substrates. We considered the silicon is totally molten when the drop is formed. Then, the contact angle decreased because of the spreading and the infiltration and finally, silicon is completely infiltrated into the substrate (Figure 4.1. 2). For carbonaceous substrates, the silicon drop infiltrates into the substrate completely in less than three minutes. However, in the case of alumina, it can be seen that unlike other materials, the spreading is only slight and the infiltration is completed only after twenty minutes.

Silicon was melted on four substrates (graphite, alumina and two types of composite) under an argon atmosphere using the sessile drop test. The variation in the contact angle and the parameters of the molten silicon drop (height and width) with the time is shown In Figure 4.1. 3. The initial time correspond when the piece of silicon started to melt.

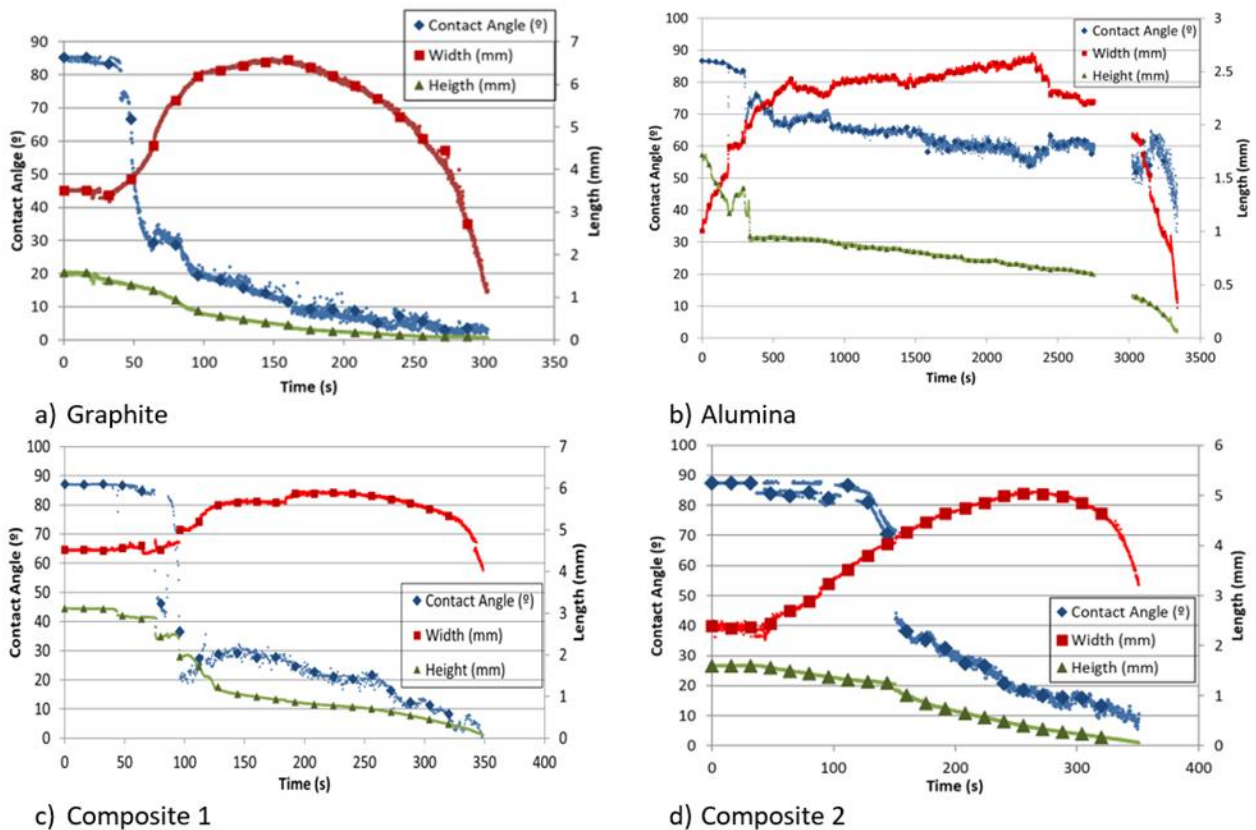
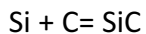


Figure 4.1. 3. Contact angle and parameters of silicon drop with time of graphite, alumina and composite 1 and 2 substrates.

In Figure 4.1. 3.a is the case of the graphite substrate. The decrease in contact angle and height of the drop with the time are linear, likewise, the increase in width with time tends to linear until it reached the maximum. This linear tendency agrees with the previous researches which have shown that wettability, spreading and infiltration were managed by the reaction between silicon and graphite.



Equation 16

The initial contact angle obtained was 85.2 then there was a drop until 23.6° at 1424°C. There is a scatter of results in the literature^{14,12,15,1,8}, and our results are in agreement with the fact that the silicon does not wet the substrate at the beginning, but once the silicon carbide layer is formed, the contact angle corresponds to the system silicon-silicon carbide²¹.

The behaviour of the molten silicon on the alumina is likely dependent on the formation of a passive layer of SiO₂ on the interface silicon-alumina. Spreading and infiltration on Alumina can be divided into several stages (Figure 4.1. 3.b). During the formation and stabilization of the drop the contact angle and the height suffers a high drop while the width increases significantly. Next, there is a change of slope in the contact angle and width whereas the height remains almost constant. This behaviour can be related to the formation of the passive layer. Then, the contact angle and the height almost linearly decrease, whereas, the width increase until a maximum, indicating, the passive layer starts to break. Once it has totally been removed, all parameters dramatically decrease until the drop disappears through infiltration.

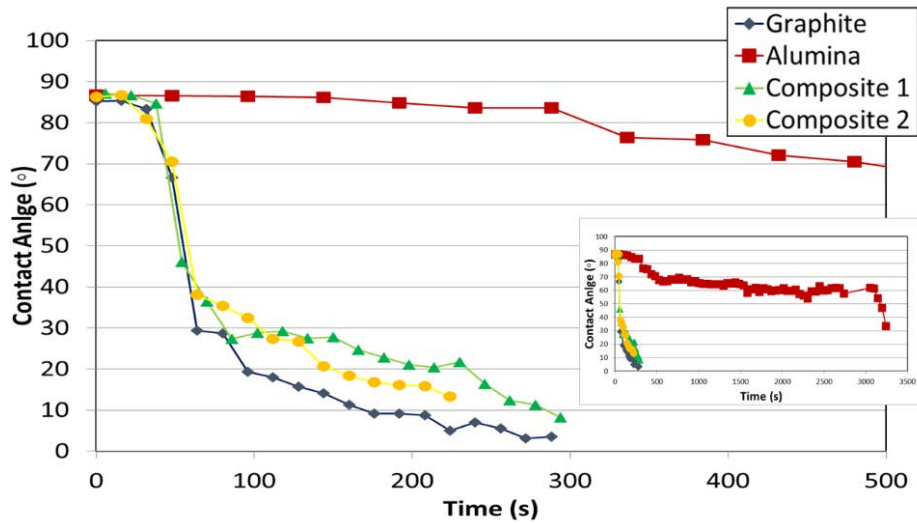
The initial contact angle obtained was 86.2° at 1424°C. According to references Yuan et al²⁷, this result is totally in agreement (86° at 1422°C under an argon atmosphere). Besides in comparison with the other substrates, spreading was minimum and infiltration was slower. However, the silicon infiltrated the whole substrate due to the high porosity of alumina. The good behaviour shown against molten silicon can be due to the possible formation of the above mentioned passive layer of SiO₂, nevertheless, the infiltration was dramatically fast once the layer was broken.

Composite 1 results are shown in the Figure 4.1. 3.c. Because of high variation in the data of contact angle and width, a moving average filter was applied. There is a drop in contact angle and the height while there is a rise in wettability for the melting of the silicon. Once the drop is formed and stabilized, the width remains almost constant, while contact angle and height show a linear decrease possibly due to the high rugosity. Once the width reaches the maximum, all parameters decrease changing the slope remarkably. The initial contact angle obtained was 85.07, and after the Si melting, 27.9° at 1425°C.

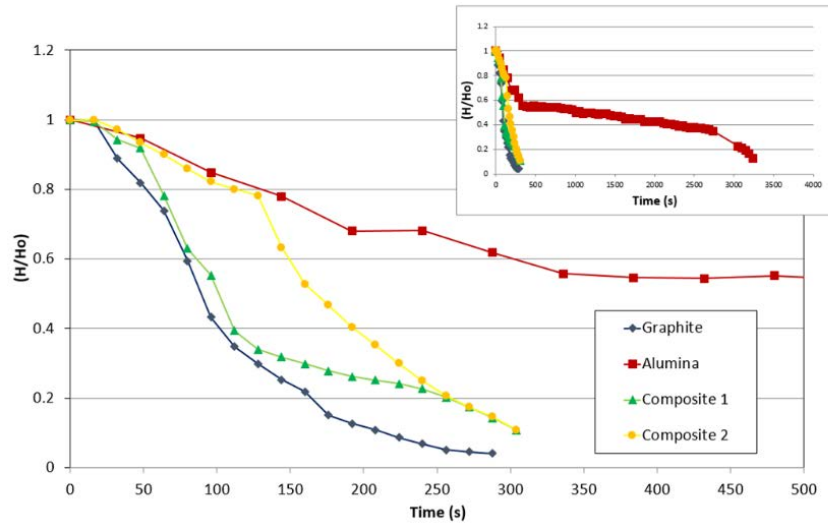
On the other hand, Figure 4.1. 3.d presents the results of composite 2. In similar way to graphite, once the drop is formed, the width linearly increases while the height and contact angle linearly decrease. The spreading could be driven by the chemical reaction between Si and C, described by equation 1. The initial contact angle obtained was 84.42 then there was a drop until 43.8° at 1422°C.

- **Analysis of the drop parameters**

The variation of contact angle and the variation of the relative height (mm/mm) of the different substrate (graphite, alumina and composites) with time are compared in Figure 4.1. 4:



(a)



(b)

Figure 4.1. 4. Comparison of variation of a. contact angle and b. relative drop height (mm/mm) of substrate with the time.

Figure 4.1. 4. a compares the variation of the contact angle of all studied materials with the time. In the beginning, silicon does not wet any substrates because the values are close to 90° . Then, the values of the contact angle of carbonaceous substrates decrease sharply in less than 3 minutes due to the formation of SiC layer. In contrast the reduction of the contact angle for Alumina is in 28 min. Thus, the wettability of silicon on alumina is much lower than on the other materials due to a passive layer that is finally removed.

When the drop is formed, the contact angles were: 23.6 for graphite, 86.2 for alumina, 27.69 for composite 1 and 43.8 for composite 2. Despite the properties difference in the carbonaceous substrates shown very similar behaviour. First of all, the contact angle remains almost constant. Then, there is a high drop, and finally, it keeps decreasing linearly but slower than before.

Figure 4.1.4.b shows the variation of the relative height (mm/mm) of different substrates with the time. The height was divided by the initial height in order to obtain relative values which are comparable.

As in the case of wettability, infiltration in alumina was much slower than in the other materials. However, silicon infiltrated entirely in alumina and, in addition, the infiltration was faster with the increment of time.

On the other hand, the relative drop height of graphite and the composite 1 decreases highly at the beginning while in the case of composite 2, this parameter decreases only slightly. Then, there is a change of the slope in every material: the values for composite 2 drop faster than in the cases of graphite and composite 1 substrates.

Table 4.1. 4. Spreading and infiltration rate measured on several substrates in the different stages.

	Graphite	Alumina			Composite 1	Composite 2
		Stage 1	Stage 2	Stage 3		
U _{spr} (mm/s)	0.012	0.0018	0.00007	0.0016	0.012	0.010

Spreading rate U_{spr} were calculated for different substrates (Table 4.1. 4). For carbonaceous substrates, the values are very similar and close to 0.010 mm/s. Besides, they showed a linear tendency in the variation of drop width with the time, showing the dependency on the chemical reaction at the triple line.

In the case of alumina, the kinetics were measured in each stage, the values of the spreading rate are significantly lower than the carbonaceous materials. It is remarkable that the stages 1 and 3 showed one order and stage 2 two orders of magnitude smaller than carbonaceous materials. These results support the formation and subsequent breakage of a passive layer of SiO_2 .

- **Optical microscopy analysis of Sessile drop samples**

Top view images were taken by an optical microscope (Figure 4.1. 5a) after sessile drop test, then the substrates were cut and cross section images were also taken (Figure 4.1. 5.b). The exception was composite 1 where scanning electron microscope was used. On the other

hand, infiltration distance and effective radius R , calculated from wetted area A ($A=\pi R^2$), were measured by image processing for each material.

On the wetted area can be observed two concentric circles on carbonaceous substrates. The smallest one match with the area of maximum infiltration distance, while the biggest one with the diffusivity of silicon. The lack of symmetry in the circles indicates that the drop was pinned by some defect, hindering the formation of SiC layer but increasing the diffusivity of silicon in certain directions.

Conversely, in alumina, there is a single circle and the silicon has infiltrated the whole substrate. The spreading was hindered by grain boundaries, boosting the infiltration.

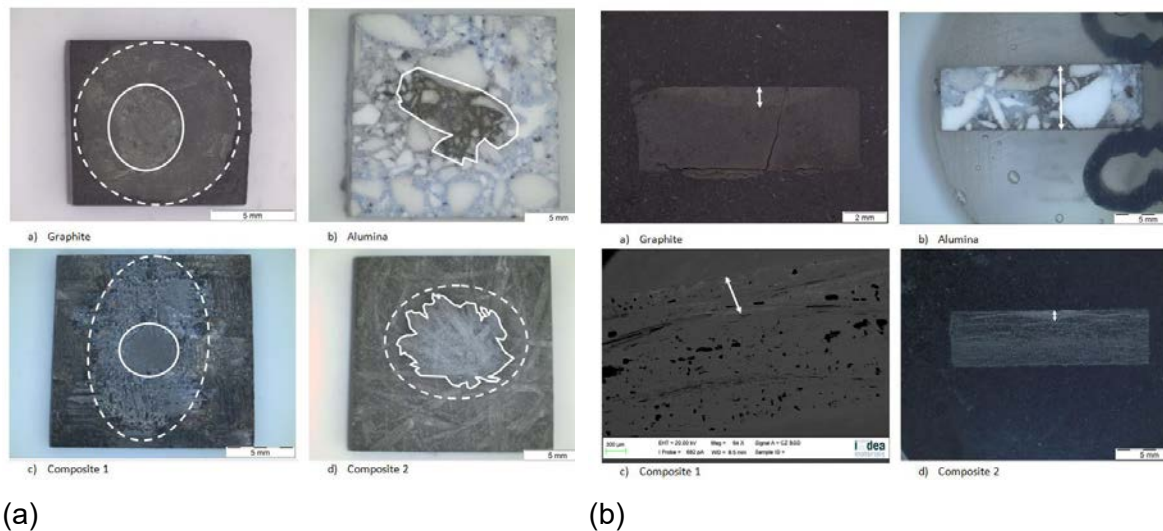


Figure 4.1. 5. a. Top view and b. cross section images of substrates after sessile drop test.

Figure 4.1. 5 provides the values of internal and external radius, the infiltration distance and the condition of the experiments. Besides, the maximum radius was measured in situ by the sessile drop method and it is also included. In addition to the infiltration rate is calculated by $U_{inf} = h_f^*/t_{inf}$ suggested by Voytovych et al²⁹, being h_f^* the maximum infiltration distance measured in the micrographs.

According to Table 4.1. 5, the values of maximum radius disagrees with the external radius. This fact could be due to the fact that the drop is not symmetric, thus, the size of the radius depends on the direction where it was recorded. Furthermore, other cause could be secondary wetting¹, related to the diffusion of silicon.

Regarding the infiltration, composite 1 is pointed out because the infiltration distance is minimum despite its high grade of porosity. However, the spreading is maximum. Its high rugosity and low grade of crystallinity boost the spreading but hinder the infiltration. However, the infiltration distance in the Alumina is maximum because of the high grade of porosity and because of the minimum spreading.

Analysing the kinetics of carbonaceous materials, the values of the spreading rates are significantly higher than the infiltration rates. Meanwhile, for alumina, the infiltration rate is higher than spreading. Although regarding the curves, the drop of the height of the drop indicates the spreading rate is not continuous, in the end, the value should be higher than at the beginning. These results support the formation and subsequent breakage of a passive layer of SiO₂.

Table 4.1. 5. Infiltration and spreading rates, values of effective radius and maximum infiltrated length according properties of graphite and work condition

	Graphite	Alumina	Composite 1	Composite 2
Internal Radius(mm)	1.85	--	1.81	2.10
External radius (r_{eff}) (mm)	3.53	3.87	5.73	4.85
Maximum radio (mm)	3.684	1.39	4.16	3.46
Infiltration (h_{total}) (mm)	0.98	5.02	0.64	0.82
Temperature	1424°C			
Atmosphere	Argon			
Ra (μ m)	4.83	3.29	4.48	7.02
Porosity	22.3%	27.92%	32.3 %	23.89%
Av pore diameter (μ m)	9.32	14.66	26.25	11.62
Uinf (mm/s)	0.004	0.0015	0.002	0.003
Uspr (mm/s)	0.012	0.00007	0.012	0.010
Uinf/Uspr	0.33	21.4	0.17	0.30

- **SEM analysis of the Sessile drop samples**

The samples were analysed by scanning electron microscope (SEM) equipped with energy dispersive X-ray spectroscopy (EDX). Besides, a compositional study was realised on the surface and cross section by X-ray diffractometion (XRD).

From the results in Figure 4.1. 7, it is apparent that the silicon reacts with the graphite during the spreading and infiltration, forming silicon carbide while a large quantity of unreacted silicon is not found. On the other hand, in the Figure 4.1. 6.a, it can be highlighted that the graphite shows pores almost closed. Figure 4.1. 6. B illustrates the micrographs of alumina after sessile drop test where silicon has infiltrated inside of the cracks of the alumina. Although the oxygen could have been able to pollute the silicon, the XRD did not reveal the formation of silicon oxide (Figure 4.1. 8).

As in the case of graphite, the micrographs of composite 1 after sessile drop test are shown where silicon has infiltrated between and has reacted with the carbon of fibres Figure 4.1. 6.c. According to Figure 4.1. 9, Silicon carbide has been formed but there is no unreacted silicon. In other words, that the reaction in the triple line is a key factor despite the rugosity.

Figure 4.1. 6.d exhibits the micrographs of composite 2, Silicon has infiltrated through the porosity of composite 2 and reacted with carbide, but unreacted silicon has been found on the surface (Figure 4.1. 10). This agrees with Novakovic⁵⁴, the 10% of silicon remains unreacted when Si/C composites are obtained by the infiltration method.

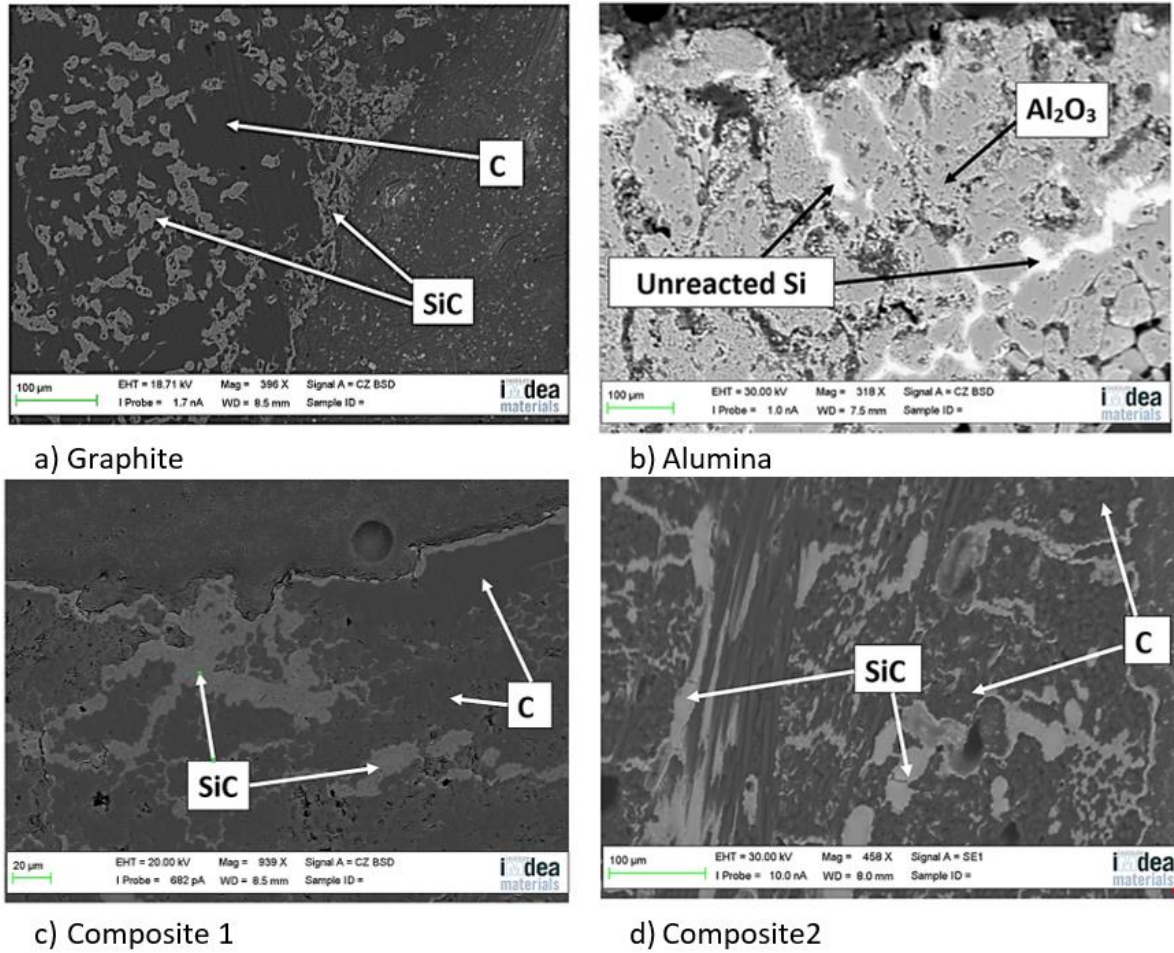


Figure 4.1. 6. Micrographs of a. Graphite, b. Alumina, c. Composite 1 and d. Composite 2 after sessile drop test

- X-Ray analysis of the Sessile drop samples

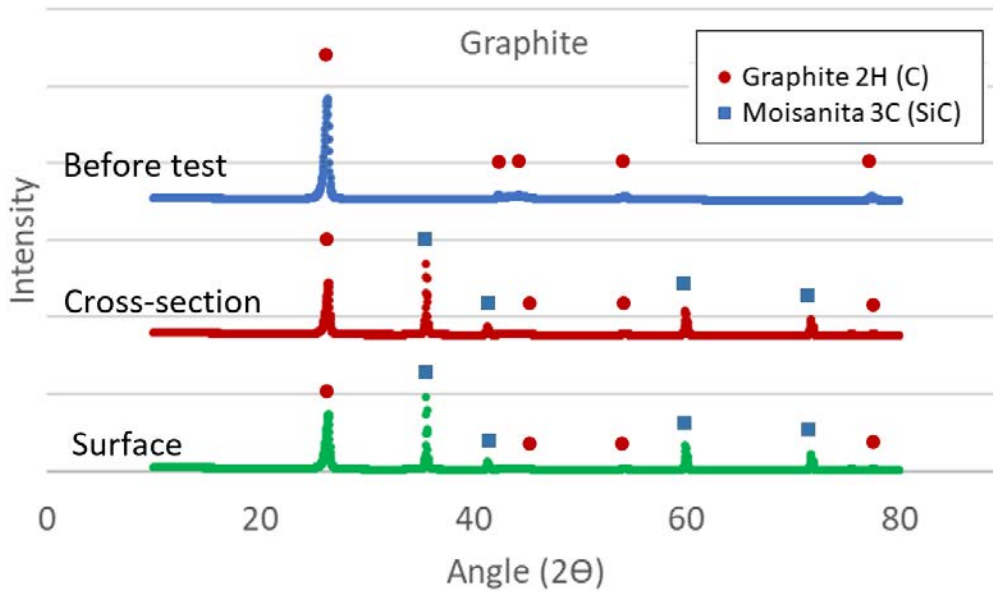


Figure 4.1. 7. . X- ray results of graphite before and after sessile drop test (cross section and surface).

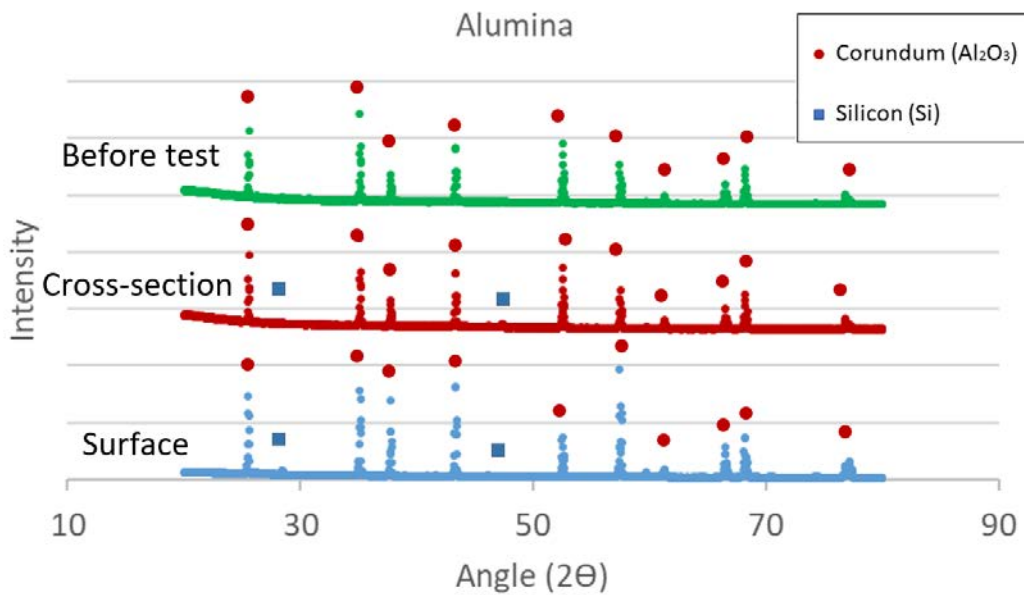


Figure 4.1. 8. X- ray results of alumina before and after sessile drop test (cross section and surface).

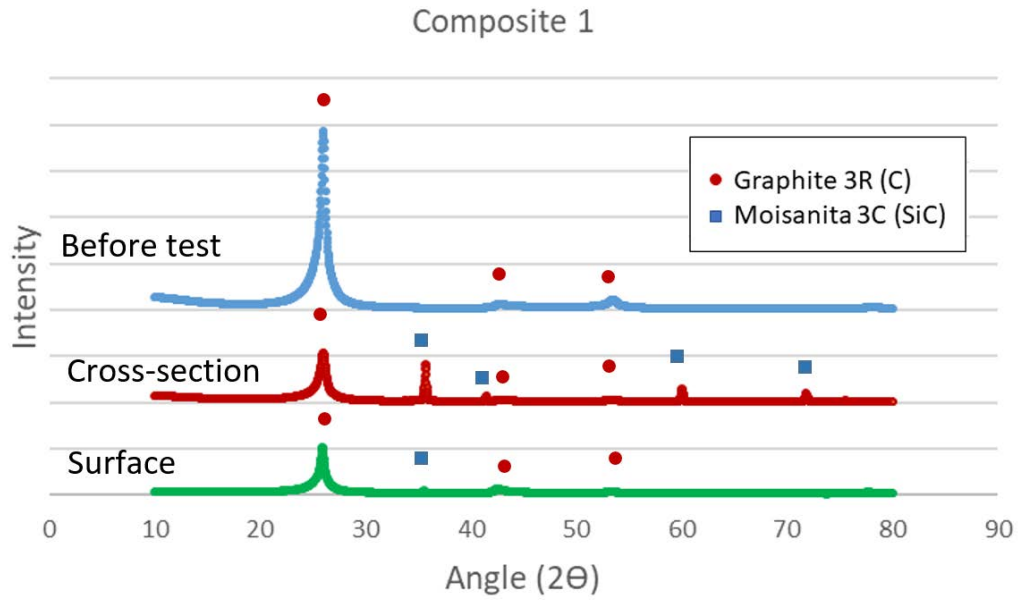


Figure 4.1. 9. . X-ray results of composite 1 before and after sessile drop test (cross section and surface).

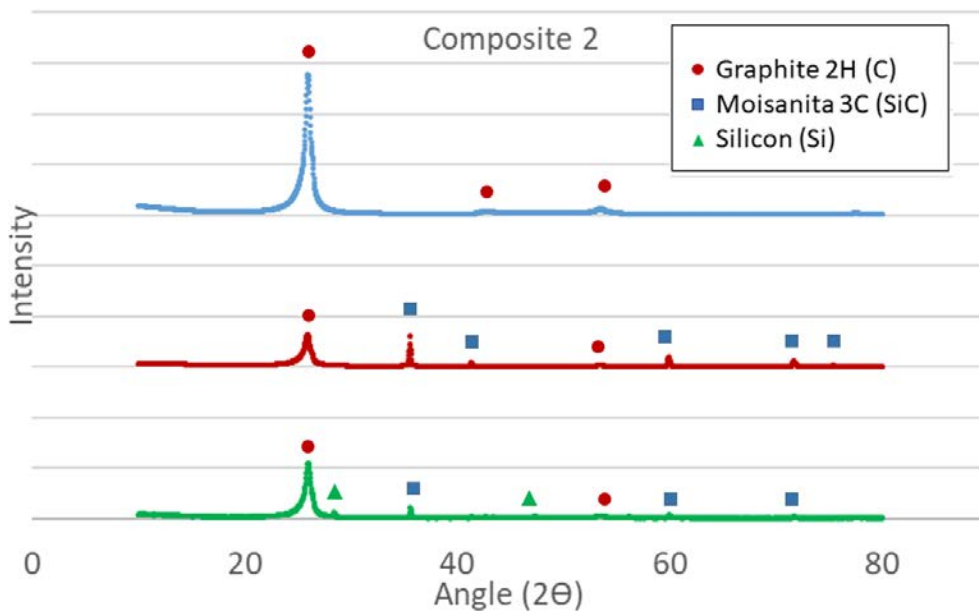


Figure 4.1. 10. X-ray results of composite 2 before and after sessile drop test (cross section and surface).

4.1.3 Discussion

Table 4.1. 6. Values of silicon-graphite substrate, silicon-composite 1 and silicon-composite2.

	Graphite	Composite 1	Composite 2
% Porosity	23.3	32.3	23.89
Grade of crystallinity	0.36	0.55	0.39
Ra (μm)	4.83	3.29	7.02
Maximum distance infiltrate	0.98	0.64	0.82
Average pore size	9.32	26.25	11.62
Uinf ($\mu\text{m/s}$)	8	11	7
Uspr ($\mu\text{m/s}$)	12	12	10
Initial Contact Angle	23.6 $^{\circ}$	27.69 $^{\circ}$	43.8 $^{\circ}$
Uinf/Uspr	0.33	0.17	0.30

Previous studies have reported that the phenomenon of infiltration and spreading happens when the silicon starts to melt, and are managed by the reaction between silicon and graphite (equation 1)^{8,10-12}.



It can be observed for the case of graphite, that the phenomena of infiltration and the spreading are managed by the reaction between silicon and carbon at the triple line. However, in the cases of the composites, it is more complicated to reach this conclusion. According to Drevet et al²¹, the initial contact angle of silicon on graphite is around 90 $^{\circ}$, which correspond to Si-C wetting, the contact angles initially obtained 85 $^{\circ}$, then while the drop is formed, the contact angle sharply decreased until 20 $^{\circ}$ -40 $^{\circ}$ corresponding to Si-SiC layer wetting. Finally, the wetting is perfect in every substrate, this means that contact angle is almost zero. There is a scatter of results in the literature (Table 4.1. 7)^{14,12,15,1,8}, and our results agree in the sense that the silicon does not wet on the substrate at the beginning, but once the silicon carbide layer is formed, the contact angle corresponds to the system

silicon-silicon carbide²¹. The variation in the contact angle values can be due to the fact that the test conditions are not the same (rugosity, temperature, atmosphere), but the high porosity is the most remarkable difference.

Regarding the rugosity, Composite 2 had the maximum value and at the same time, the highest initial value. This seems to be in disagreement with Li and Hausner¹⁴, whose results showed that the contact angle was smaller due to the high rugosity. However, in our case, the big holes affected the calculated average rugosity (Ra).

Table 4.1. 7.Values of contact angle according properties of graphite

Authors	Li and Hausner¹⁴	and Dezellus¹²	Whalen and Anderson¹⁵	Ciftja¹	Israel⁸
Initial cont. angle (°)	~18	~48	146	25-30	~100 ~95 ~90
Final cont. angle (°)	3	35	35-40	5-15	0 ~30 ~12
Temperature (°C)	1430	1430	1502	1600	1460
Atmosphere	Argon	Vacuum	Vacuum	Argon	Argon
Ra (µm)	3.18	0.005	0.002- 0.004	1.27	0.09 0.77
Silicon mass (mg)	60			10-50	
Porosity (%)				18	15
Av pore diameter (µm)				2.5	2.3

According to Caccia et al, the system which shows linear spreading curves and has low values of spreading rate (U_{spr} (dR/dt) $\sim 10\mu\text{m}$) is managed by the reaction at the triple line. Besides they concluded that the value of the infiltration rate and the spreading rate have to be similar, so that $U_{inf}/U_{spr} = (0.65-0.95)^{17}$. Regarding our results, every material had a rate of around $10\mu\text{m}$ and a linear tendency, but the relation spreading with time was not totally linear, particularly in composite 1. Thus, the spreading and infiltration were affected by the rugosity. Moreover, the values of infiltration rate were significantly smaller than the spreading rate.

According to Eustathopoulos et al¹³, the spreading and infiltration kinetics are both controlled by the reaction in the triple line, so that the values of the kinetics should be similar. However, the infiltration is hindered by the porosity. Thus, the infiltration rate is equal to infiltration spreading divided by the tortuosity factor, ξ .

$$\frac{dh}{dt} = \frac{dR/dt}{\xi}$$

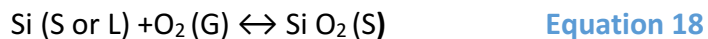
The tortuosity is defined as the ratio between the way chosen by a fluid lying inside a porous body and the geometrical distance between two points⁸. Besides, they related the tortuosity factor with the inverse of porosity of the substrate. Composite 2 and graphite substrate showed a similar tortuosity regarding kinetics rate, and they also had a similar percentage of porosity (Table 4.1. 6). Thereby, a qualitative relation was founded but not quantitative. Except in the case of composite 1, the infiltration rate is minimum but the percentage of porosity is higher than other carbonaceous materials. These differences can be due to the high rugosity which boosted the spreading or the presence of oxide which hindered the infiltration.

Regarding the top and side view of carbonaceous substrates, the results suggest that the more the silicon spreads, the fewer substrates will be infiltrated, independently of rugosity, porosity or average pore diameter. Israel *et al.*⁸ affirm that the infiltration ends when the pores are closed. In our case, the pores are big so that silicon infiltrated thoroughly and then the pores were closed only after infiltration. Thanks to that, silicon reacted totally. On the micrographs, unreacted silicon was not found, these results are remarkable for the method of the ceramics fabrication of reaction bonded silicon carbide (RBSC), because it is often found unreacted silicon after this process¹⁸.

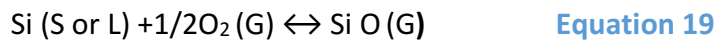
On the other hand, SEM and X-ray analysis reveal a silicon carbide layer on the surface of the graphite and closed pores for the cases of graphite and composite1 substrates. Besides, there are not significant impurities in the composites. However, X-ray results show unreacted silicon on the surface in composite 2 and, according to Novakovic et al⁵⁴, the 10% of silicon does not react when Si/C composites are obtained by the infiltration method.

In spite of that differences between the graphite, composite 1 and composite 2 substrates are managed by the reaction in the triple line. In the case of composite 1, the different directions of the fibres boosted the spreading and hindered the infiltration and the reaction in the triple line. On the other hand, the X-ray results reveal, in all the case silicon, carbide layer has been formed. Thus, the spreading and infiltration was controlled by the SiC reaction and were affected by the rugosity.

The behavior of silicon on the alumina substrate was completely different. This system is governed by the formation and the breakage of a passive layer of SiO₂. According to Drevet et al²¹, molten silicon can dissolve the oxygen of alumina, and after the saturation, precipitate as SiO₂. The SiO₂ forms a passive layer which avoids the infiltration.



However, the breakage of the passive layer is possible because of the molten silicon can dissolve the oxides following equation 3:



Thanks to the flowing argon presence, the oxides can be evacuated. At the same time, the same process happens on the wall of the pores of alumina. First of all, a passive layer is formed on the wall of the pores and the infiltration was hindered, but when the passive layer was eliminated the infiltration started. Infiltration depends on the evacuation of the oxides. In addition, the spontaneous infiltration only takes place if the liquid wet the substrate, in fact, for contact angle less than 60°²³. The lower values of the kinetic and also the change in the curves, hence, the increase of the kinetics with the time agrees in the fact the process is likely managed by the deoxidation of SiO. The initial contact angle calculated in this study agrees with the literature²¹. The corrosion rings reported for other authors^{25,26} are not found in this analysis. This material is not used in the solar silicon industry due to the pollution of silicon.

CONCLUSIONS

The behaviour of several substrates (graphite, carbon composites and high purity alumina) against melted silicon was studied by classic Sessile drop method⁴⁵. The most important phenomena, wettability and infiltration, were analysed and compared with the properties of the substrates (porosity, rugosity, crystallinity).

According to the obtained results, the reaction of the triple line silicon-graphite-atmosphere manages the infiltration and wetting phenomena. This is showed by the linear variation of contact angle and parameters of silicon drop with the time in the substrates: Graphite, composite 1 and Composite 2. However, the graphics of composite 1 indicate that the reaction has been hindered by the rugosity.

Also, the crystallinity has influenced on the wettability and infiltration^{18,24}. In this study, the amorphous material showed worse infiltration and wettability.

In the case of Alumina, due to the presence of oxygen, a passive layer is formed and subsequently eliminated by chemical reactions silicon-oxygen^{17,45}, delaying the processes.

Regarding the contact angle and infiltration behaviour, Alumina is the best material against molten silicon. However, regarding the reactivity, silicon was contaminated so that this material is not recommended for solar silicon application. However, composite 2 is compatible with the application as it shows a high initial contact angle, good behaviour in spreading and infiltration in comparison with the other materials and also contains unreacted silicon at the surface.

5. Graphite substrates

5.1 Graphite from Tokai Carbon Co, LTD

In order to analyse the behaviour of the molten silicon against several graphite substrates, four commercial graphite substrates were chosen from the same company. Firstly, the substrates were characterized and prepared to execute the experiments. Then, Sessile drop and induction furnace tests were done, and finally, the microstructural and chemical characterization was realised.

5.1.1 Characterisation of material

The characterization and preparation of the substrates is a key factor in this dissertation, due to the fact that the aim of the study is to know the influence of these parameters in the behaviour of molten silicon against several substrates.

- **Porosity analysis**

Open porosity and total density were measured by Archimedes method. Besides, the percentage of porosity and the pore mean size were calculated by X-ray tomography analysis and the results are shown in Table 5.1. 1. and Figures 5.1.1 and 5.1.2.

Table 5.1. 1 Density results

Material	Apparent Density	Total Density	Archimedes porosity %	Tomography porosity %	Pore mean size (µm)
G330	1.93	1.71	11.41	22%	10.29
G347	2.08	1.77	15.16	14%	7.48
G348	2.16	1.83	15.19	11%	9.02
G530	2.12	1.75	17.47	23%	11.69

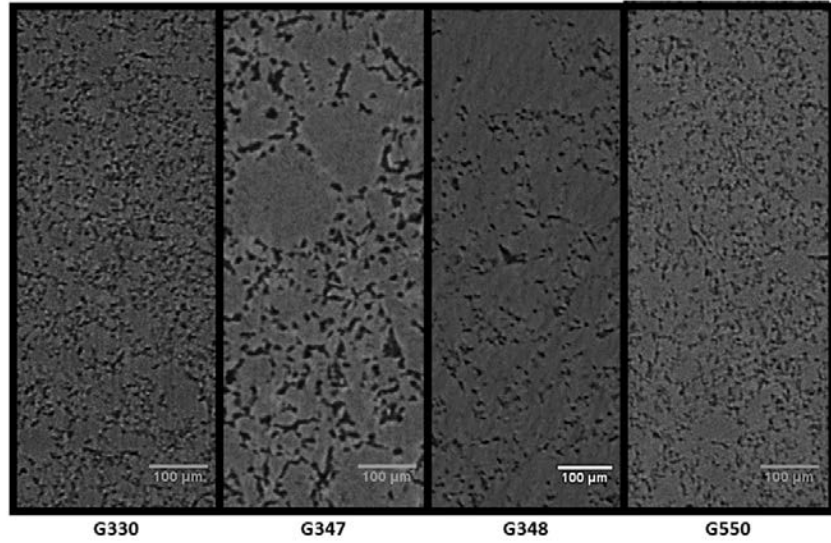


Figure 5.1. 1. Image of the distribution of pores in different graphite, being a) G330, b) G347, c) G348 and d) G550.

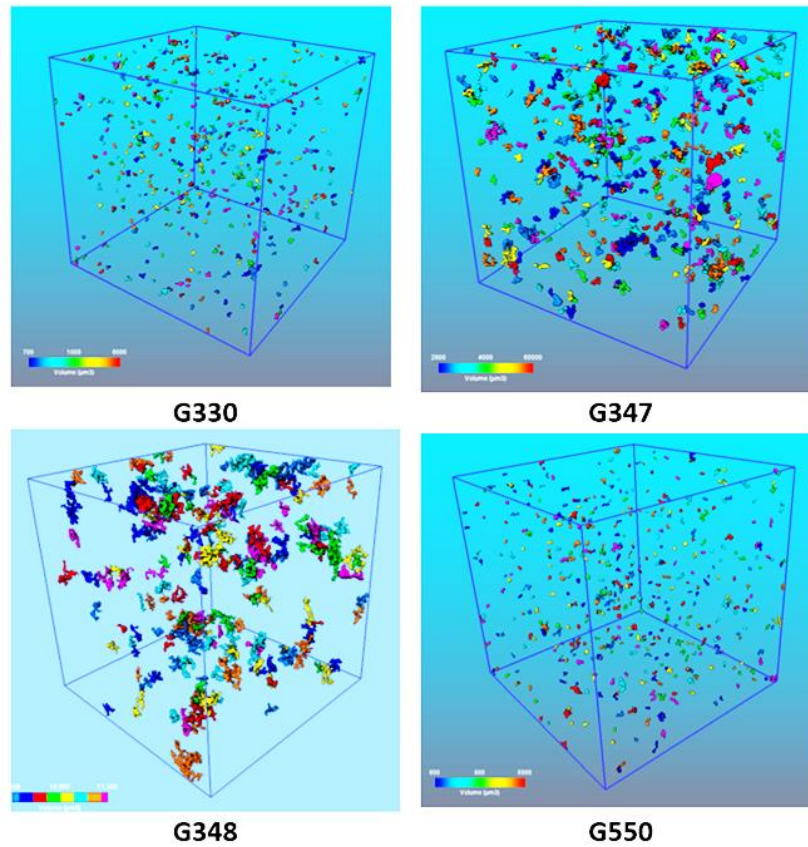


Figure 5.1. 2. Image of the interconnectivity of pores in different materials, being a) G330, b) G347, c) G348 and d) G550.

The differences between Archimedes porosity and the porosity obtained by X-Ray tomography are due to the error of each technique. As we can see in Figure 5.1. 1, the pores are situated on the grain boundaries in every substrate. G347 and G348 have a bigger grain size than G330 and G550 but less percentage of porosity. Besides G347 and G348 show more interconnectivity between their pores, namely, there are more isolated pores in G330 and G550 in spite of their high percentage of porosity.

- **Crystallinity analysis**

The crystallinity was measured by the ratio $D1/(D1+D2+G)$ obtained by Raman Microspectroscopy according to Beyssac et al⁴⁴.

Table 5.1. 2. Ratio to quantify the grade of crystallinity

	G330	G347	G348	G530
$D1/(D1+D2+G)$	0.398	0.398	0.398	0.398

The value of crystallinity is the same in each sample because they are made of with the same graphite and the differences of properties such as density or pore size are linked with the fabrication method.

- **Rugosity analysis**

The results of average rugosity (Ra) are shown in Table 5.1. 1

Table 5.1. 3.Values of average rugosity

	G330	G347	G348	G530
Ra (μm)	0.48	0.22	0.49	0.49

The substrates G330, G348 and G530 were polished until $1\mu\text{m}$. In contrast, G347 was grounded until $4000\mu\text{m}$ in order to analysed the influence of the rugosity. The polished samples obtained a less rugosity surface but the pores were opened, because of that the value of average rugosity is higher than the G347 value whose rugosity surface is higher but their pore were closed. In this case, some scratches can affect the wetting behaviour.

5.1.2 Sessile drop test

The sessile drop method is largely used in order to know the contact angle and kinetics rate of the spreading and infiltration phenomena. The classic method was used, in this thesis, for every material under argon atmosphere, and then the microstructure was analysed as well as the composition interaction.

5.1.2.1 Classic method

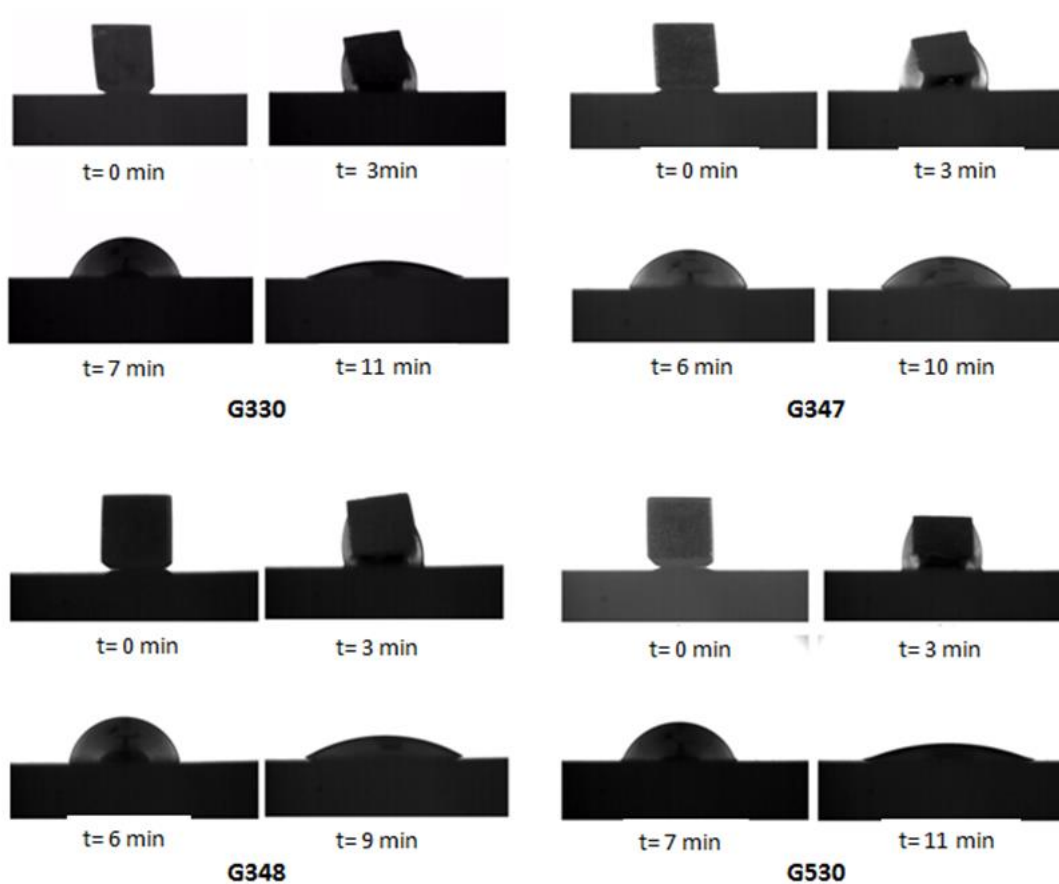


Figure 5.1. 3. Images of sessile drop test, a) on G330, b) on G347 c) on G348 and d) on G350.

During the classic sessile drop test, silicon samples were directly melted on the substrates under Argon atmosphere until 1450°C, the process was recorded by a camera linked to a computer and then, the videos were analysed by matlab software thanks to an images

analysis program. Figure 5.1. 3. Illustrates how the drop of silicon reached the equilibrium around 10 min in all the cases.

- **Analysis of the Sessile drop test**

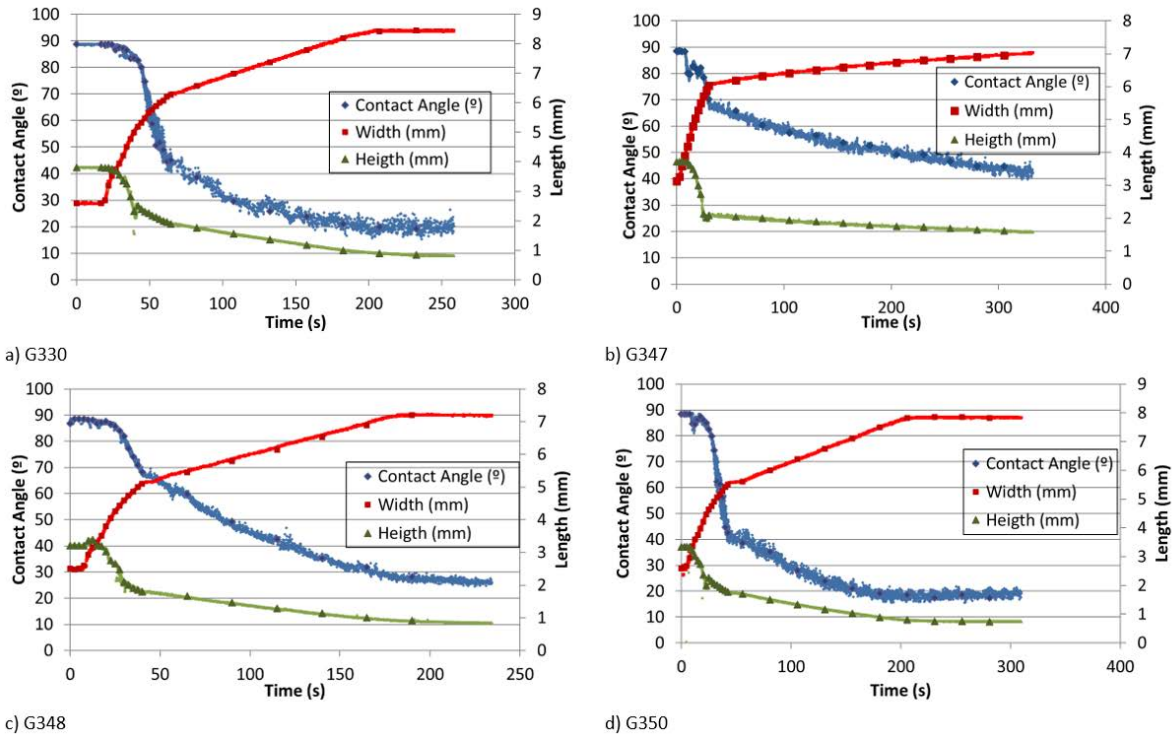


Figure 5.1. 4. Contact angle and parameters of silicon drop with time a) on G330, b) on G347 c) on G348 and d) on G350.

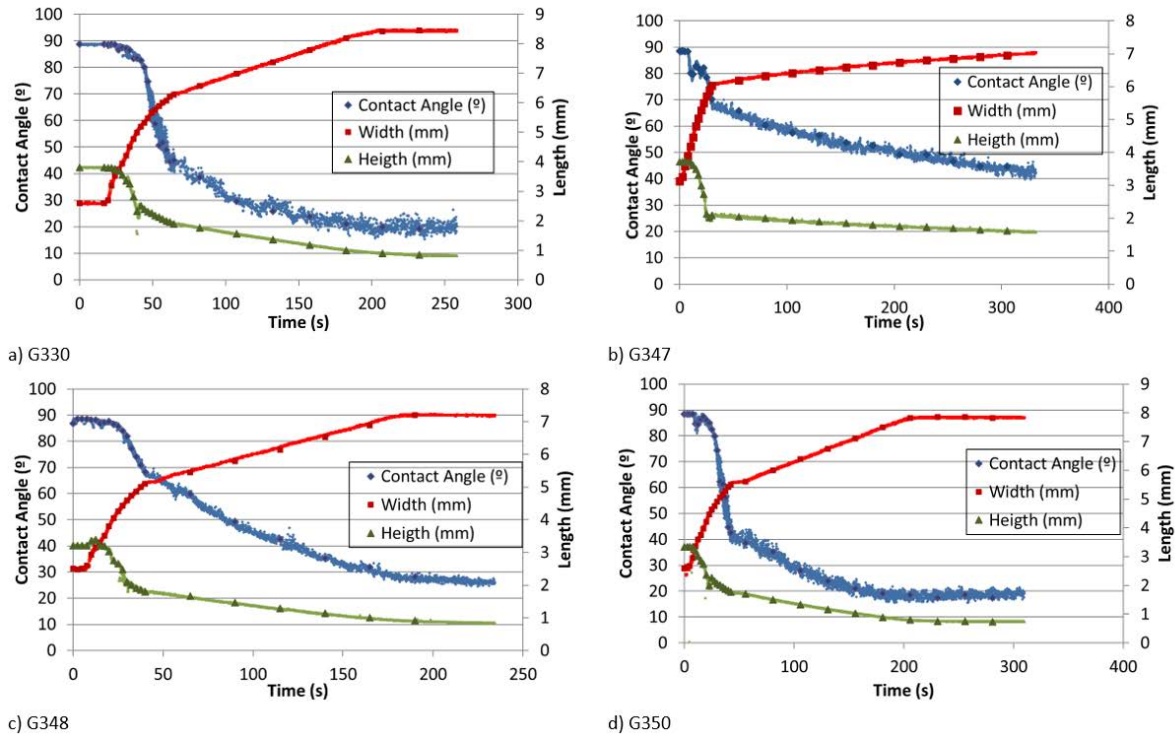
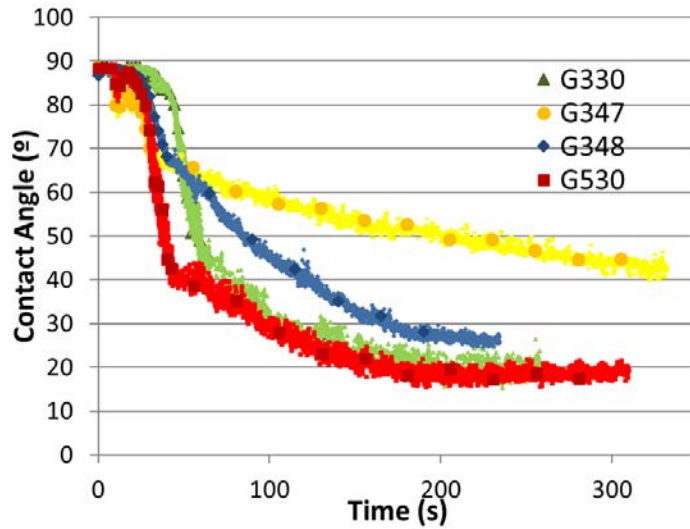


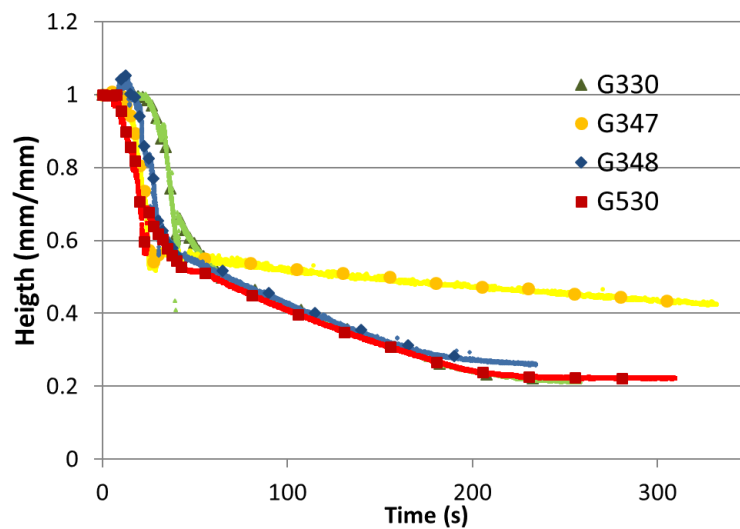
Figure 5.1. 4 illustrates the variation in contact angle and the height and width of the drop with the time. The graphics show the whole process from the start of melting to get the equilibrium. The equilibrium is reached when the contact angle and drop parameters become constant with the time.

Every sample shows a linear relation of the width of silicon drop with the time, indicating the reaction between silicon and carbide in the triple line⁵.

Once the drop is formed, and after the first sharply drop, the contact angles for G347 and G348 ($\sim 70^\circ$) are higher than G330 and G530 values ($\sim 45^\circ$). In contrast, the final or equilibrium contact angle for the G347 ($\sim 40^\circ$) is higher than the rest of the other samples ($\sim 20^\circ$). Previous studies⁸⁻¹⁵ have reported large results for initial contact angle from 18° to 146° and for final contact angle from 0° to 40° , these values agree with firstly system show the contact angle the carbon-silicon but, after the formation of silicon the contact angle corresponds to Si/SiC system.



a)



b)

Figure 5.1. 5. Comparison of variation of a. contact angles and b. relative drop height (mm/mm) of substrates with the time

Figure 5.1. 5.a presents the variation of the contact angle with the time. From the beginning of melting to the time when the drop is formed, a significant decrease of the height is shown, above all, G330 and G530 substrates. Then, the slope changes in every case, the values of the contact angle keep decreasing but slower than before. Particularly, the variation in G347 is lower than the other substrates. Besides it has the highest initial and final contact angle.

On the other hand, Figure 5.1. 5.b illustrates the variation of the height of the drop with the time. In order to compare values, the height was divided by the initial height to obtain a dimensionless value (mm/mm). As in the case of the contact angle, firstly there is a large decrease in all the samples and then a change in the slope. Once the drop is formed, the decrease is slower than before, especially in G347 due to the rugosity on the surface.

Table 5.1. 4. Spreading measured on several graphite substrates before and after drop formation

	G330	G347	G348	G530
Uspr (mm/s)	0.014	0.013	0.014	0.011

Table 5.1. 7 shows the values of the spreading rate measured by $U_{spr} = \frac{1}{2} \frac{dD}{dt}$, considering the diameter as the width of the drop. Every substrate showed linear relation with the time and the spreading time lies between $10-10^4$ s, thus, it is considered that the spreading is controlled by the reaction at the triple line²¹.

- **Optical microscopy analysis of Sessile drop samples.**

Regarding the top images of substrates after sessile drop test presented in Figure 5.1. 6a, a good symmetry is observed in all substrates. In spite of the difference in the rugosity, the spreading of drop is similar, indicating that the drop was not pinned by any impurity or scratch. Although, in the case of G347, the external ring is not so symmetric, and besides, it is much bigger than the internal ring. This could be due to the fact than the infiltration can be boost in this substrate in comparison with the others, due to the interconnectivity of the pores is higher than the others.

On the other hand, Figure 5.1. 6.b presents the cross section images after de sessile drop test. The samples were cut in order to observe the infiltration section. As we can see, the deepest infiltration was for G347, and also it had the more regular shape in the infiltration area. Generally, the infiltration has a semicircle shape, in other words, in the centre of the drop the infiltration is maxima, and as it moves away from the centre, the infiltration distance is less. This means that for G330, G348 and G550 the infiltration was hindered.

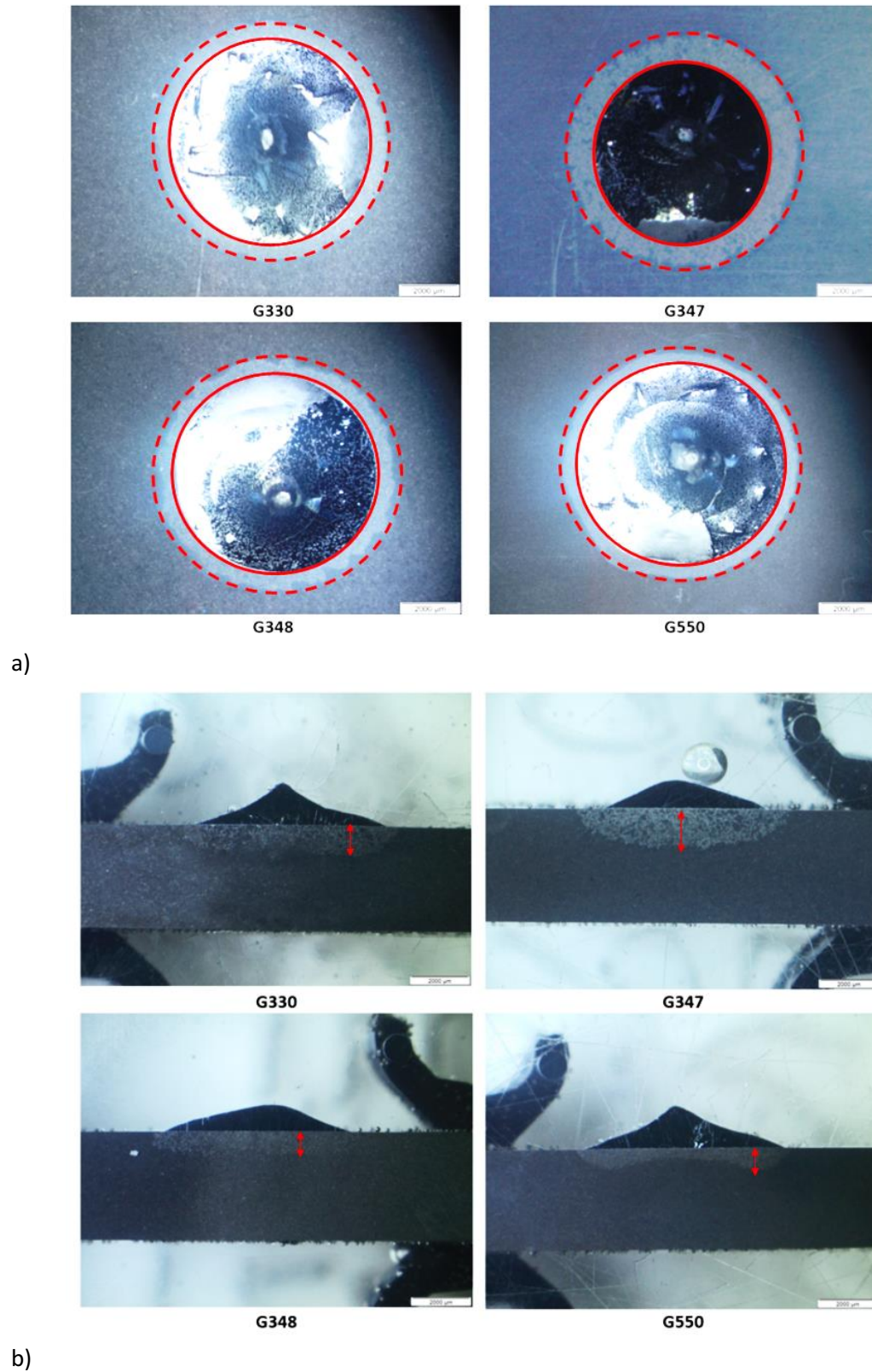


Figure 5.1. 6. a. Top view and b. side view images of substrates after sessile drop test.

Table 5.1. 5. Values of effective radius and maximum infiltrated length according properties of graphite substrates and work condition

Substrates	G330	G347	G348	G530
Internal Radius (mm)	3.574	3.071	3.529	3.772
External radius (r_{eff}) (mm)	4.243	4.067	4.177	4.281
Maximum radio (mm)	4.235	3.57	3.61	3.92
Infiltration (h_{total}) (mm)	1.232	1.458	0.996	0.846
Temperature	1450°C			
Atmosphere	Argon			
Ra (μm)	0.48	0.22	0.49	0.49
Porosity	22%	14%	11%	23%
Av pore diameter (μm)	10.29	7.48	9.02	11.69
U_{inf}	0.006	0.005	0.004	0.003
U_{spr}	0.014	0.013	0.014	0.011
U_{inf}/U_{spr}	0.42	0.36	0.32	0.25

Table 5.1. 5 provides the values of effective radius and maximum infiltrated depth according to the properties of the graphite substrates and test conditions. Besides, the maximum radius during the sessile drop test was calculated. G550 substrate shows the largest external and internal radius while G347 substrate shows the smallest ones. This agrees with the values of maximum infiltration for G347 and minimum one for G550.

According to the properties, the rugosity is linked to the spreading because the values of the effective radius are similar for G330, G348 and G550 substrates. However, it cannot be set a relationship between the rugosity and the values of maximum infiltration length.

On the other hand, the infiltration rate was calculated by $U_{inf} = \frac{h_{total}}{t_{inf}}$, where h_{total} is the maximum infiltration distance. Camel et al¹⁷ suggested that U_{inf} and U_{spr} have the same order of magnitude because both are managed by the reaction in the triple line. However,

the U_{inf} is hindered due to the tortuosity. For that, the ratio U_{inf}/U_{spr} lies from 0.65 to 0.95. The ratios U_{inf}/U_{spr} in every substrate show values down to 1 but lower than those obtained in the literature⁵⁵. The differences can be due to the differences to the rugosity.

- SEM analysis of the Sessile drop samples

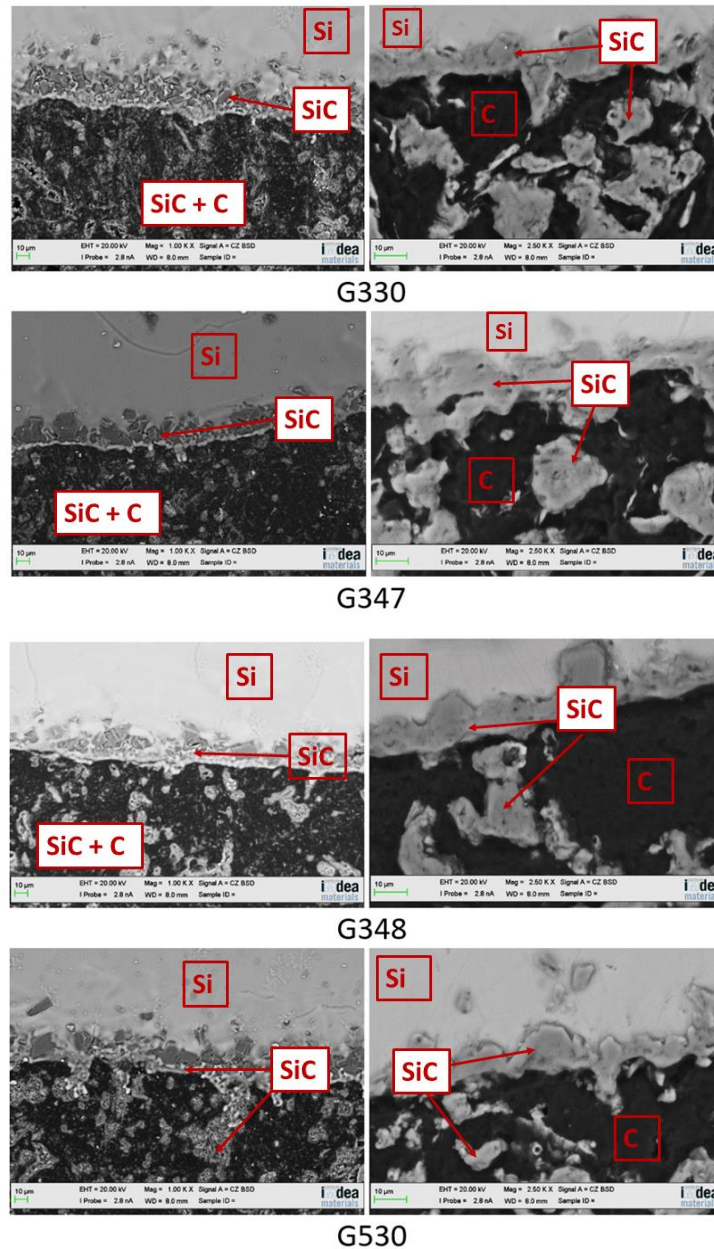


Figure 5.1. 7. Top and cross side micrographs of a. G330, b. G347, c. G348 and d. G550 after sessile drop test

Top and cross-section micrographs of G330, G347, G348 and G550 after sessile drop test are shown in Figure 5.1. 7.

In each case, the silicon has infiltrated and the pores have been closed by SiC. Besides, a SiC layer was formed at the surface preventing the infiltration. This agrees with Israel et al⁹, according to this author the silicon infiltrates into the pores, and then the reaction between silicon and carbide starts on the wall of the pore until the pore is closed by SiC. At the same time, a SiC layer is formed owing to the spreading of the drop on the surface, that boosts the reaction on the surface. In addition, large SiC crystals are formed around the silicon droplet, as shown in the top micrographs. These large crystals form a SiC layer less continuous than the interface layer but probably influence the propagation.

The average thickness of the interface layer (e) and the thickness of the SiC crystals formed (e_d) are calculated in Table 5.1. 6. The values for e lie between 12 and 15 μm and for e_d , between 21 and 26 μm . These results agree with the literature¹⁰.

Table 5.1. 6. Values of the SiC layer thickness (e) and the thickness of the SiC crystals formed around the silicon droplet (e_d)

	G330	G347	G348	G530
$e(\mu\text{m})$	13.3	15.1	12.6	13.8
$e_d(\mu\text{m})$	23.7	21	22.86	26.38

- **X-Ray and Raman analysis of the Sessile drop samples**

The chemical compositions formed on the surface of the substrates were observed by X-ray analysis (Figure 5.1. 15). Silicon carbide was found, showing that silicon reacted with the graphite in the interface. There was a large quantity of carbon so that the signal was very strong hiding the Silicon and silicon carbide signal, thus the cross section was analysed by Raman. Figure 5.1. 16 shows silicon infiltrated in the porous of substrates and reacted with the graphite. However, unreacted silicon was found in the centre of the pore,

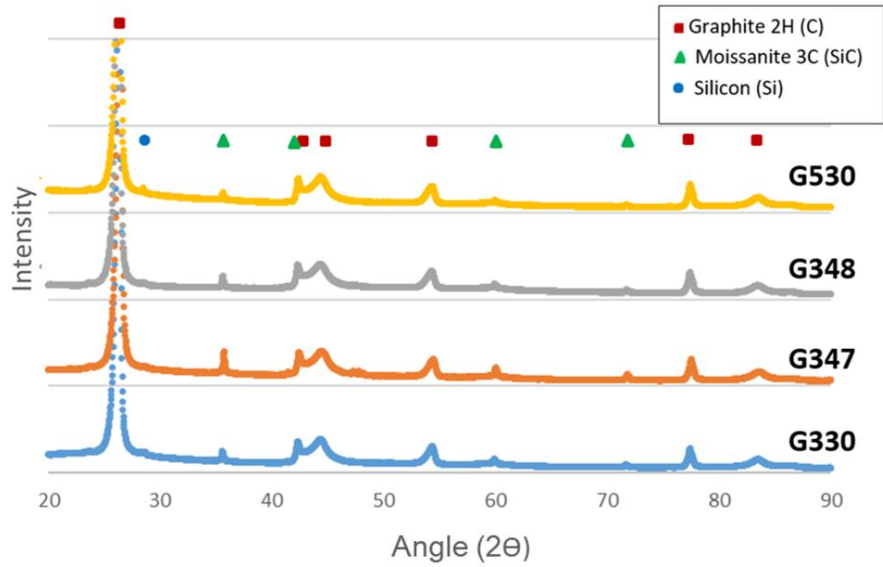


Figure 5.1. 8. X-Ray results of graphite substrates after Sessile drop test.

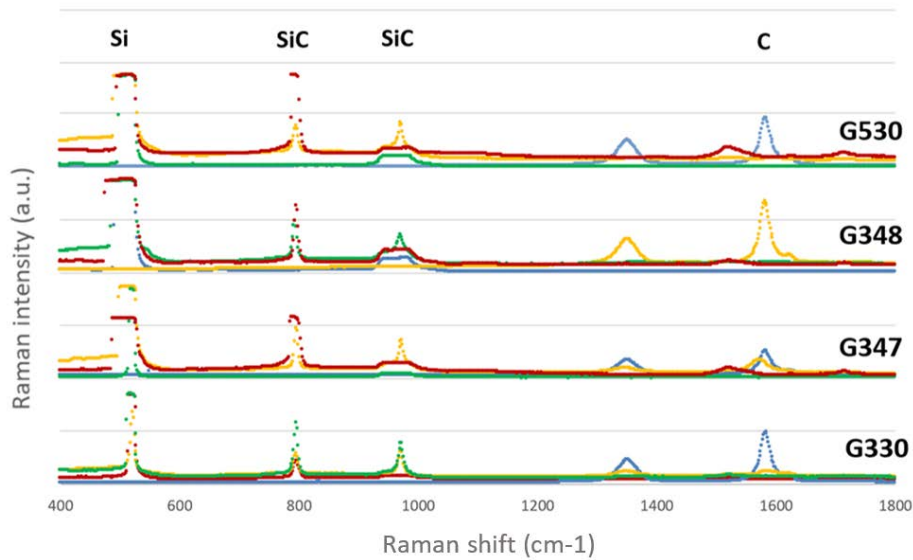


Figure 5.1. 9. Raman shift results of graphite substrates after Sessile drop test.

5.1.2.2 Dispensed drop

In addition to the classic method, two samples were analysed by the dispensed drop method. The dispensed drop method consists in to cast silicon inside a BN plunger, and when the temperature of 1450°C is reached, silicon is dropped on the substrates. Due to the complex and the high price of the experiment only two samples could be measured,

these samples showed a good behavior in a previous test in the induction furnace. The main advantages of the “dispensed drop” method, are: 1) the drop is free of oxide, 2) the temperature is uniform in the whole drop and 3) the wetting behavior is not affected by the melting process³¹. As in the other cases, chemical and microstructural characterization were done after the experiments.

- **Analysis of the Dispensed drop test**

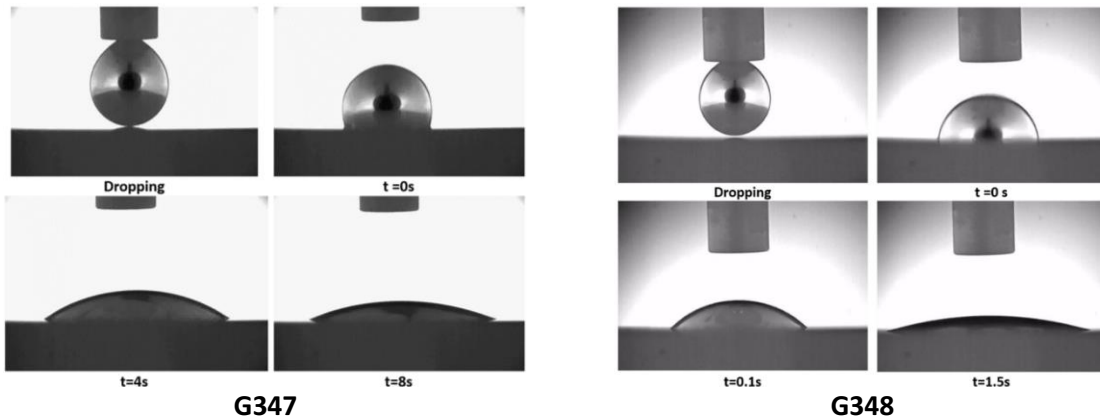


Figure 5.1. 10, Images of sessile drop test, a) on G330, b) on G347 c) on G348 and d) on G350.

In comparison with the classic method, silicon reached faster the equilibrium angle. Particularly in the case of G348, the drop spreads very fast, indicating that the scratches of the surfaces were likely to influence the process.

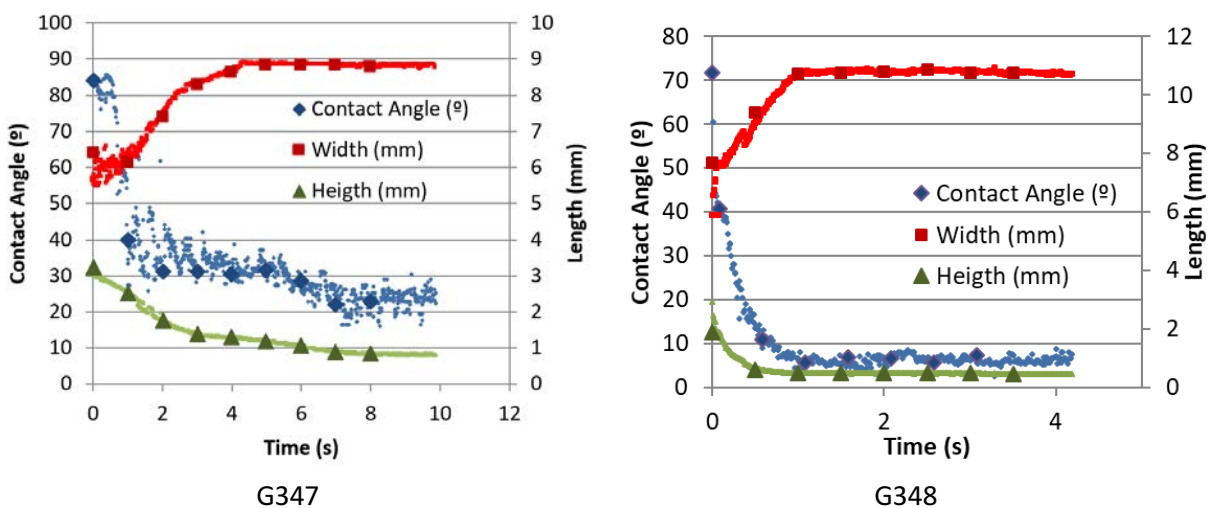


Figure 5.1. 11. Contact angle and parameters of silicon drop with time on G347 and G348 during dispensed test

Figure 5.1. 11 illustrates the variation in contact angle and the height and width of the drop with the time. The origin of the time is when the silicon was dropped on the substrates by a plunger. The drop was recorded until the equilibrium was reached, in other words, when the contact angle and drop parameters become constant.

As in the classic method, both samples show the linear trend between the contact angle and the drop parameters with the time, suggesting the reaction between silicon and carbide on the triple line¹³⁻⁵.

Initial contact angles for G347 ($\sim 85^\circ$) are higher than G348 values ($\sim 70^\circ$). In addition, the equilibrium contact angle for the G347 ($\sim 40^\circ$) is also higher than the G348 values ($\sim 5^\circ$). Dezellus also used the dispensed drop variant of the sessile drop technique under vacuum at 1430° ¹². However, the values obtained were 35° for vitreous graphite and 0° for pseudo-monocrystal of graphite were infiltrated fully by the silicon. Other studies⁸⁻¹⁵ have reported large results for initial contact angle from 18° to 146° and for final contact angle from 0° to 40° .

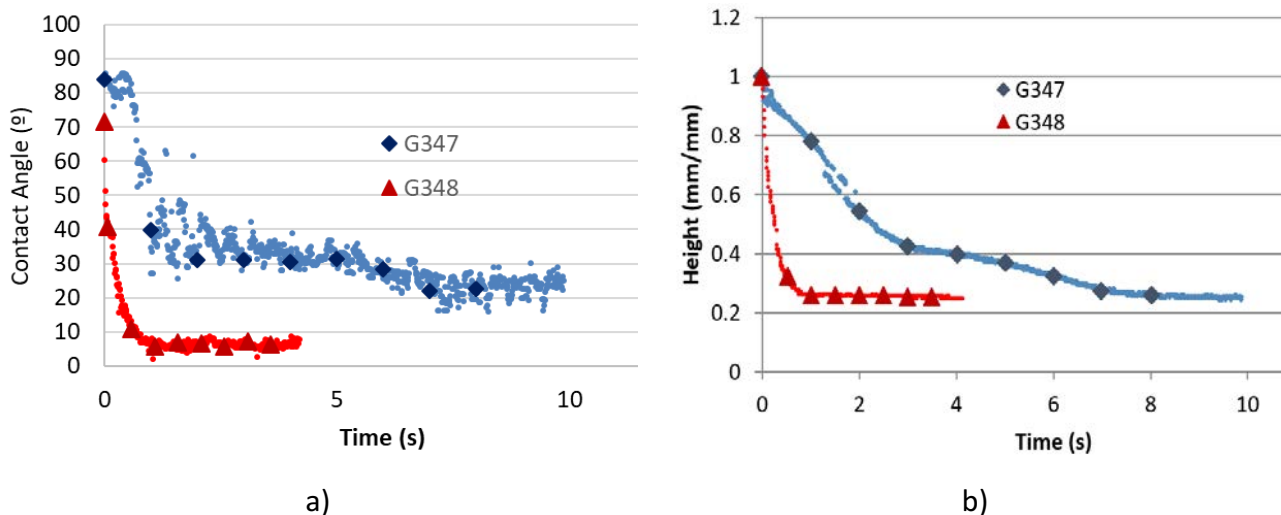


Figure 5.1. 12. Comparison of variation of a. contact angles and b. relative drop height (mm/mm) of substrates with time

Figure 5.1. 12. a shows the variation of the contact angle with the time. As in the classic sessile drop method, there was a remarkable decrease just after the silicon was dropped in both cases. Then, for G347 substrate the decrease is slight. Likewise, for the comparison

of the height, shown in Figure 5.1. 12. b, the height declines sharply a few seconds after the dropping in both case. After, for G348 remains almost constant and for G347 keep decreasing but slower than before. The high speed on the G348 substrates suggests that some scratches boost the spreading, affecting the contact angle and the infiltration.

Table 5.1. 7. Spreading and infiltration rate measured on G347 and G348 substrates during dispensed sessile drop method.

	G347	G348
Uspr (mm/s)	0.49	1.95

As in the classic method, the spreading rate was measured by $U_{spr} = \frac{1}{2} \frac{d \text{width}}{dt}$. The spreading rate of G348 is much faster than of G347. The value of G347 agrees with the literature but the value of G348 is higher than the literature. According to Camel¹⁷, if the reaction in the triple line manages the spreading, the relation with the time is constant and close to 10 μm . The silicon and substrate were heated in the same chamber, a SiC layer could be formed on the surface of the substrate before to dispense the drop due to the fact the silicon can evaporate before to reach the melting point⁸ and condensed on the surface of the substrate. In addition, the silicon started to spread at 1450°C while in the classic sessile drop method the spreading starts at 1414°C. This factor and the effects of the scratches might have affected the kinetics.

- **Optical microscopy analysis of the Sessile drop samples**

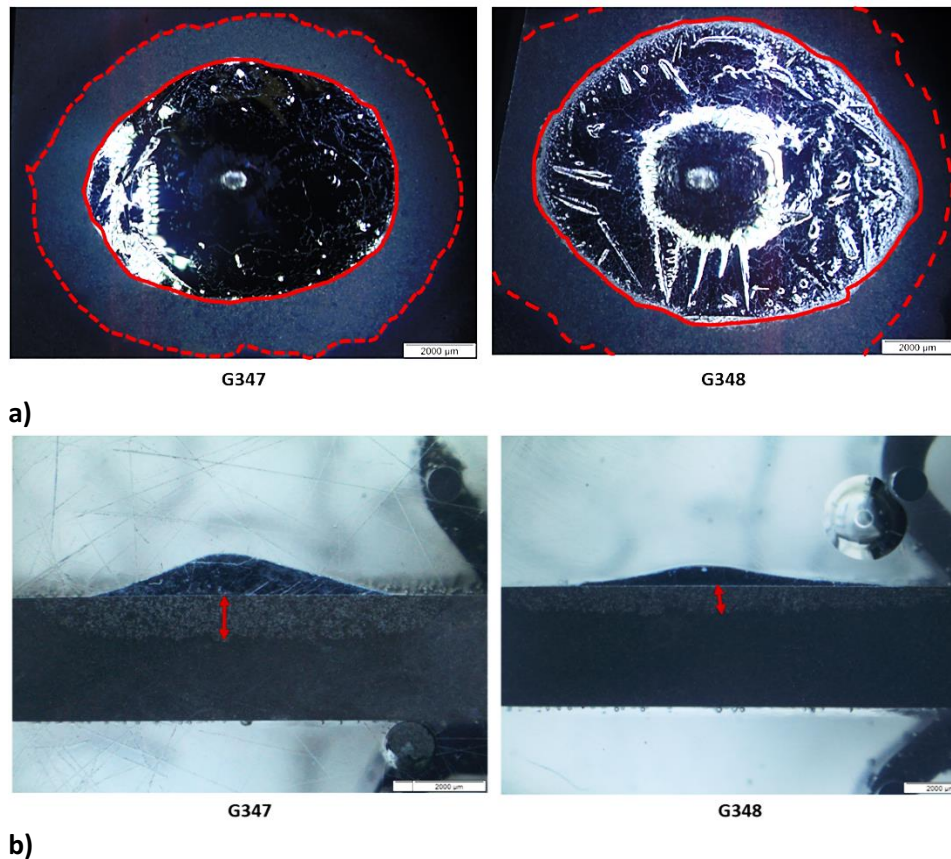


Figure 5.1.13 a. top and cross section images of substrates after sessile drop test.

Figure 5.1.13 illustrates top and cross-section of the substrates after the dispensed sessile drop. Around the drop, there is a SiC area where silicon spreads and then infiltrates. However, the shape, in this case, is oval, instead of a symmetric circle. Therefore, the silicon drop could have been pinned by impurities and boosted by the scratches of the surface. These effects are emphasized in the G348 substrate where the spreading distance is higher than G347 substrate but the infiltration distance is lower. Table 5.1.8 quantifies these same results. Remarkably, the difference of internal radius and maximum radius measured during the experiment is due to the fact that the drop is asymmetric, thus, the size of the radius depends on the direction where it was recorded. Besides, the infiltration rate was measured by $U_{inf} = \frac{h_{total}}{t_{inf}}$, and these results and the ratio between kinetics rate are included.

Table 5.1. 8. Values of effective radius and maximum infiltrated length according properties of graphite and work condition

Material	G347	G348
Internal radius (mm)	3.45	4.55
	4.55	5.73
External radius (r_{eff}) (mm)	5.01	6.26
	6.40	7.20
Maximum radius (mm)	4.85	13.46
Infiltration (h_{total}) (mm)	0.53	0.87
Temperature	1450°C	
Atmosphere	Argon	
U_{inf} (mm/s)	0.11	0.53
U_{spr} (mm/s)	0.49	1.95
$U_{\text{inf}}/U_{\text{spr}}$	0.22	0.28

The kinetics rate for both materials are lower than those obtained in the literature (0.65-0.95)⁸, and the Si evaporation and the influence of the scratches can be the main differences.

- SEM analysis of the Sessile drop samples

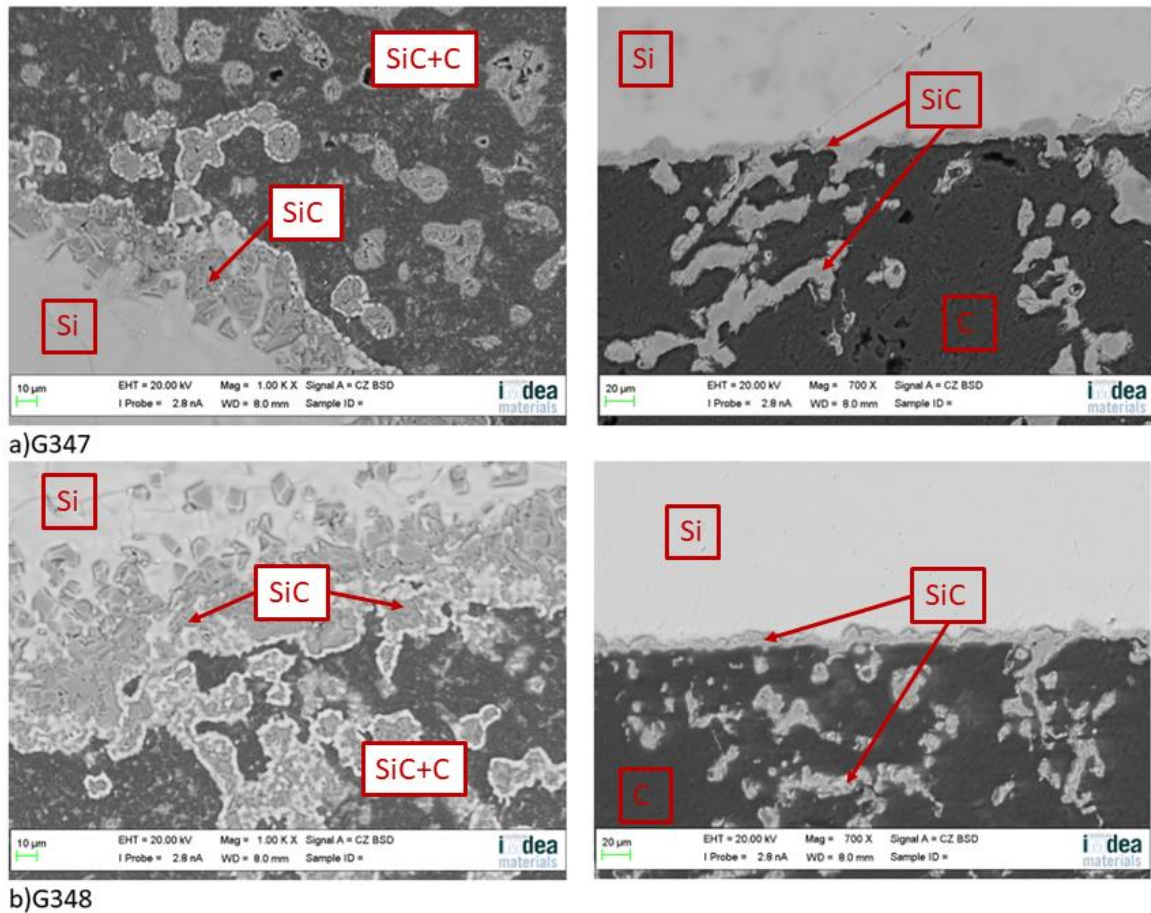


Figure 5.1. 14 top and cross section micrographs of a. G347 and b. G348 after dispensed sessile drop test.

Table 5.1. 9. Values of the SiC layer thickness (e) and the thickness of the SiC crystals formed around the silicon droplet (e_d)

	G347	G348
$e(\mu\text{m})$	7.89	7.25
$e_d(\mu\text{m})$	22.88	53.7

The top (on the left) and cross section (on the right) of the samples were analysed by SEM analysis (Figure 5.1. 14). On the surface, it is seen the porosity of the graphite substrate filled by silicon carbide while silicon carbides crystals are found on the edge of the drop. A

higher quantity of crystals is present in the G348 substrate despite it has reached the equilibrium faster than G347 substrate. Table 5.1. 9 shows the values of the thickness of the SiC layer formed interface (e) and also the values of the thickness of the SiC crystals formed around the silicon droplet (e_d). On the one hand, the values of e are lower than in the literature and the obtained results by the classic method. However, for G347, e_d agrees with the classic results but the value for G348 is especially higher.

Regarding the cross-section, a SiC layer is found on the interface Silicon-Graphite. Besides, the silicon has infiltrated and reacted into SiC and closed the pores. In the comparison of the sessile classic methods, the results are similar. Although the main difference is the number of crystals on the edge of the drop.

- X-Ray and Raman analysis of the Sessile drop sample

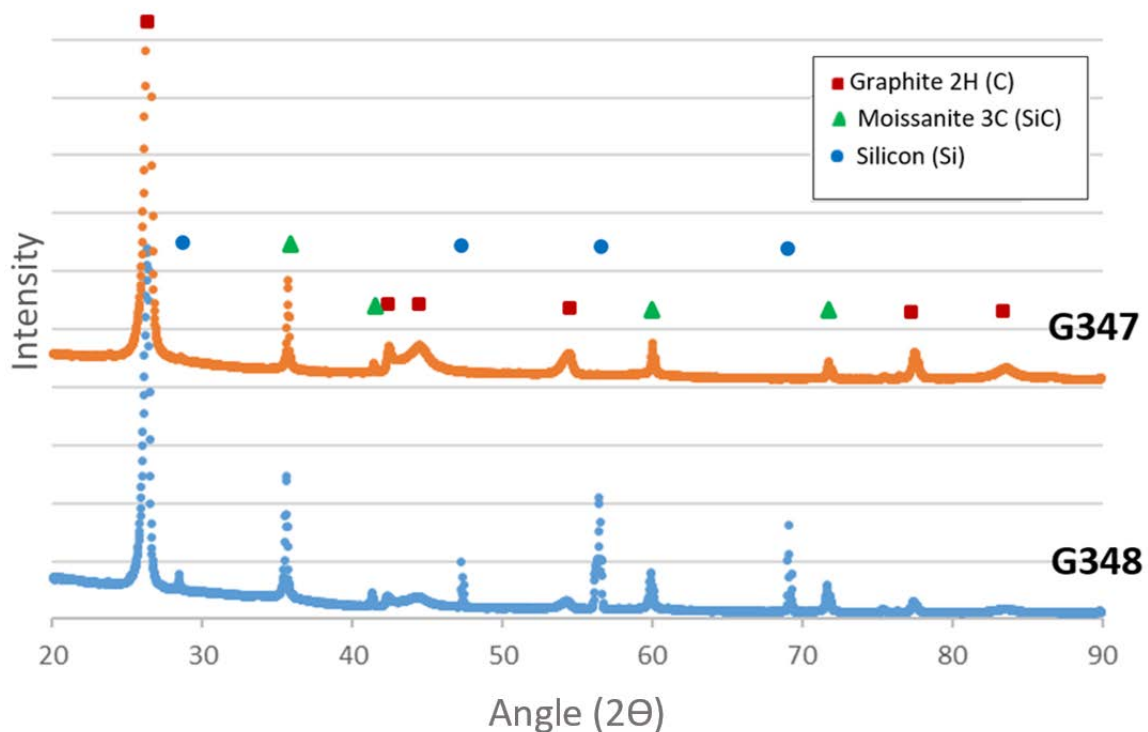


Figure 5.1. 15. X-Ray results of graphite substrates after Sessile drop test

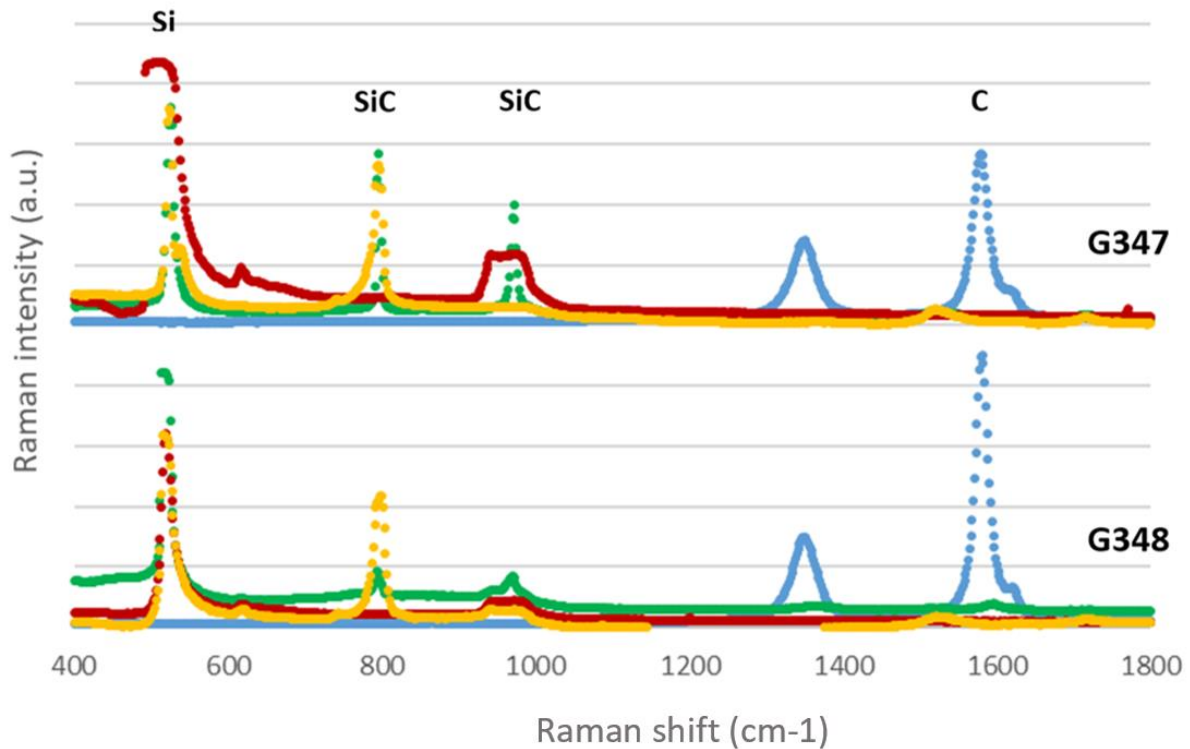


Figure 5.1. 16. Raman shift results of graphite substrates after Sessile drop test.

The surface of the samples was analyzed by XRD (Figure 5.1. 15) and the cross section by Raman Spectroscopy. Through the two methods can be confirmed that silicon reacted with the graphite on the interface and the pores, forming silicon carbides. Although, unreacted silicon was found.

5.1.3 Induction furnace test

In order to analyse the behaviour of the molten silicon against graphite, an induction furnace was used. The silicon samples were melted on the graphite substrates under the high vacuum atmosphere. It was not possible to record the process, but when the test is finished, the samples were microstructural characterized and regarding the microstructure and composition.

- **Optical microscopy analysis of the induction furnace samples**

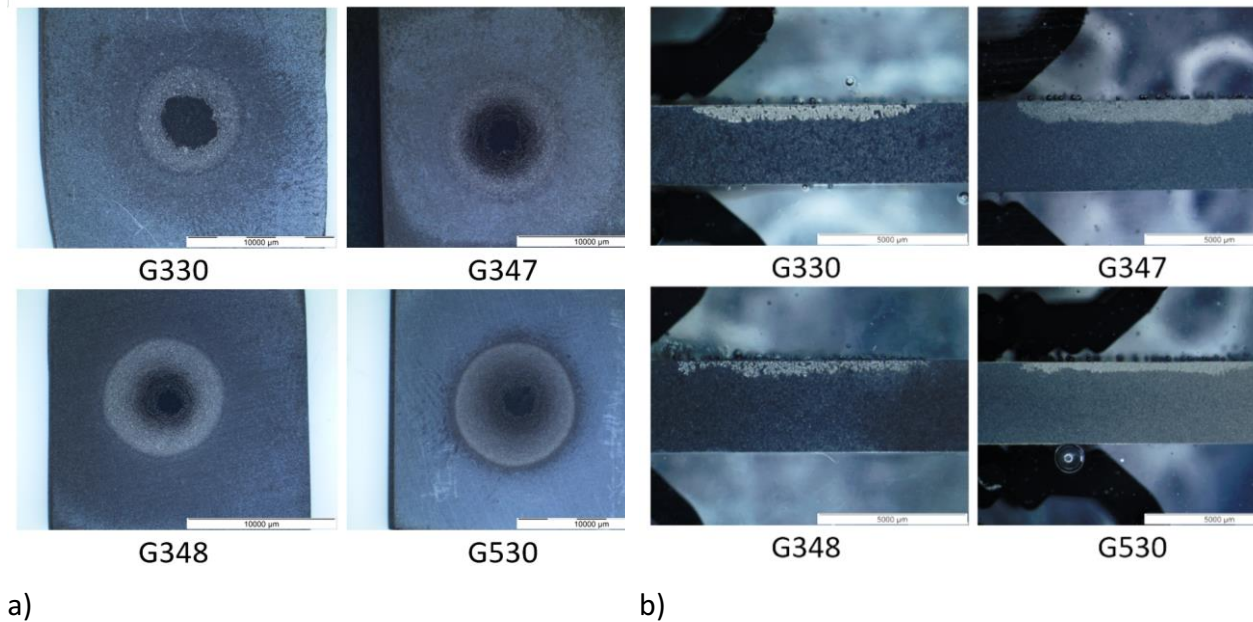


Figure 5.1. 17. a. top and cross section images of substrates after high vacuum test.

Figure 5.1. 17, shows the top and cross-section of substrates after the induction furnace test. Under high vacuum atmosphere, it is remarkable there is not any drop over the substrate, indicating the probably evaporation of the silicon. Molten silicon infiltrated completely, but it could be that the drop also evaporated as reported by Israel et al⁸. Besides, as under argon atmosphere, the drop produces two concentric circles as well as the molten silicon infiltrated through by the pores.

Table 5.1. 10 shows the values of the obtained parameter from the images in comparison with the properties and work conditions, internal and external radius are measured from the top view, while maximum radius and infiltration distance are analyzed from the cross-section. The values of the infiltration distance are smaller than the values obtained under Argon atmosphere. On the contrary, the values of the maximum radius are larger than argon's ones. These results agree with the evaporation of the silicon, on one hand boosted the spreading and elimination because of the vacuum atmosphere.

Table 5.1. 10. Values of effective radius and maximum infiltrated length according properties of graphite substrates and work condition

Material	G330	G347	G348	G530
Internal Radius (mm)	3.45	4.77	3.77	2.17
External radius (r_{eff}) (mm)	7.49	8.73	8.37	8.68
Maximum radius (mm)	7.73	8.29	8.72	8.35
Infiltration (h_{total}) (mm)	0.58	0.88	0.58	0.44
Temperature	1450°C			
Atmosphere	Vacuum			
Ra (μm)	0.48	0.22	0.49	0.49
Porosity	22%	14%	11%	23%
Av pore diameter (μm)	10.29	7.48	9.02	11.69

- SEM analysis after induction furnace test

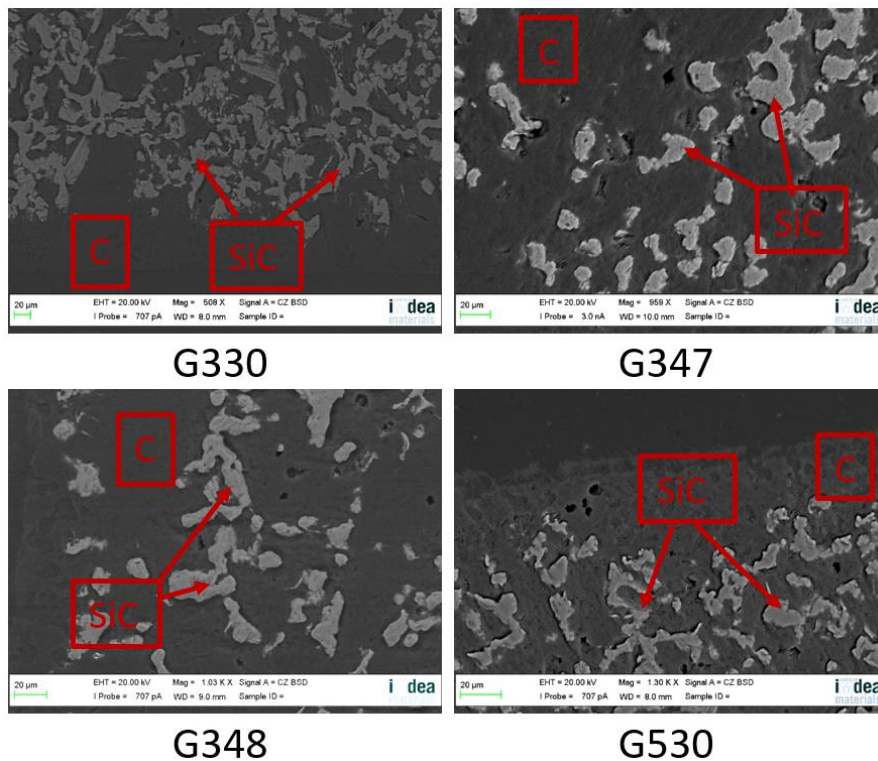


Figure 5.1. 18. Cross-section micrographs of G330, G347, G348 and G530 after induction furnace test.

The cross-section micrographs are found in Figure 5.1. 18, as in the argon experiments, silicon infiltrated by the pores, and reacting with the carbon of the wall of the pores of the graphite substrates, finally, were closed by SiC.

- X-Ray analysis after the induction furnace test

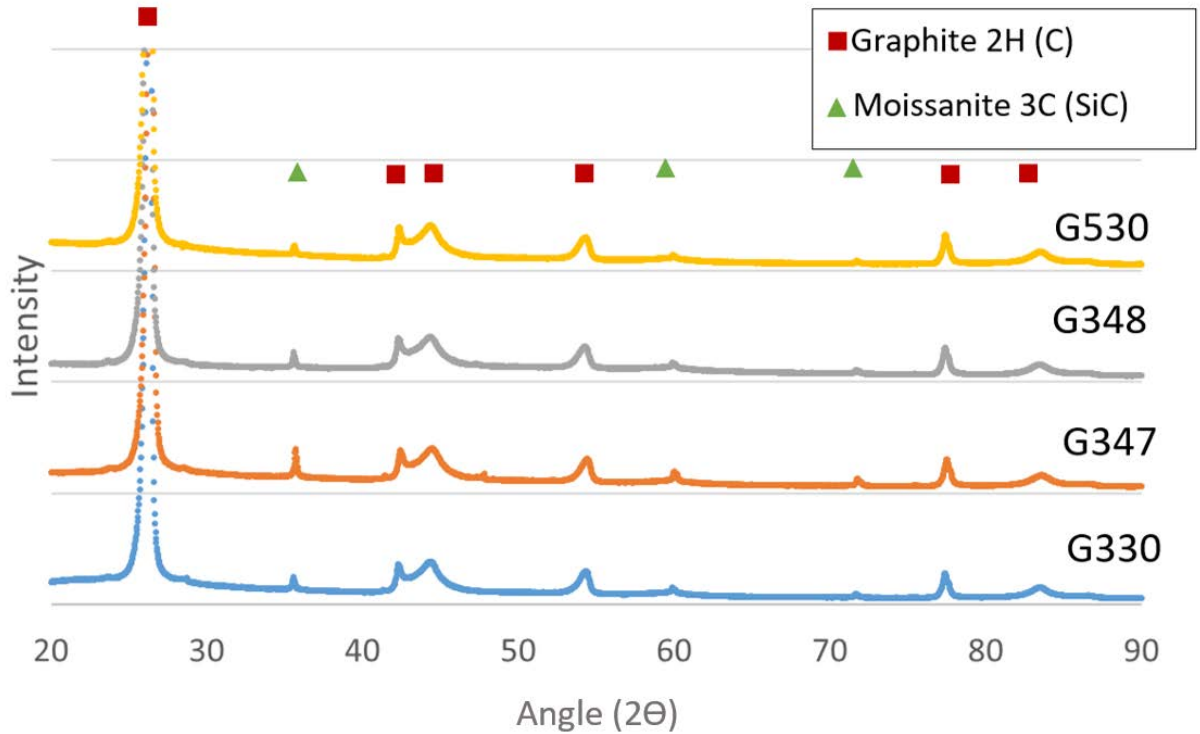


Figure 5.1. 19. X-ray results of graphite substrate after induction furnace test.

Figure 5.1. 19 shows the results of graphite substrate after induction test, as under atmosphere, the composition of the samples was carbon and silicon carbides, unreacted silicon was not found. These results support the evaporation of the silicon, the mass of silicon which not reacted nor infiltrated was eliminated by the silicon evaporation.

5.2 Graphite from Sigrafine and Carbon-lorraine

Other commercial graphite substrates from different companies were chosen in order to compare and get more information. As for Tokai substrates, the substrates were characterized and prepared before to perform the experiments. Then, the wetting, spreading and infiltration were analysed by Sessile drop method, and finally, the microstructural and chemical characterization was made.

5.2.1 Characterization of material

- Porosity analysis

Table 5.2. 1 Density results

Material	Apparent Density	Total Density	Archimedes porosity %	Tomography porosity %	Pore mean size (μm)
Lorraine	2.13	1.71	19.55	18%	10.62
R6650	2.08	1.74	16.38	20%	8.94
R6710	2.11	1.79	15.06	22%	7.52

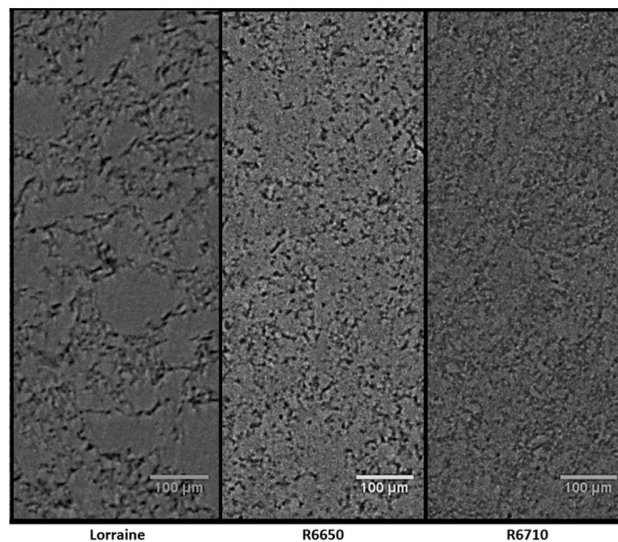


Figure 5.2. 1. Image of the distribution of pores in different graphite substrates, being R6650, R6710 and Lorraine

The porosity was analysed by the Archimedes method and by X-ray tomography. In Figure 5.2. 1 is observed the distribution of the pores in each material. R6650 substrate shows small grains and the pores are in the grain boundaries, similar to R6670, but in this case, the pores are smaller. On the other hand, Lorraine substrate has bigger grains and bigger pores in the grains boundaries.

This distribution of pores agrees with the obtained results in Table 5.2. 1The maximum pore mean size is for Lorraine and the minimum is for R6710. The differences of the percentage of porosity are due to the fact that the small pores hindered the measured porosity.

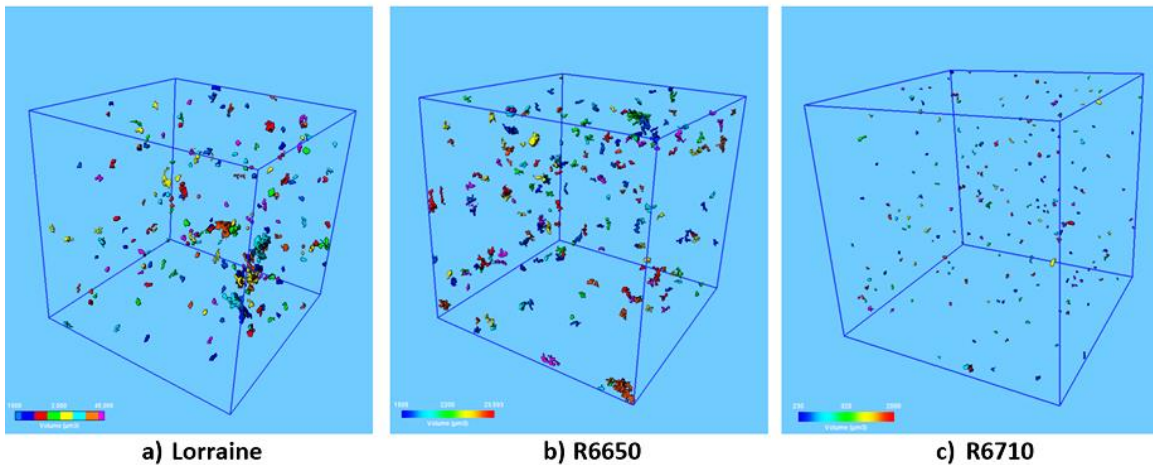


Figure 5.2. 2. Image of the interconnectivity of pores in different materials, R6650, R6710 and Lorraine

Figure 5.2. 2, can be seen that R6710 substrate has isolated pores while R6650 and Lorraine have more interconnected pores

- **Crystallinity analysis**

Table 5.2. 2. Ratio to quantify the grade of crystallinity

	Lorraine	R6710	R6650
D1/(D1+D2+G)	0.423	0.37	0.37

Regarding the crystallinity, Lorraine substrate is more crystalline than the other because the value of the ratio is higher (Table 5.2. 2.). Similarly, the obtained ratio for Tokai graphite substrates is 0.398.

- **Rugosity results**

The substrates were grounded until 4000 μm as in the case of G347. The value of the average rugosity are in Table 5.2. 3. The values for R6650 and Lorraine are similar while the minimum value is for R6710.

Table 5.2. 3. Values of average rugosity

	Lorraine	R6650	R6710
Ra (μm)	0.34	0.32	0.19

5.2.2 Sessile drop test

- **Analysis of the Sessile drop test**

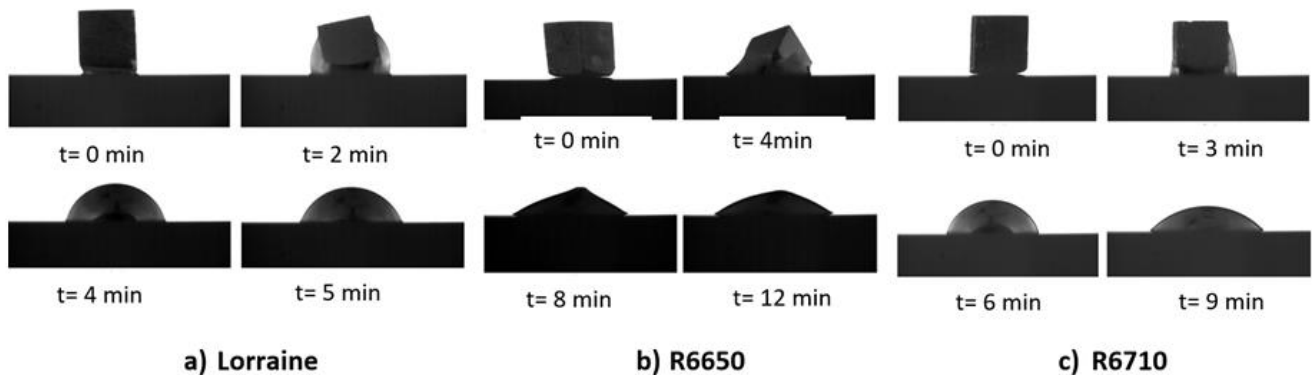
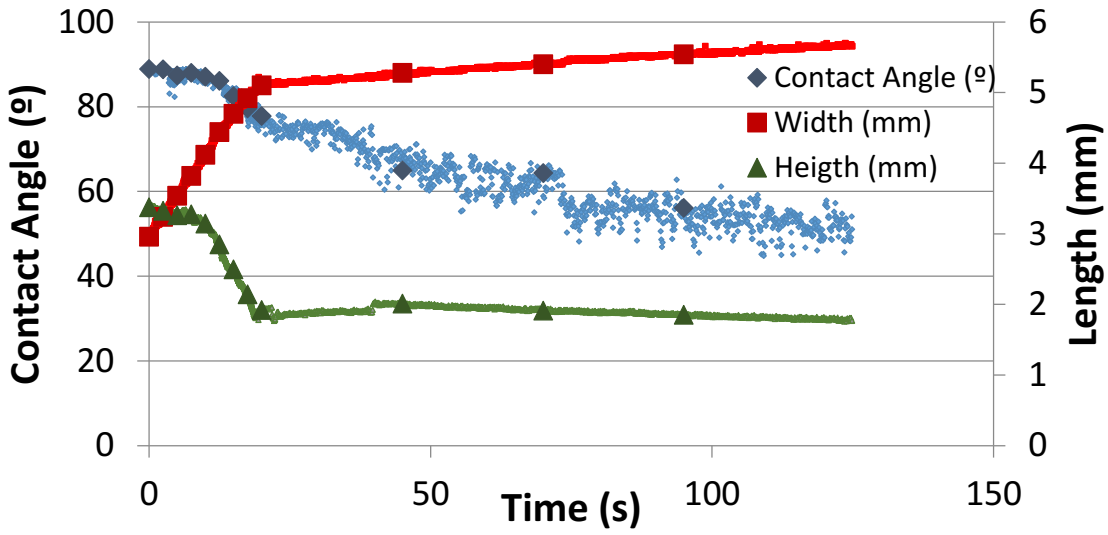
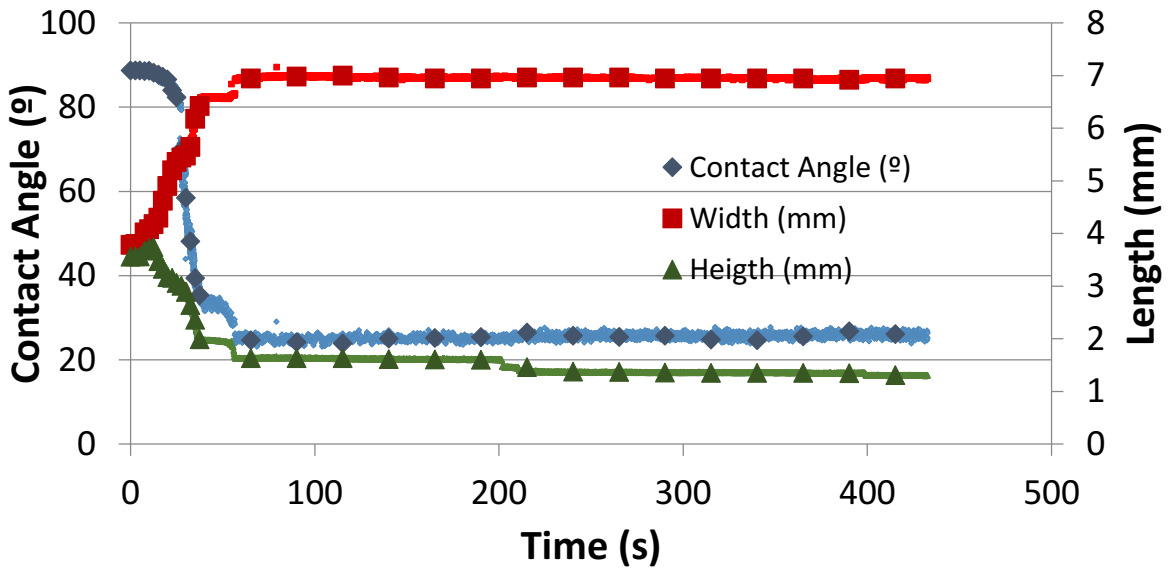


Figure 5.2. 3. Images of classic sessile drop test, a) on Carbon-Lorraine b) on R6650 and c) on R6710.

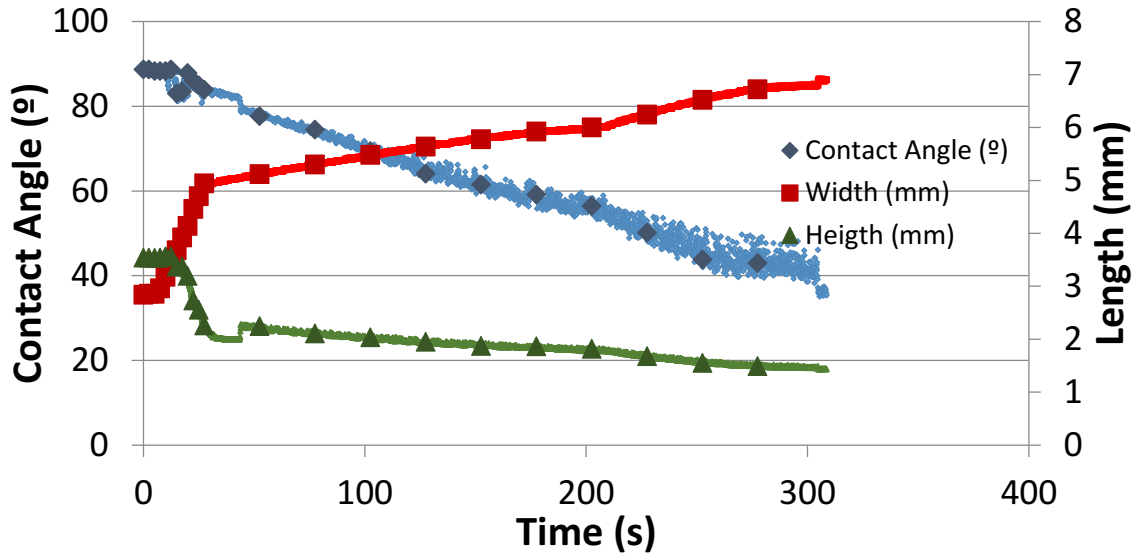
Silicon was melted on several substrates by the classic sessile drop and some images of the process are found in Figure 5.2. 3. The initial time corresponds with the starting of the melting of the silicon and the experiment was over when the equilibrium has been reached. This process takes around 10 min according to Tokai carbon results (Figure 5.1. 3) alike R6650 and R6710, while the process was faster in the Lorraine substrate case. Regarding the drop, the lack of symmetry in R6650 indicates impurities and scratches pinning the drop.



a) Lorraine



b) R6650



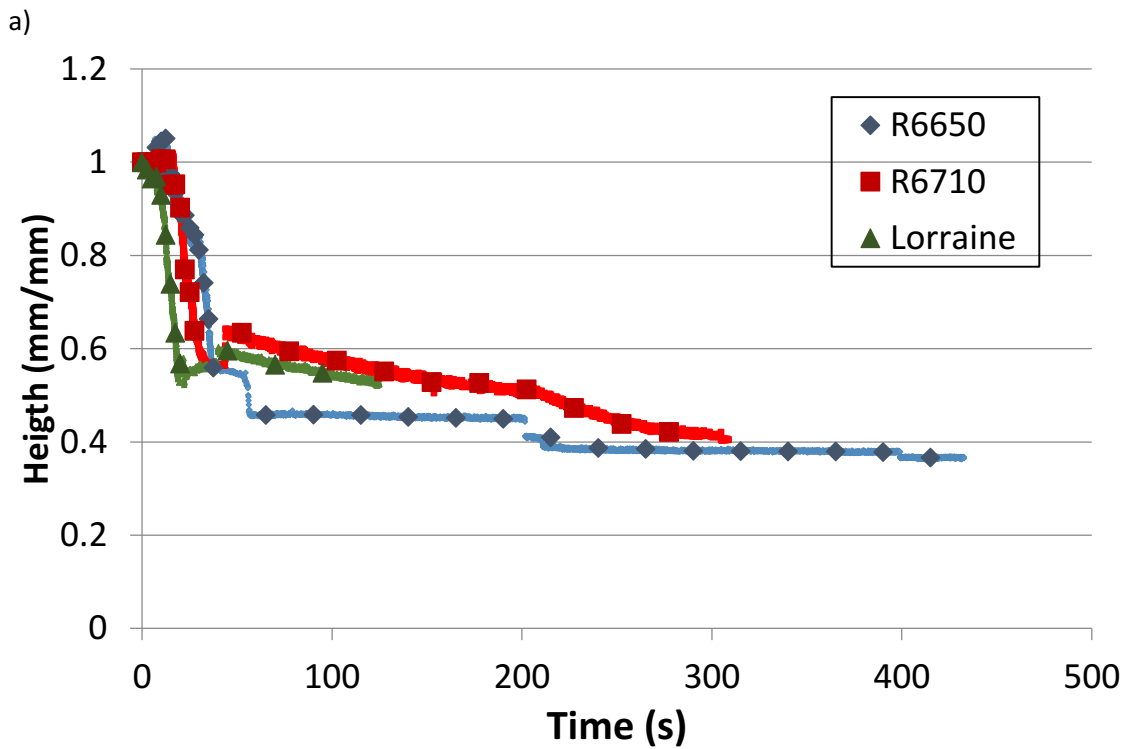
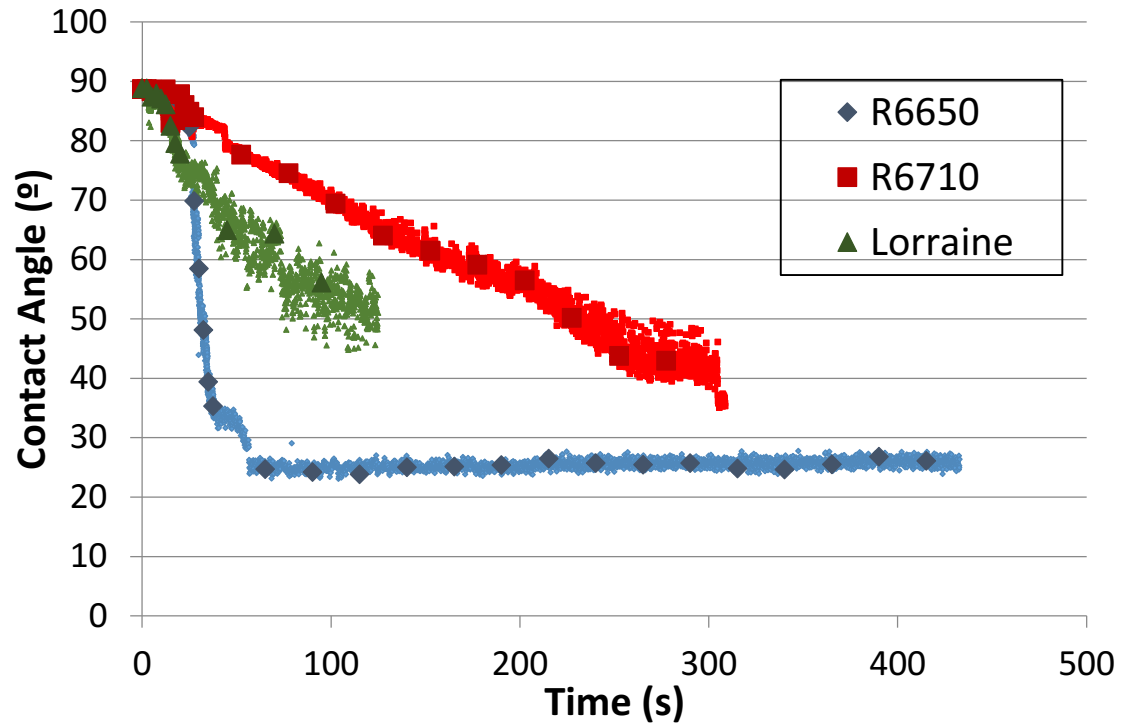
c) R6710

Figure 5.2. 4 Contact angle and parameters of silicon drop with time of a) on Lorraine, b) on R6650 and c) on R6710.

Figure 5.2. 4.a illustrates the variation of the contact angle and parameters of the drop (height and width) with the time on Lorraine substrates. In the beginning, the contact angle and the drop height decrease, while the drop width increases. Then, there is a change in the slope in every parameter: the contact angle and the height keep decreasing as the width increasing, but at slower rate than before. The evolution in every case is linear, indicating the reaction in the triple line.

Regarding R6650 (Figure 5.2. 4.b), there is a remarkable drop of the contact angle and drop height as well as a sharp increase in the drop width. After that, every parameter remains almost constant although there are some slight variations. The tendency also, in this case, is linear.

Like for the Lorraine substrate, the variation of contact angle and drop parameters with the time has a linear tendency for R6710. However, there is a change of the slope, namely, the process was faster than before as we can see in Figure 5.2. 4.c.



b)
Figure 5.2. 5. Comparison of variation of a. contact angles and b. relative drop height (mm/mm) of substrates with the time

Figure 5.2. 5. a illustrates the comparison of variation of the contact angle with time, the initial contact angle in every case is 90° . Then, there is a decrease where the slope indicates how fast the drop gets the equilibrium in each substrate. The fastest case was R6650 and the slowest was R6710. The equilibrium angles were 48.34° , 25.28° and 35.34° , respectively for Lorraine substrate, R6650 and R6710.

On the other hand, the variation of the dimensionless height (h/h_0) with the time is compared in Figure 5.2. 5.b. The remarkable initial drop is common for every substrate, but after that, the variation is different. The decrease was continuous for the Lorraine substrate and R6710, while was stepped for R650 due to the scratches. Spreading rate (U_{spr}) was calculated by $U_{spr} = \frac{1}{2} \frac{d \text{width}}{dt}$. The values agree with the literature⁸, although the R6710 values were slightly lower than the other materials.

Table 5.2. 4. Spreading and infiltration rate measured on several graphite substrates before and after drop formation

	Lorraine	R6650	R6710
U_{spr} (mm/s)	0.009	0.013	0.006

- **Optical microscopy analysis of the Sessile drop samples**

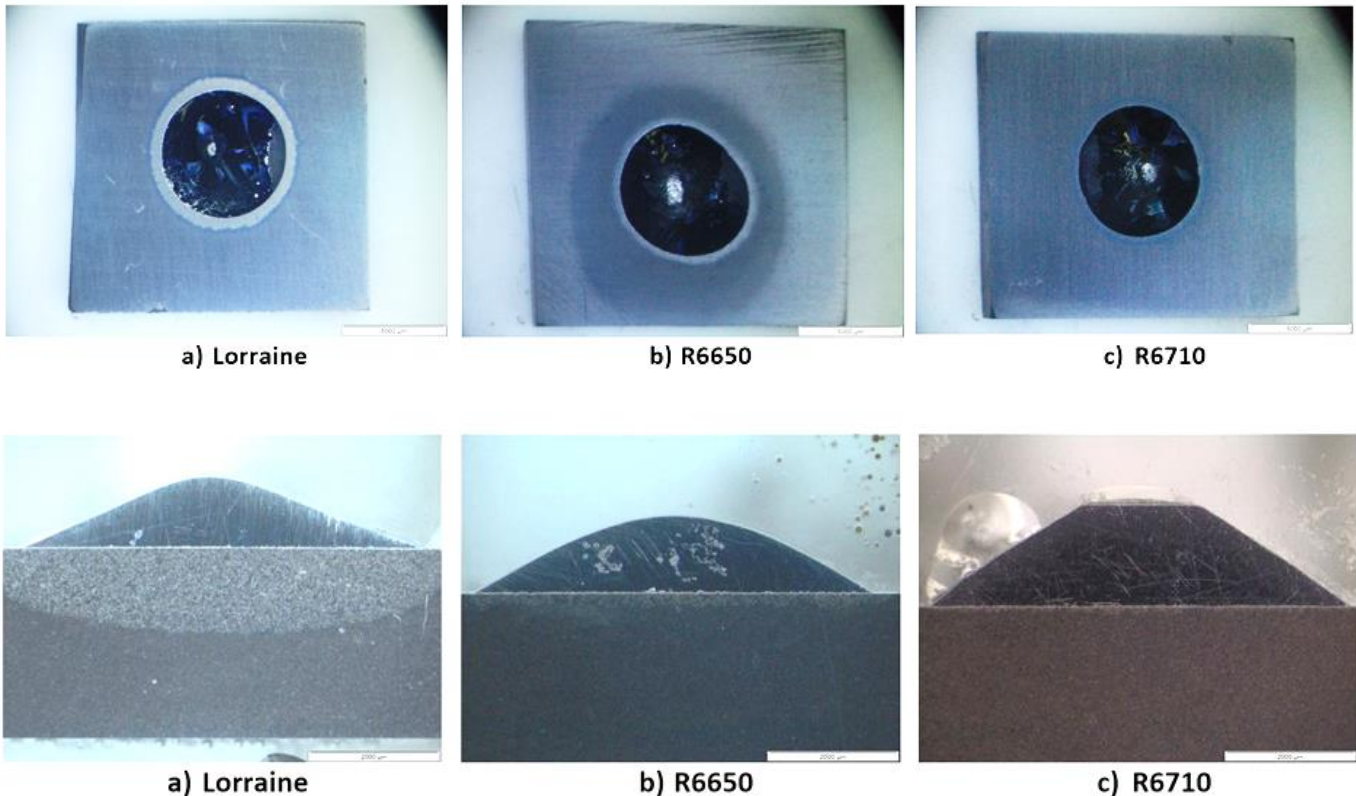


Figure 5.2. 6. a. Top view and b. cross side images of substrates after sessile drop test.

The top and cross side images of substrates after the sessile drop test are showed in Figure 5.2. 6. On the surface, it is observed the drop of silicon and around of it a SiC ring in every case. However, the diffusivity of the silicon by the scratches is only significant on the R6650 substrate. Regarding the cross side images, the infiltration is almost negligible in R6650 and R6710 substrates, while Lorraine substrate shows a similar infiltration as Tokai substrates.

The results obtained for the Lorraine substrate, show values in agreement with the literature (0.65-0.95)⁸, but for R6650 and R6710 the value of infiltration rate are minimum, so in these cases, the infiltration was not managed by the reaction in the triple line.

Table 5.2. 5 contains the most relevant values from the top and cross section images, with properties of graphite substrates and work conditions included. The minimum spreading is for Lorraine substrates, while the minimum of infiltration is for R6710. According to this results is hard to find a relation with the characteristic parameters, such as porosity or

rugosity. Moreover, the infiltration rate was measured by $U_{inf} = \frac{h_{total}}{t_{inf}}$, where h_{total} is the maximum distance infiltrated as well as the ratios between the kinetics rate are included.

The results obtained for the Lorraine substrate, show values in agreement with the literature (0.65-0.95)⁸, but for R6650 and R6710 the value of infiltration rate are minimum, so in these cases, the infiltration was not managed by the reaction in the triple line.

Table 5.2. 5. Infiltration and spreading rates, values of effective radius and maximum infiltrated length according properties of graphite substrates and work condition

Material	Lorraine	R6650	R6710
Internal Radius (mm)	3.05	3.24	2.97
External radius (r_{eff}) (mm)	3.60	3.62	3.34
Maximum radio (mm)	2.85	3.58	3.46
Infiltration (h_{max}) (mm)	1.41	0.31	-
Temperature	1424°C		
Atmosphere	Argon		
Ra (μm)	0.34	0.32	0.19
Porosity	18%	20%	32%
Av pore diameter (μm)	10.62	8.94	7.52
Uinf	0.008	0.001	0
Uspr	0.009	0.013	0.006
Uinf/Uspr	0.89	0.07	0

- **SEM analysis of the Sessile drop samples**

Figure 5.2. 1. shows the top (right side) and the cross-section (left side) micrographs of the different substrates after sessile drop test. The scratches due to the fact of the substrates were ground, are remarkable on the surface of all substrates. As on the surface of Tokai

graphites, SiC crystals are found on the ridge of the silicon drop. However, the quantity of crystals is less on R6650 and R6710 substrates. Regarding cross-section, silicon has infiltrated and SiC layer was formed on the interface between silicon and graphite.

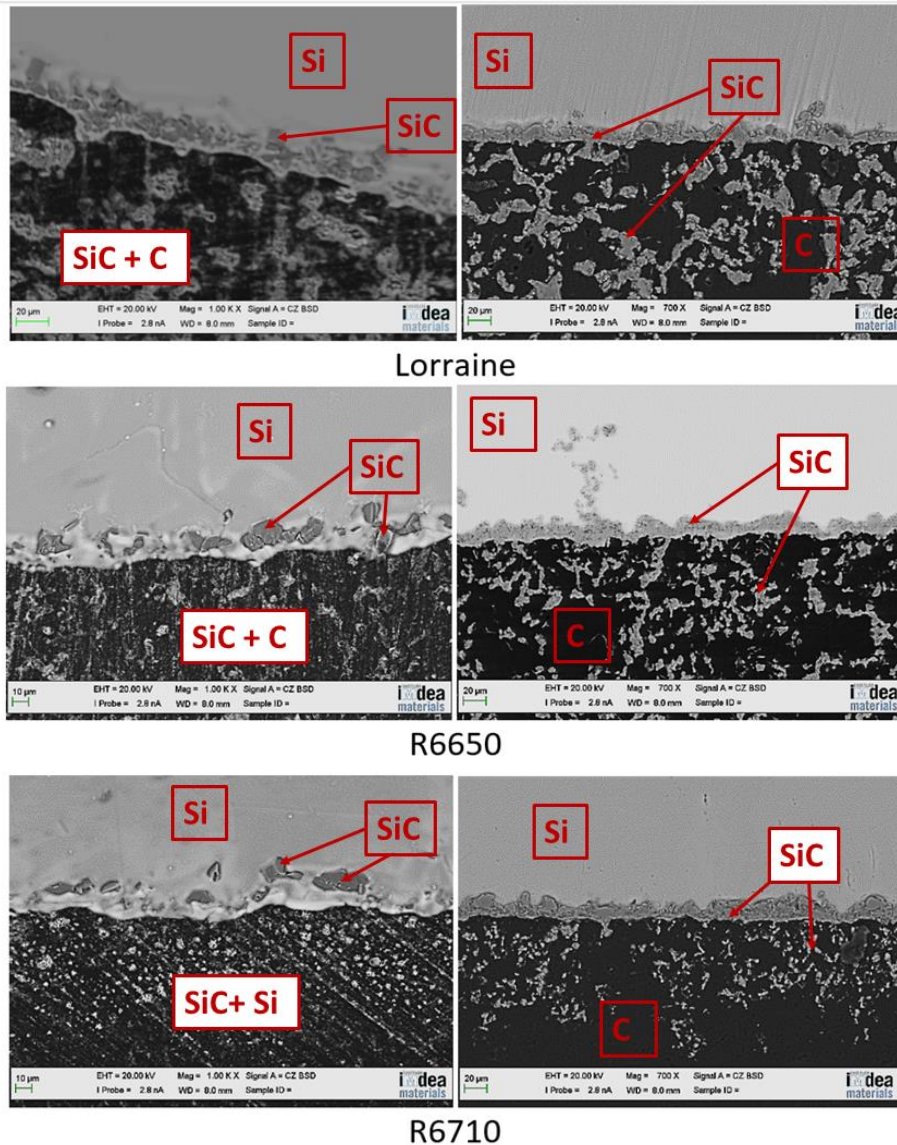


Figure 5.2. 7. Micrographs of a. Lorraine, b. R6650 and c. R6710 after sessile drop test

Figure 5.2. 7 shows the values of the thickness of the SiC layer formed on the interface. The values, as well as the thickness of the SiC crystal formed on the silicon close to the triple line, are in agreement with the literature and with the obtained results for Tokai graphite substrates

Table 5.2. 6. Values of the SiC layer thickness (e) and the thickness of the SiC crystals formed around the silicon droplet (e_d)

	Lorraine	R6650	R6710
$e(\mu\text{m})$	15.9	15.9	14.6
$e_d(\mu\text{m})$	19.4	22.6	19

- **X-Ray and Raman analysis of the Sessile drop samples**

X-ray (Figure 5.2. 8) and Raman (Figure 5.2. 9) analysis show how the silicon spreads and reacts with the carbon on the surface. Besides, during the infiltration silicon also reacts with the graphite from the wall of the pores although unreacted silicon was found in both cases.

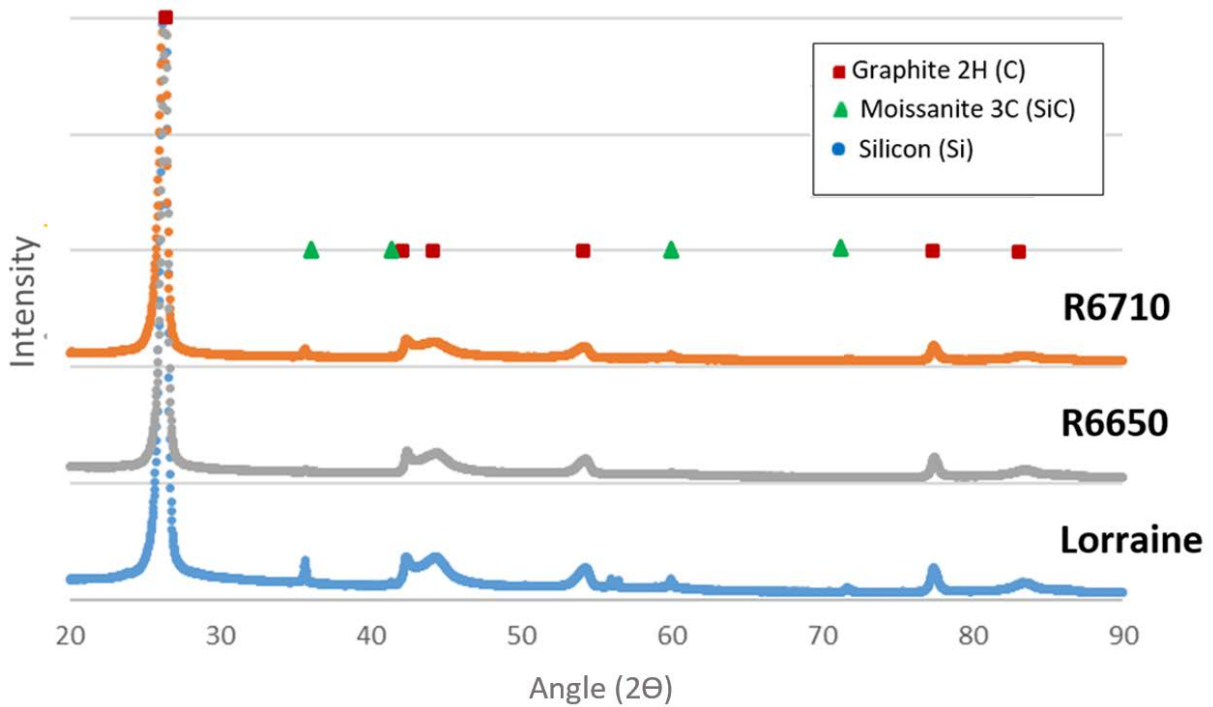


Figure 5.2. 8. X-Ray results of graphite substrates after Sessile drop test.

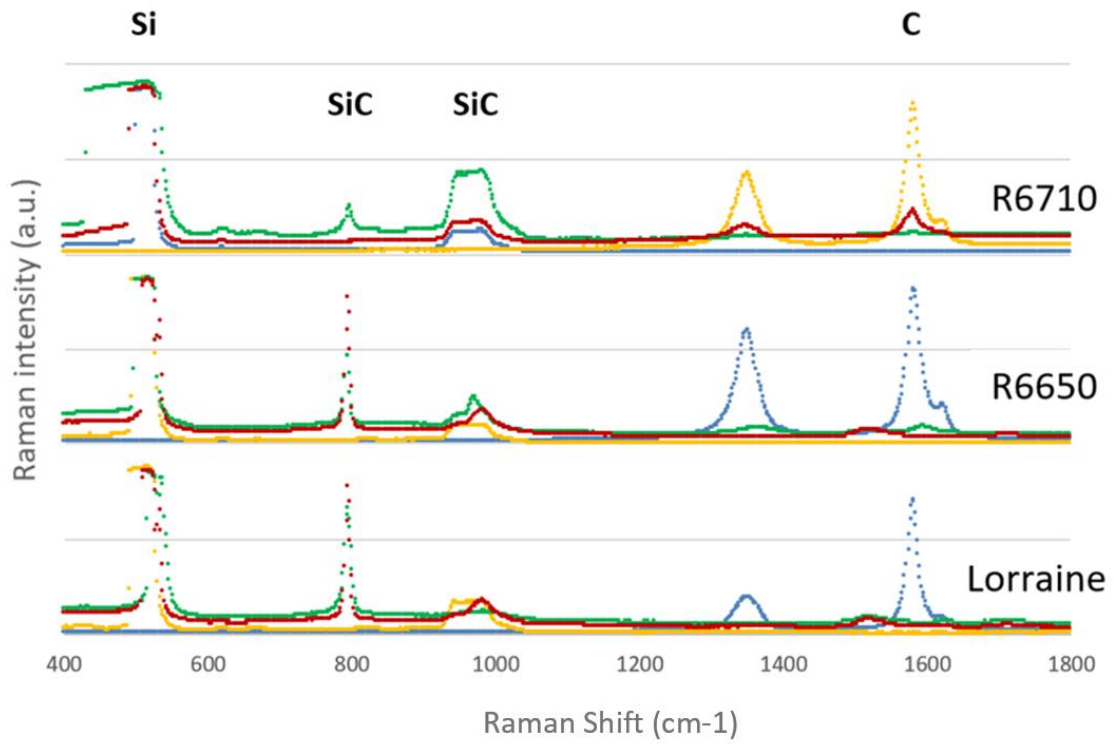


Figure 5.2. 9. Raman shift results after the Sessile drop.

5.3 Discussion

In this chapter, the behaviour of melting Silicon against different graphite substrates was analysed by the Sessile drop method in order to get knowledge about spreading and infiltration. In addition, the effect of the atmosphere was analysed by induction furnace tests.

Regarding the porosity analysis, the density of the graphite is quite similar ($\sim 2.10 \text{ g/cm}^3$), while there is a scatter of values for the percentage of porosity from 11% to 23% as well as the pore mean size from 7.48 to 11.69 μm .

The pores were on the grain boundaries, and the quantity or size depends on the size of the grain. Thus, some of the substrates have big grains such as G347 or the Lorraine substrate, although others like G330 or R6710 have small grains. On the other hand, none of the substrates show a noteworthy interconnectivity, but it is considered that silicon can dissolve graphite allowing the infiltration.

Some of the substrates were ground until 4000 μm and others were polished until 1 μm . The values of the average rugosity of the polished substrates were higher than the grounded ones, indicating that the pores were closed during the grinding of the substrates. However, deeper scratches were also found in these cases.

The Tokai, Lorraine and Sigrafine substrates lasted about 10 min to melt the silicon sample and to reach the equilibrium in the classic sessile drop. However, for the dispensed sessile drop, the equilibrium was reached in less than 10 s. According to Dezellus¹², this method allows to study the spreading kinetics, independently of the melting. In order to compare both methods, several points should be taken into an account:

- All of the substrates were heated until 1450 $^{\circ}$, but the process in the classic sessile method started at 1414 $^{\circ}$ while in the dispensed sessile method was at 1450 $^{\circ}$. Thus, the properties of the silicon are not the same.
- As the heating of the silicon took place in the same chamber, silicon can have been evaporated, condensed and reacted with the substrate.

On the other hand, the obtained curves in the Sessile drop test reveal certain similarities.

Firstly, there was a remarkable decrease in the contact angle and the height of the drop and then, the parameters kept decreasing but getting slower, as well as the width of the drop. At the beginning, the increase was sharp and after that, the spreading rate is slower. However, the ground substrates show a slower variation of the contact angle and the height drop than in the polished ones. In fact, they had the biggest final contact angle (40° - 50°), except R6650 where the silicon diffusion affects the final results. Despite the value of the average rugosity is lower for grounded substrates, the polished samples obtain less rough surface but with open pores. Thus, the Si-C reaction was hindered and also the infiltration. Other reason to believe that the reaction between silicon and carbide manage the behaviour against molten silicon is the fact that the width drop variation with the time is linear as Caccia et al⁵⁶ affirm. Only in the classic drop experiments, the values of spreading rate ($U_{spr} (dR/dt) \sim 10\mu\text{m}$)⁵⁶ were lower. Besides, the initial contact angles were close to 90° , indicating, that silicon does not wet substrates until the SiC layer is formed²¹

Observing the top view, the drops showed symmetry for the classic sessile method, except for R6650 substrate. The maximum radius measured during the experiment agrees with the obtained with the images after the experiment, indicating that the diffusivity or secondary wetting happened only in R6650. Meanwhile, the shape of the drop were ovals for the dispensed sessile method. The diffusivity was a key factor for the asymmetric results. On one hand, the deep scratches boosted the diffusivity for R6650. And, on the other hand, the higher temperature increases the speed of the reaction and decrease the silicon density boosted the diffusivity by the scratches.

Regarding infiltration, it is hard to define which factor affects this process. On one hand, the substrate used in the dispensed drop method shows a rise in the spreading distance and a reduction of the infiltration distance.

According to the curves, the variation in the dimensionless height drop of grounded substrates was slower than polished ones. However, carbon Lorraine substrate and G347 have the highest value of infiltration distance. There is also no clear relationship with the interconnectivity or the size of the pores. However, R6710 showed almost negligible

infiltration. Therefore, the recommendation is the low percentage of porosity and interconnectivity and small pore mean size.

Furthermore, the obtained micrographs in all the experiments are similar: on the top, SiC crystals are found on the ridge of the silicon drop. Meanwhile, on the cross-section, silicon has infiltrated and SiC layer was formed on the interface between silicon and graphite. The scratches due to the fact of the substrates were grounded are remarkable on the surface of grounded substrates.

During the experiment under high vacuum, the evaporation of the silicon was remarkable, so that, there was not a droplet over the graphite substrates. Besides, the values of the maximum spreading distances are larger than under argon atmosphere while the values of infiltration distances were smaller than argon ones.

In order to know the composition, X-ray and Raman analysis were done. The results illustrate that silicon spread and react with the carbon on the surface. Besides, during the infiltration silicon also react with the graphite from the wall of the pores, although unreacted silicon was found in both cases. This agrees to Novakovic et al⁵⁴, the 10% of silicon does not react when Si/C composites are obtained by the infiltration method.

CONCLUSIONS

In this chapter, the behaviour of melting Silicon against graphite substrates from several companies was analysed by the Sessile drop method in order to get knowledge about the spreading and infiltration. For this purpose, some of them were polished and other grounded and were used two different sessile methods: classic and the dispensed method.

The phenomena of infiltration and spreading for every substrate were managed to the reaction in the triple line. The grounded substrates showed the variation of contact angle slower than the polished ones, in fact, they were obtained the highest final contact angles. As well as the variation of infiltration was slower, but in this case, some of them were largely infiltrated. It is remarkably the superficial rugosity as a key factor for the spreading.

The results of the dispensed sessile drop method are quite different from the others. The equilibrium was reached in less than 10 s and the maximum spreading distance is very large on comparison with the other method. Initially, the obtained contact angle was close to 90° , thus the evaporation and the later condensation can be dismissed. On the other hand, the curves are alike the classic method. Therefore, the higher temperature can be the main factor of the remarkable speed and spreading showed in these experiments.

The effect of the silicon evaporation was a key factor during the vacuum experiment so that the infiltration was hindered and the spreading was boosted.

Finally, the best behaviour against molten silicon is showed by R6710, where the final contact angle is the highest, the spreading distance is low and the infiltration is negligible.

6. Coated graphite substrates

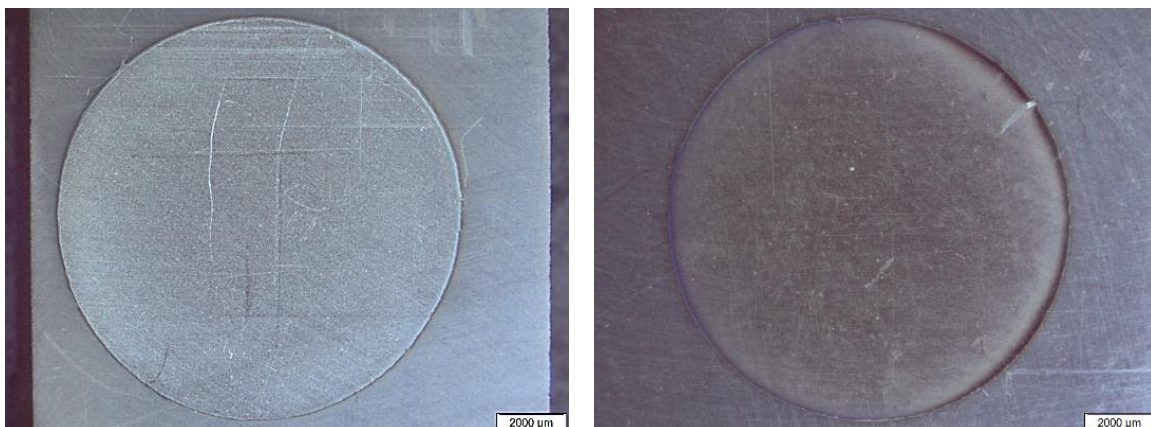
In this chapter will be studied the availability of the coated made of B_4C and TiO_2 for photovoltaic applications. Nowadays, several studies about coatings are being developed, for example, Si_3N_4 is used as a mechanical fusible during the crystallization of photovoltaic silicon in order to avoid the sticking⁴⁷. Besides, the coating avoids the infiltration and reduces the pollution of the molten silicon due to the coating is formed by a thin layer.

6.1 Boron carbide (B_4C)

Boron carbide is a covalent ceramic whose contact angle is not very high, but it is a reactive system, namely, the behaviour of molten silicon is controlled by the reaction. This fact could reduce the infiltration and the pollution would be controlled. In addition, the influence of the thickness of the coating will be analysed.

6.1.1 Characterisation of material

- **Optical microscopy analysis of Sessile drop samples.**



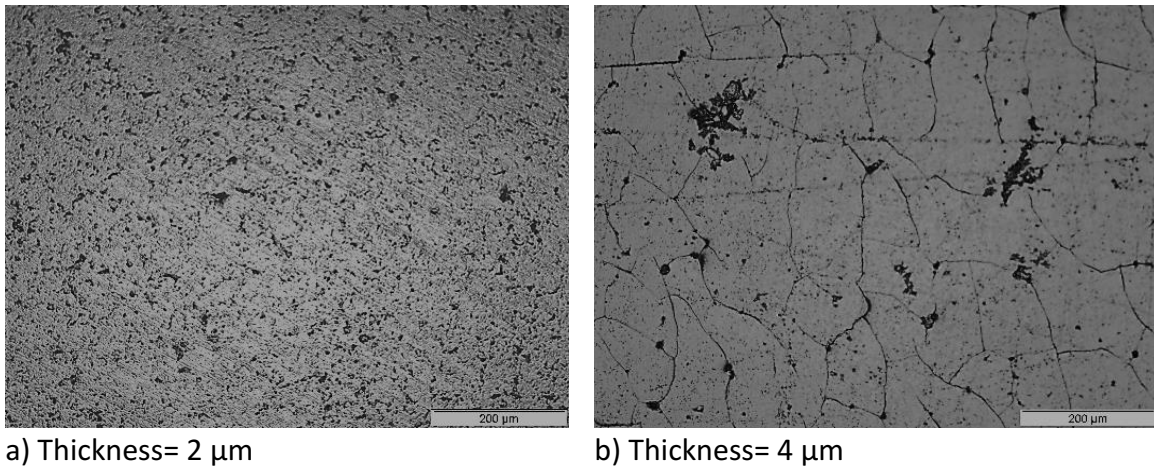


Figure 6.1. 1. Images of B₄C coatings a. 2 μm and b. 4 μm

The graphite substrates were coated with B₄C by chemical vapour deposition (CVD), the coating thickness of the samples obtained were 2 μm and 4 μm.

Figure 6.1. 1, show the samples with a higher coating thickness contains a higher quantity of the cracks.

6.1.2 Sessile drop test

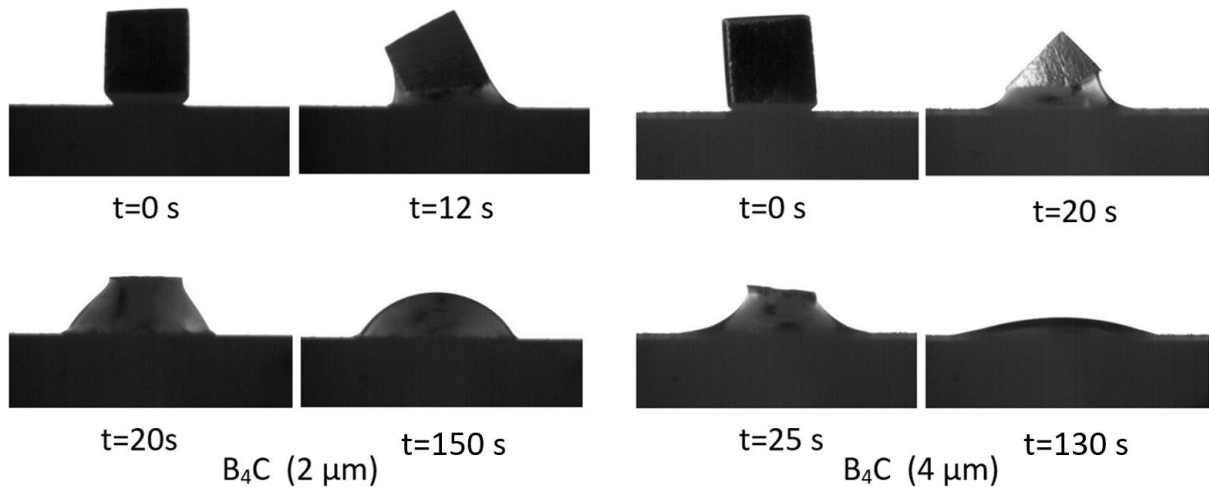


Figure 6.1. 2 Images of sessile drop test of B₄C coatings a. 2 μm and b. 4 μm

Silicon was melted on B₄C coated graphite substrates during the Sessile drop test. The silicon area in contact with the substrate started to melt, then the drop was formed and

finally, the equilibrium was reached in less than 150 s. The equilibrium is considered when the contact angle remains constant. In both cases, the drop looks like symmetric but the final value contact angle is higher for the 2 μm . In comparison, these processes are faster than the graphite substrate without coatings.

- **Analysis of the Sessile drop test**

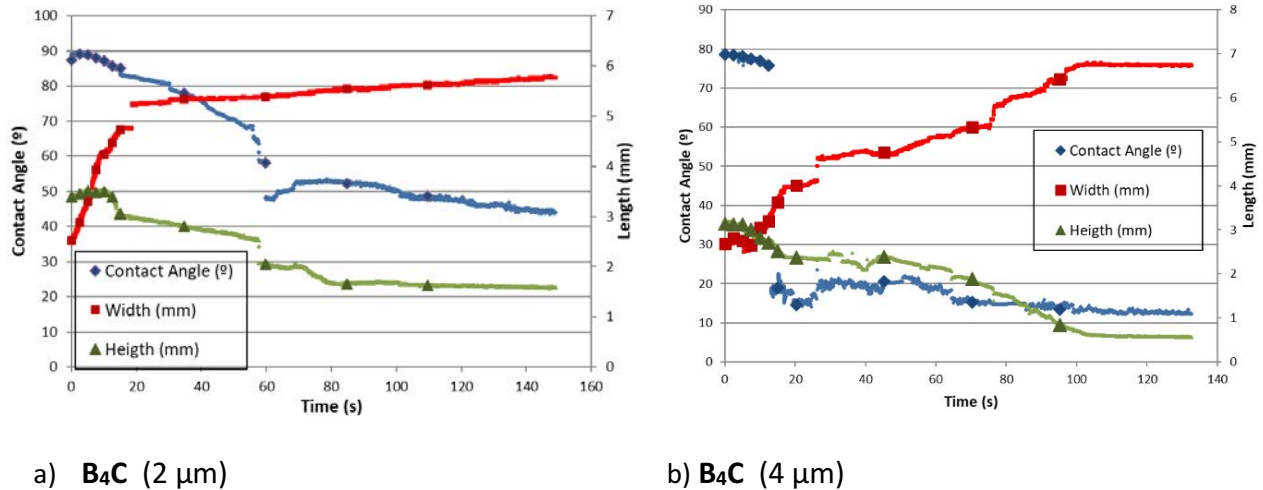
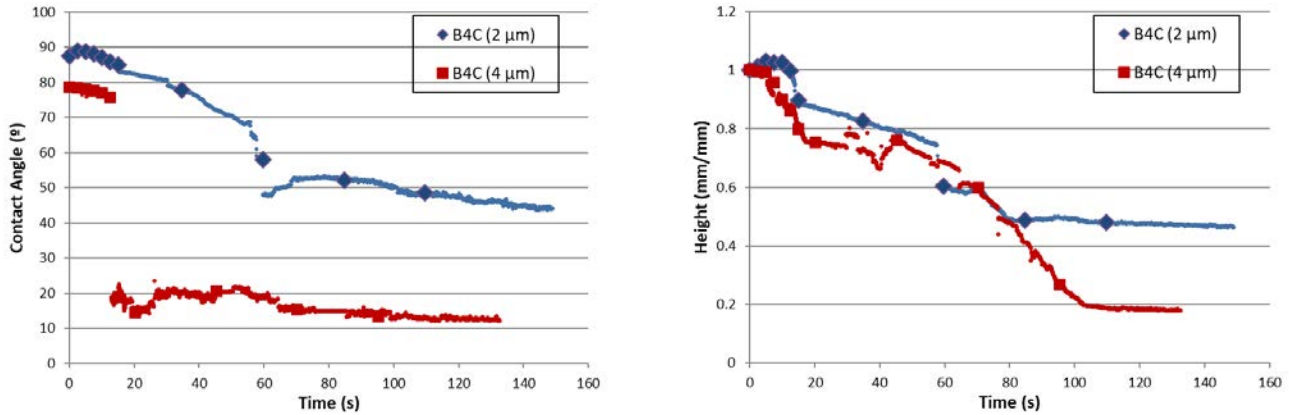


Figure 6.1. 3. Contact angle and parameters of silicon drop with time a) on B₄C (2 μm), b) B₄C (4 μm).

Figure 6.1. 3.a. shows the variation the contact angle with the time on the 2 μm B₄C coatings. In the beginning, contact angle and the height of the drop remains almost constant with the time, then there is a drop and finally, it keeps gently decreasing until reached the equilibrium. While the width of the drop increases linearly with the time, firstly very fast and then slower. This is a consequence of a chemical reaction that has taken place. Figure 6.1. 3.b illustrates the variation of contact angles and drop parameters (height and width) with the time on the 4 μm B₄C coatings. As in the previous case, contact angle and the height of the drop remains almost constant at the beginning, then there is a drop and finally reached the equilibrium while the width of the drop linearly increased with the time.



a)

b)

Figure 6.1. 4. Comparison of variation of a. contact angles and b. relative drop height (mm/mm) of substrates with the time

On the other hand, the comparison of the contact angle variation is shown in Figure 6.1. 4.a. The behavior is similar but there are remarkable differences such as the value of initial and equilibrium contact angle. The substrate with the thinner coating has an initial contact angle close to 90°, as in the case of carbon-silicon system. Then, the value decreases but the equilibrium is obtained around 45°. However, the initial contact angle for the thicker coated substrate shows a slightly lower value than the carbon-silicon system. Besides, there is a sharp drop which significantly reduces the value of the equilibrium angle until 15°.

Figure 6.1. 4. illustrates the variation of the dimensionless height of the drop, being the behavior very similar for both coatings. The only difference is that the thinner coated substrate reaches the equilibrium faster than the thicker coated substrate

Table 6.1. 1. Spreading and infiltration rate measured on several graphite substrates before and after drop formation

	B ₄ C (2 μm)	B ₄ C (4 μm)
Uspr (mm/s)	0.004	0.015

The Table 6.1. 1 provides the value of the spreading rates. The values are around 10 μm/s as in the Silicon- Carbide system.

- **Optical microscopy analysis of Sessile drop samples.**

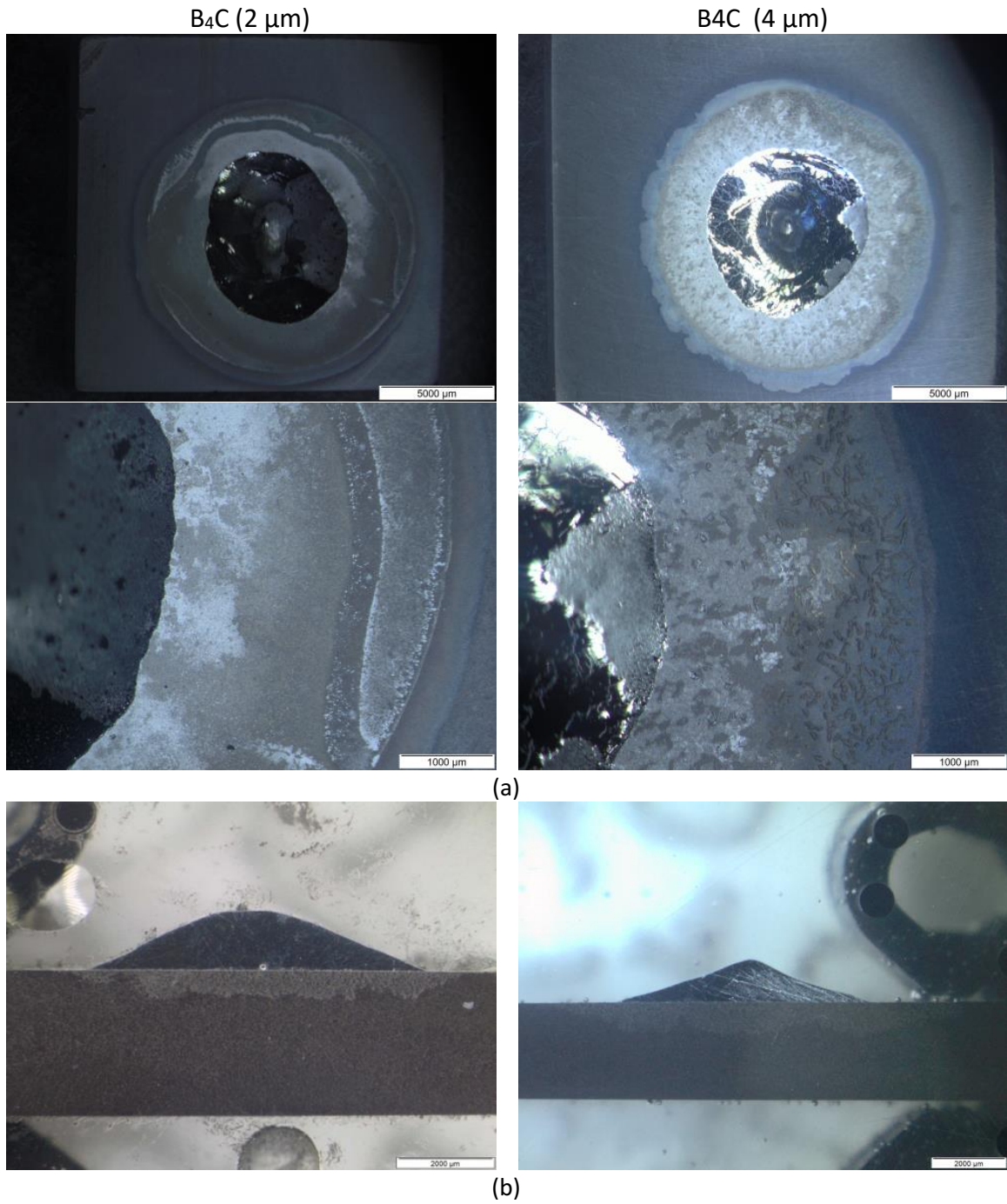


Figure 6.1. 5. a. Top view and b. side view images of substrates after sessile drop test.

After the sessile drop test, top and side view images of the coatings substrates were taken by the optical microscope and are shown in

Figure 6.1. 6. According to the images, silicon has broken through the B₄C coating, so that the drop, in both cases, is not symmetric. Spreading was more hindered in the thinner coated than the thicker. However, the infiltration was reduced in both samples. Hence, the cracks in the thicker coating substrate are a key parameter in this study.

Table 6.1. 2 provides the effective radius measured after the test by the optical microscope and the maximum radio measured during the experiment, the values are no similar due to the lack of the symmetry of the drop. The values of maximum spreading and infiltration are higher in the thicker coating sample than the thinner ones. This is possibly due to the thinner coating is more homogenous while the thicker have several cracks, facilitating the silicon spreading. Moreover, provides the value of the kinetics rates. These values correspond with the values obtained by the silicon-graphite system. The values are around to 10 $\mu\text{m/s}$ and the ratio between kinetics rate lie between (0.65-0.85)⁸. Although the kinetics rate for B₄C (2 μm) slower than B₄C (4 μm) and in comparison of graphite substrate.

Table 6.1. 2. Values of effective radius and maximum infiltrated length according properties of graphite substrates and work condition.

Material	B₄C (2 μm)	B₄C (4 μm)
Internal Radius (mm)	3.23	3.84
Maximum radio (mm)	2.87	3.37
Infiltration (h_{total}) (mm)	0.67	1.07
Temperature	1450°C	
Atmosphere	Argon	
U _{inf} (mm/s)	0.004	0.008
U _{spr} (mm/s)	0.005	0.015
U _{inf} /U _{spr}	0.8	0.55

- SEM analysis of the Sessile drop samples

a. B₄C (2 μm)

b. B₄C (4 μm)

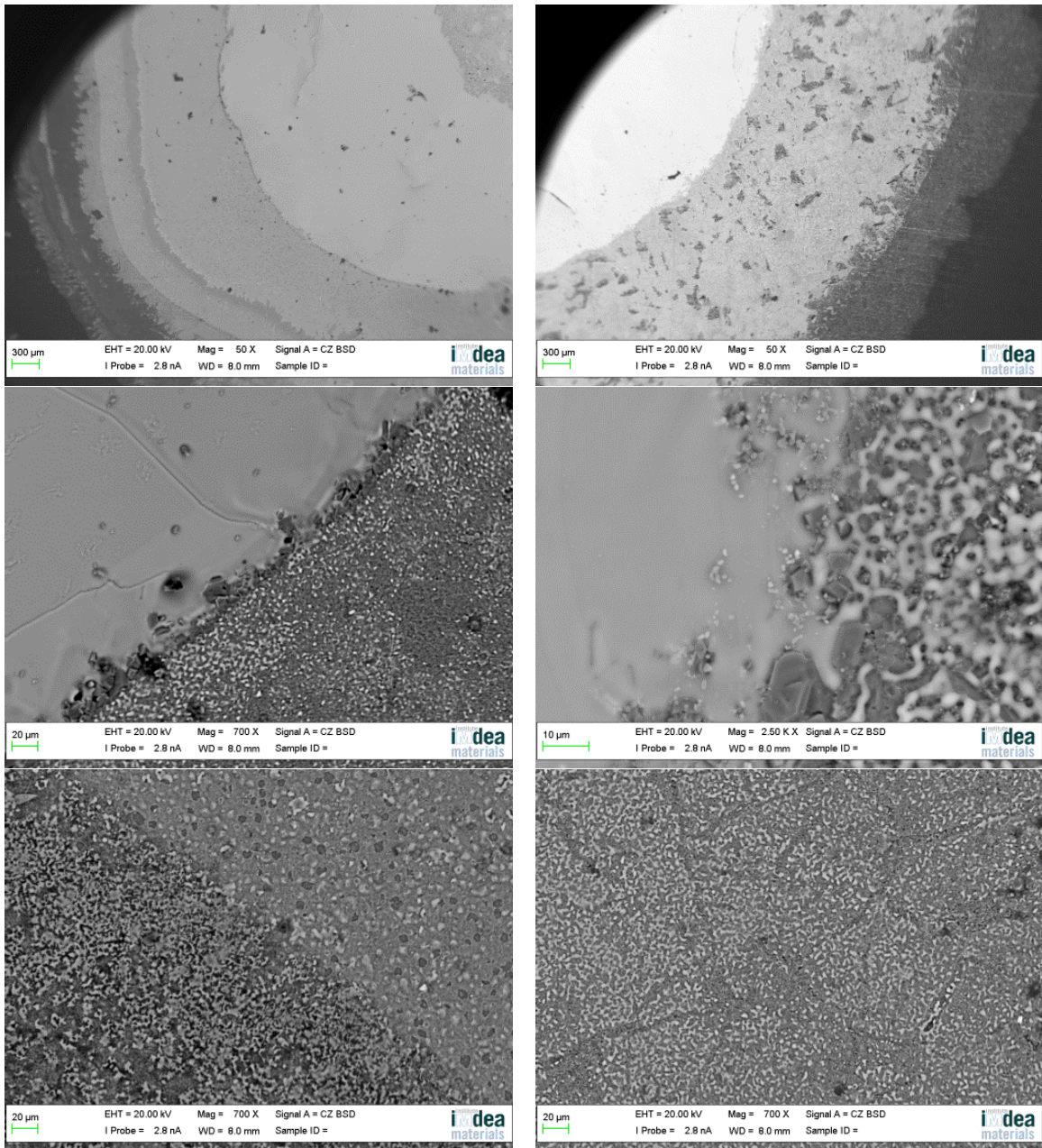
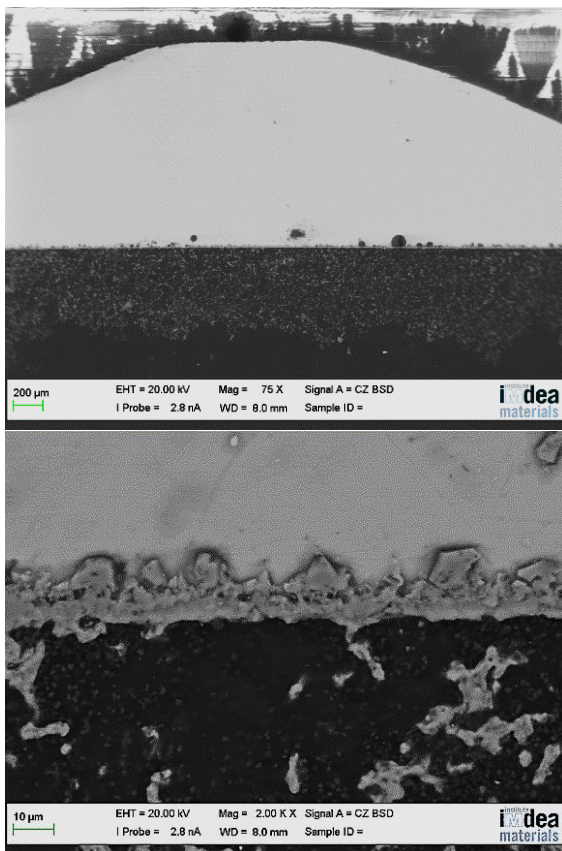
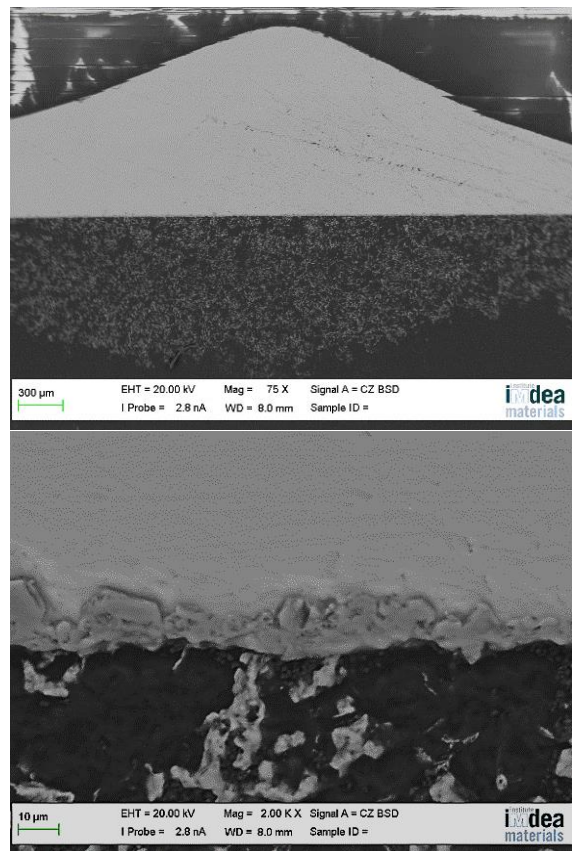


Figure 6.1. 6. Top view micrographs of a. B₄C (2 μm) and b. B₄C (4 μm).

Figure 6.1. 6. shows the micrographs on the left side the $4\mu\text{-B}_4\text{C}$ coating and the right side the $2\mu\text{-B}_4\text{C}$ coating. For the thinner coating substrate, several concentric rings around the drop can be seen. According to the EDX analysis, the main difference between each area is the quantity of silicon and carbide; as one moves away from the centre, the amount of pure silicon decreases and the quantity of silicon carbides increases until the ends of the sample, there is only graphite and silicon carbide. It is significant that boron is not found in the EDX analysis. On the other hand, $4\mu\text{-B}_4\text{C}$ coating shows around the silicon drop ~~an~~ only one ring formed by silicon and SiC but no boron is found. These results indicate that the silicon dissolved the B_4C coating, and due to the cracks this process was faster in the thicker coating substrate obtaining a more homogeneous compounds area. Besides, the ease of spreading makes the contact angle decreases.

a. B_4C (2 μm)b. B_4C (4 μm)

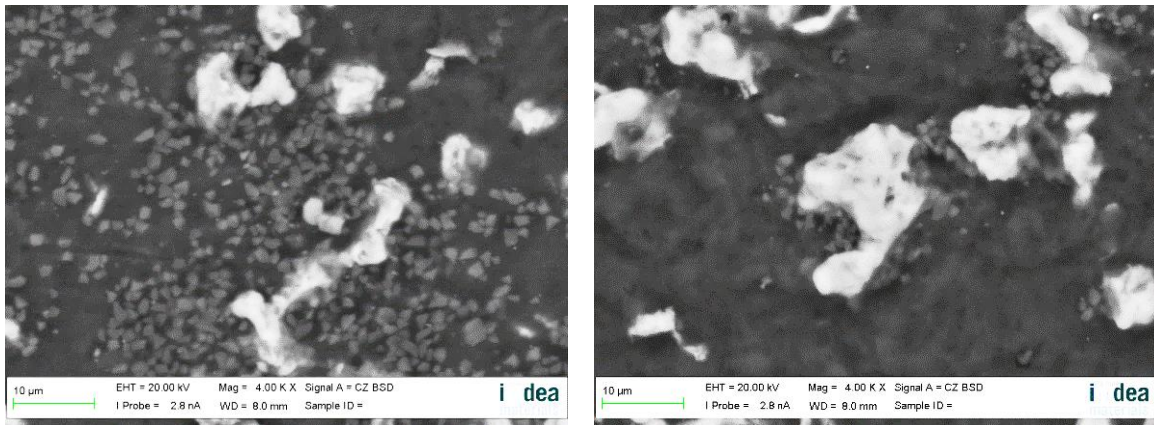


Figure 6.1. 7. Cross section micrographs of a. B₄C (2 μm) and b. B₄C (4 μm).

Figure 6.1. 7 shows the cross section micrographs of B₄C coating substrates after sessile drop test. SiC layer was formed on the interface silicon drop and substrate in both samples. Silicon infiltrated the pores which were closed by SiC as silicon-carbide system, but unlike, there are several small Si₂O crystals. Silicon was polluted by the oxide from the coatings. Table 6.1. 3 shows the values of the SiC layer thickness (e), these values correspond to Si/C system.

Table 6.1. 3. The values of the SiC layer thickness (e).

	B₄C (2 μm)	B₄C (4 μm)
e(μm)	13.1	12.6

- X-Ray and Raman analysis of the Sessile drop samples

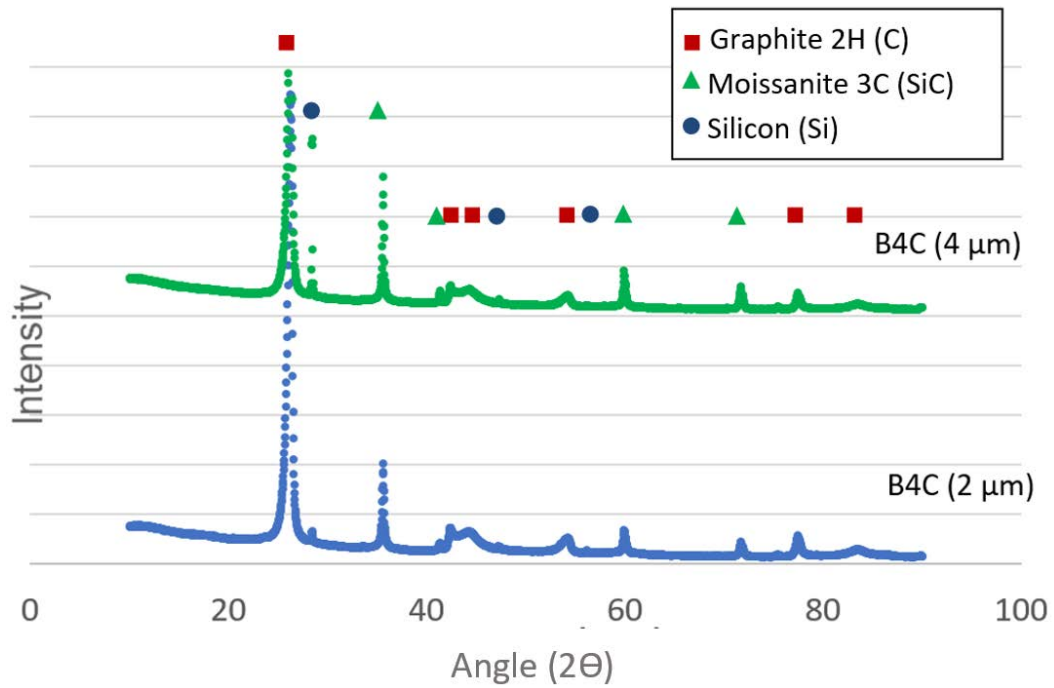


Figure 6.1. 8. X-Ray results of coating graphite substrates after Sessile drop test.

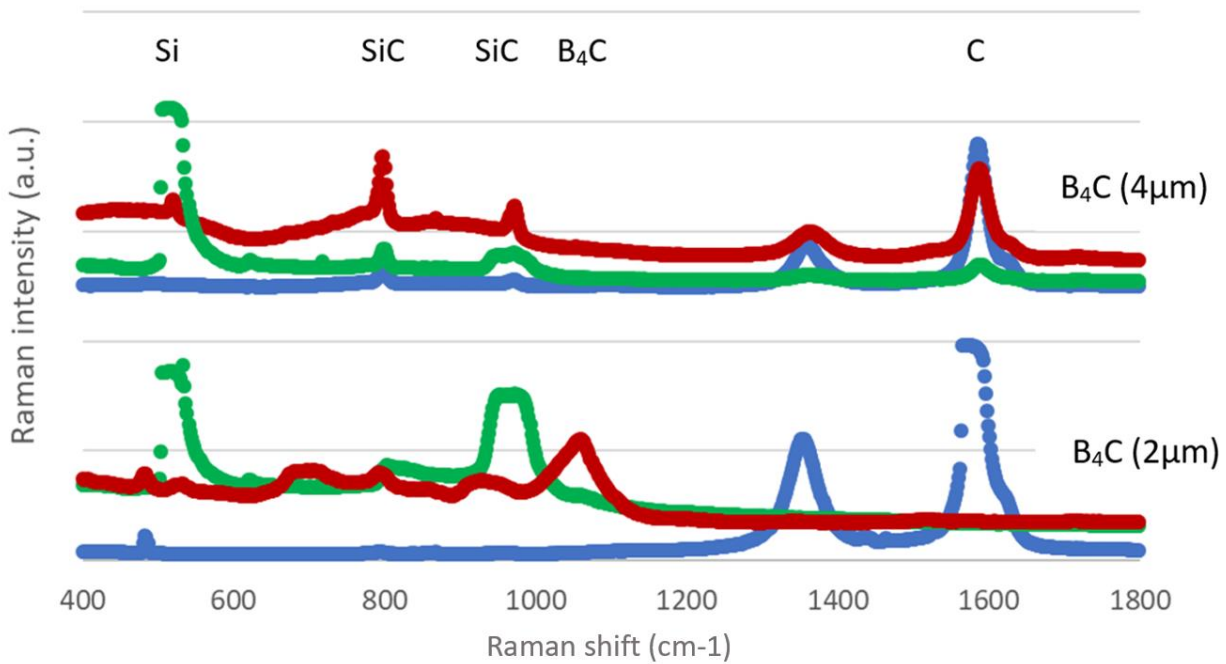


Figure 6.1. 9. Raman shift results of graphite substrates after Sessile drop test.

The chemical composition was analyzed by X-ray diffraction (Figure 6.1. 8) and by Raman micro-spectroscopy (Figure 6.1. 9). The results are similar to Silicon-carbon system, silicon carbides have been formed by reaction of pure silicon from the drop and the graphite, from the substrates. It is remarkable that a low quantity of B_4C has been found in the $2\mu\text{m}$ -coating substrates. This reinforces the theory that silicon dissolves the coating during Sessile Test and that this process was much faster for the thicker coating, despite the greater amount of B_4C , due to the cracks. Moreover, the oxides or impurities present in the micrographs are not found in these studies, likely, the quantity is very low and the signal is hidden by the others.

6.2 TiO₂ Coatings

In general, the titanium improves the wetting for metals, but there is not any study about its effects on silicon²¹. Besides, the oxides show a high contact angle and the titanium has also a high affinity for the oxygen.

6.2.1. Characterisation of materials

In order to get TiO₂ coatings were obtained by a sputtering in spite to use pure titanium as a wafer, a passive layer was formed by TiO₂ instantaneity due to the oxygen of the air and the coating thickness was 0.5 μm to obtain a homogenous lawyer.

6.2.2.1 Sessile drop test

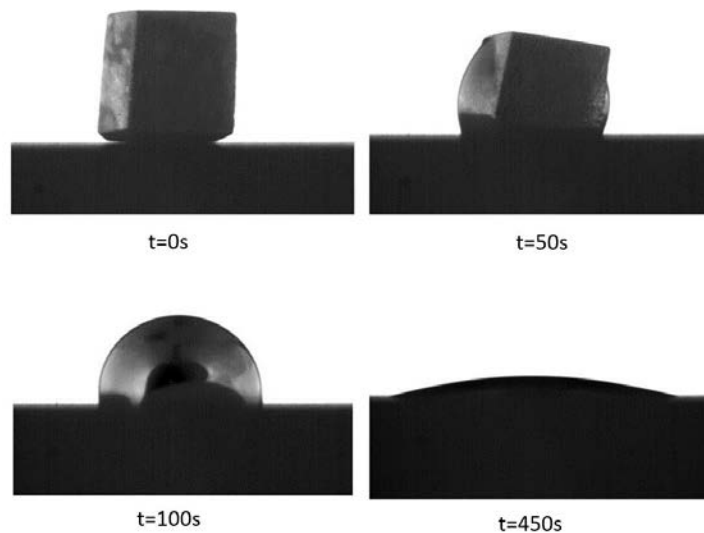


Figure 6.2. 1. Images of sessile drop test on TiO₂ coating substrate.

Silicon was melted on TiO₂ coatings graphite substrates during Sessile drop test under argon. As it happened in the other cases, the silicon started to melt at the bottom of the sample, then the drop was formed and finally, the equilibrium was reached in less than 8 min. The equilibrium is considered when the contact angle and the other parameters remain constant. Regarding the images, the drop seems symmetric and, finally silicon wet perfectly the TiO₂ coating substrate, and namely, the final contact angle is zero.

- **Analysis of the Sessile drop test**

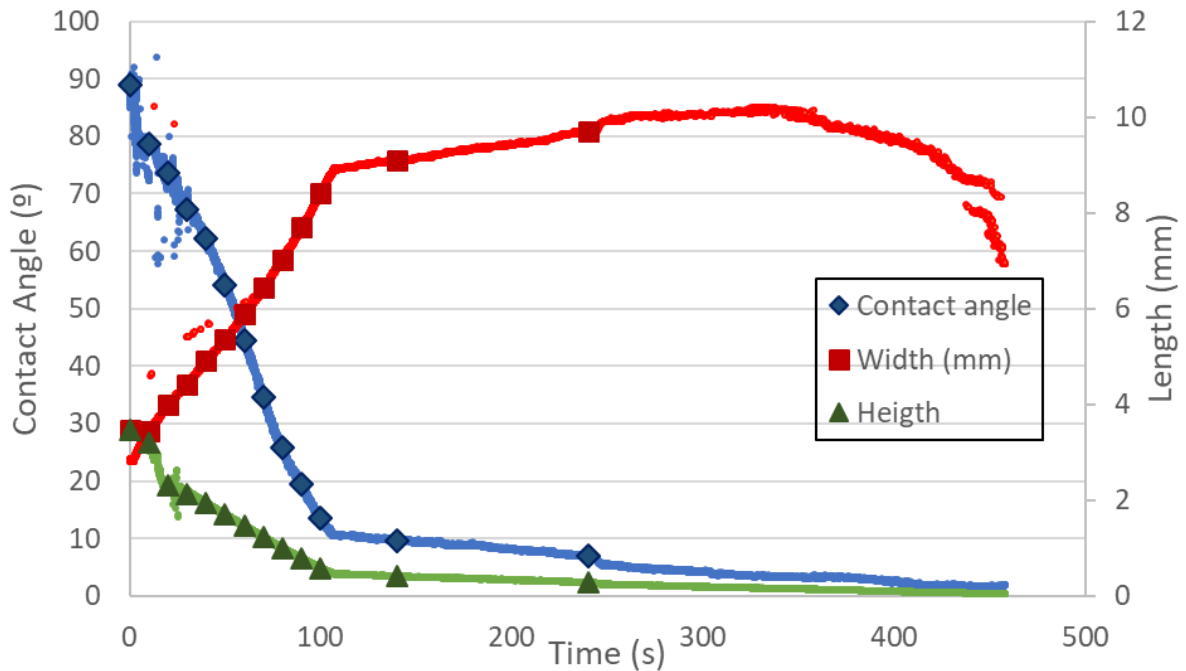


Figure 6.2. 2. Contact angle and parameters of silicon drop with time on substrate coated by TiO_2 .

As Figure 6.2. 2 in the beginning, the contact angle is close to 90° , as was in the silicon-graphite system, then there is a drop and then, it keeps decreasing slower until 0° . In the same way, the height of the drop sharply decreases firstly, but then the reduction is slower until the silicon infiltrated by the pores of the material. Whereas the width of the drop highlighted increased at the beginning, then there is also an increase but slower than before and finally, there was a reduction of the width due to the totally infiltration of the drop. The linear increase of width with the time indicates the reaction of silicon with the graphite manages the spreading and the infiltration. Besides, the spreading rate ($U_{\text{spr}} = dR/dt$) is close to $10 \mu\text{m/s}$ and the relation of kinetics rate ($U_{\text{inf}}/U_{\text{spr}}$) lies in the interval 0.65 and 0.952 shown in Table 6.2. 1.

Table 6.2. 1. Spreading rate of TiO₂ coating after Sessile drop test.

	TiO ₂
Uspr (mm/s)	0.012

- **Optical microscopy analysis of Sessile drop samples.**

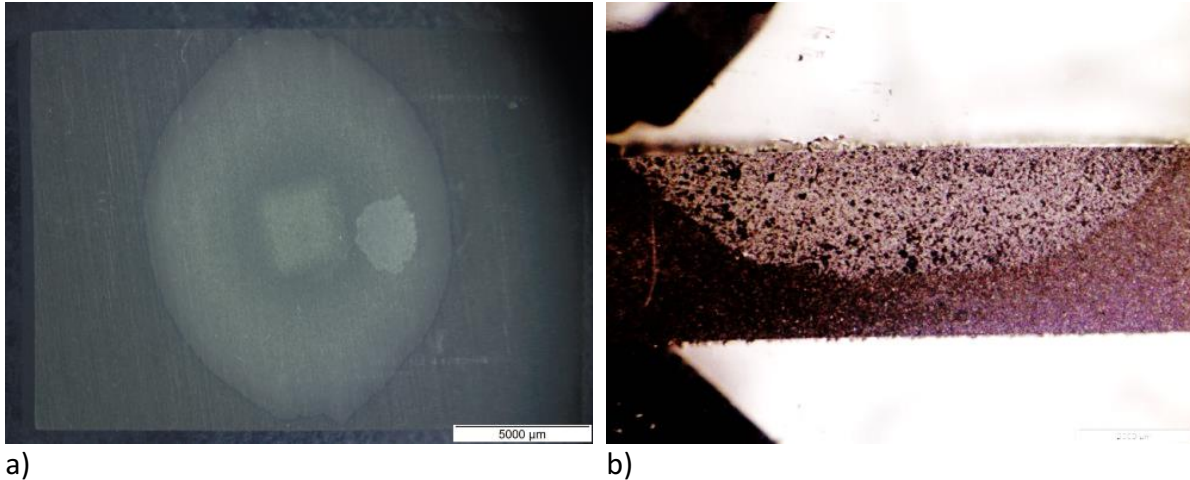


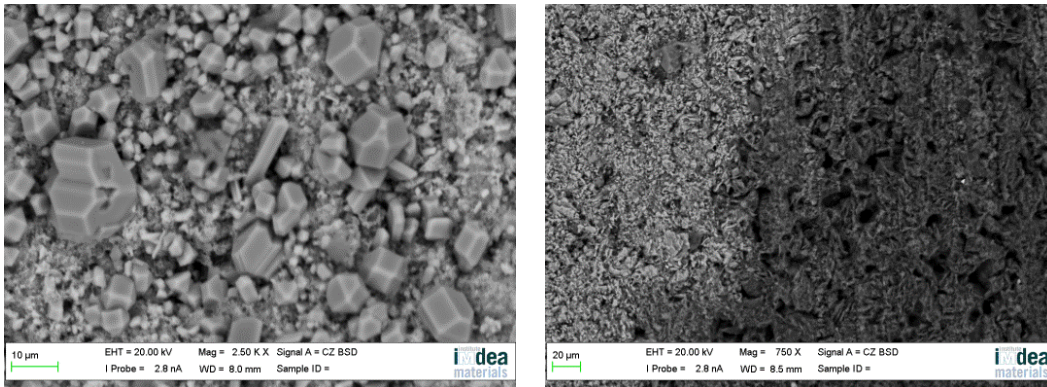
Figure 6.2. 3. a. Top view and b. side view images of TiO₂ coating substrates after sessile drop test.

Figure 6.2. 3 shows the top and side view of the TiO₂ coating after having been melted silicon on it during the Sessile drop test. Regarding the top side, the drop was not symmetric and the spreading was faster in one direction. The cross section indicates that silicon could infiltrate deeply by the pores. Table 6.2. 2 shows the values of the effective radius measured from the images from the optical microscope, as the shape of the drop is an ellipse two effective were measured from the main diameters. However, the value of maximum radio measured during the Sessile drop test is lower than the effective radius due to the lack of symmetry of the drop. Besides, the kinetics rate are included, the values of the Uinf and Uspr agrees with Si/C system but the ratio is lower than the theoretical values²¹.

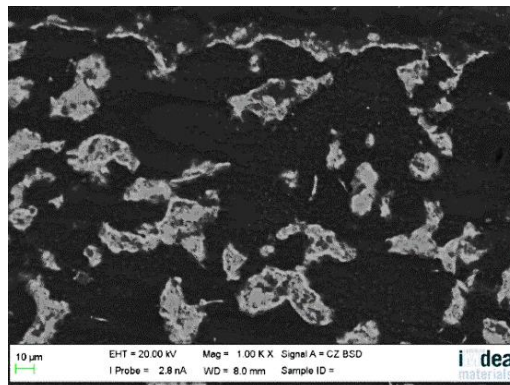
Table 6.2. 2. Values of effective radius and maximum infiltrated length according properties of graphite substrates and work condition.

Material	TiO ₂
Effective Radius (mm)	11.4 14.04
Maximum radio (mm)	10.22
Infiltration (h_{total}) (mm)	2.37
Temperature	1450°C
Atmosphere	Argon
Uinf (mm/s)	0.005
Uspr (mm/s)	0.012
Uinf/Uspr	0.43

- SEM analysis of the Sessile drop samples



a)



b)

Figure 6.2. 4. Micrographs of TiO₂ coating substrate a. top view and b. cross section.

On the top view micrographs and according to EDX- analysis, Si crystals are shown in the center of the sample (left side of Figure 6.2. 4.a), and as we move away from the center, these crystal are decreasing until becoming a thin SiC lawyer (left side of Figure 6.2. 4.a). Besides, oxides impurities are also found in the EDX-analysis but in a low quantity.

On the cross section micrographs (Figure 6.2. 4.b), pores closed by SiC are found as in the silicon-graphite system. However, there are also oxides impurities from the TiO₂.

- **X-Ray and Raman analysis of the Sessile drop samples**

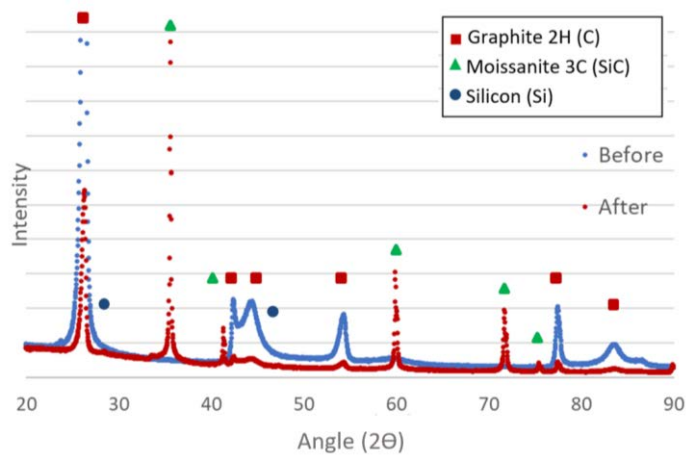


Figure 6.2. 5. X-Ray results of TiO₂ substrates after Sessile drop test.

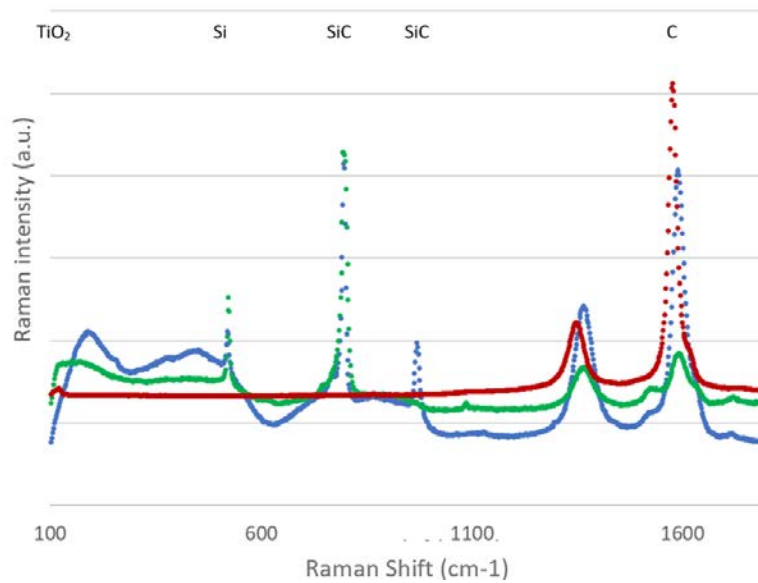


Figure 6.2. 6. Raman shift results of TiO₂ substrates after Sessile drop test.

Figure 6.2. 5 show the X-ray results before and after the sessile drop test, TiO_2 is not found in any of the analysis due to the layer is very thin and other signals are more intensive. However, the results reflect that silicon has reacted with graphite obtaining silicon carbides as the silicon and graphite system. On the other hand, TiO_2 is found in Raman results (Figure 6.2. 6), showing molten silicon dissolve the titanium oxide and then, reacted with the graphite of the substrate.

CONCLUSIONS

In this chapter was studied the behaviour of the coated substrates against molten silicon, B₄C coatings were obtained by CVD (chemical vapour deposition) and TiO₂ by sputtering.

Regarding the spreading and infiltration, the system silicon-carbide is slower than the coating, indicating, that the reaction in the triple line does not manage the phenomena despite the linear relation between the variations of the width with the time. However, the kinetic rates of TiO₂ coating agree with the values for silicon-graphite system²¹.

According to reactivity, the silicon carbide layer was formed on the surface and the pores of the graphite were closed by SiC. However, impurities were found in the micrographs from the oxides of the coating.

First of all, silicon likely spread and infiltrated faster than graphite substrate due to the coating. The thicker was the coating, the faster silicon reached the equilibrium. Then, silicon started to dissolve the coating. Once the coating was dissolved, silicon reacted with the graphite from the substrate and the oxides from the coating.

These coating can not be used in solar application because of the oxide pollution. However, B₄C hindered the infiltration.

7. Study of the surface

7.1 Introduction

According to several authors^{12,17,24}, the reaction on the triple line between silicon and carbide is a key factor in the system molten silicon and carbide. In fact, the molten silicon does not wet graphite, but once silicon carbide is formed, the obtained contact angle is around 25°-40°. The spreading and the infiltration are also affected because of the reaction; these phenomena's are faster than in non-reactive system²¹. The system presents a linear variation of the width with the time, the spreading is around 10 mm/s and the kinetic rate (U_{inf}/U_{spr}) laid between 0.65-0.95, is assumed that it is managed by the reaction in the triple line¹⁷.

There are plenty of studies using the sessile drop test, Israel et al⁹ explain that at the beginning silicon starts to melt at the bottom of the sample where is in at beginning silicon start to melt at the bottom of the sample on the are in contact with the graphite substrate. The reaction is spontaneous at 1414°C at room pressure and under argon atmosphere¹³. So that, when the molten silicon is in contact with the graphite the reaction stars at the same time, and silicon starts to infiltrate through the pores. Then, when the silicon is placed in silicon starts infiltrate by the pores. Once the pores are closed by silicon carbide, the infiltration is over and a silicon carbide layer is formed in the interface⁹.

According to several authors³²⁻³⁵, the SiC layer formed on the interface is a bilayer, namely, firstly a thin layer of SiC is formed then, because of the saturation of the silicon SiC crystal are formed until homogenous thicker layer is formed. However, there are some distinctions about the formation and the thickness of the layer. In spite of the large existing literature, there is a not accuracy study about the formation of silicon carbide layer, thus, this chapter is focused on the reaction in the triple line, the formation of silicon carbide and the infiltration.

7.2 Induction furnace test and characterisation of the material

The G348 graphite was chosen as substrate. The samples were ground and polished to avoid scratches and the quantity of the silicon samples were around 80mg. The tests were done by induction furnace and as a consequence the heating and cooling steps are faster than in other furnaces, but during the experiment, it was not possible to record it. The samples were heated a certain time and then fast cooled in order to reproduce the process of molten silicon against graphite substrate, but analysing every step. Thanks to a previous study in the induction furnace, it is known the working conditions when the system reaches the equilibrium. Thus, the duration of experiments was 12, 13, 14, 15, 17 and 22 min, being at 12 min when the interaction silicon- graphite starts and at 22 min when the equilibrium is reached. The maximum temperature was 1450°C and the atmosphere used was argon, although previously, there were cycles of vacuum performed in order to avoid the oxidation.

7.3 Analysis of results

- **Optical microscopy analysis of Sessile drop samples.**

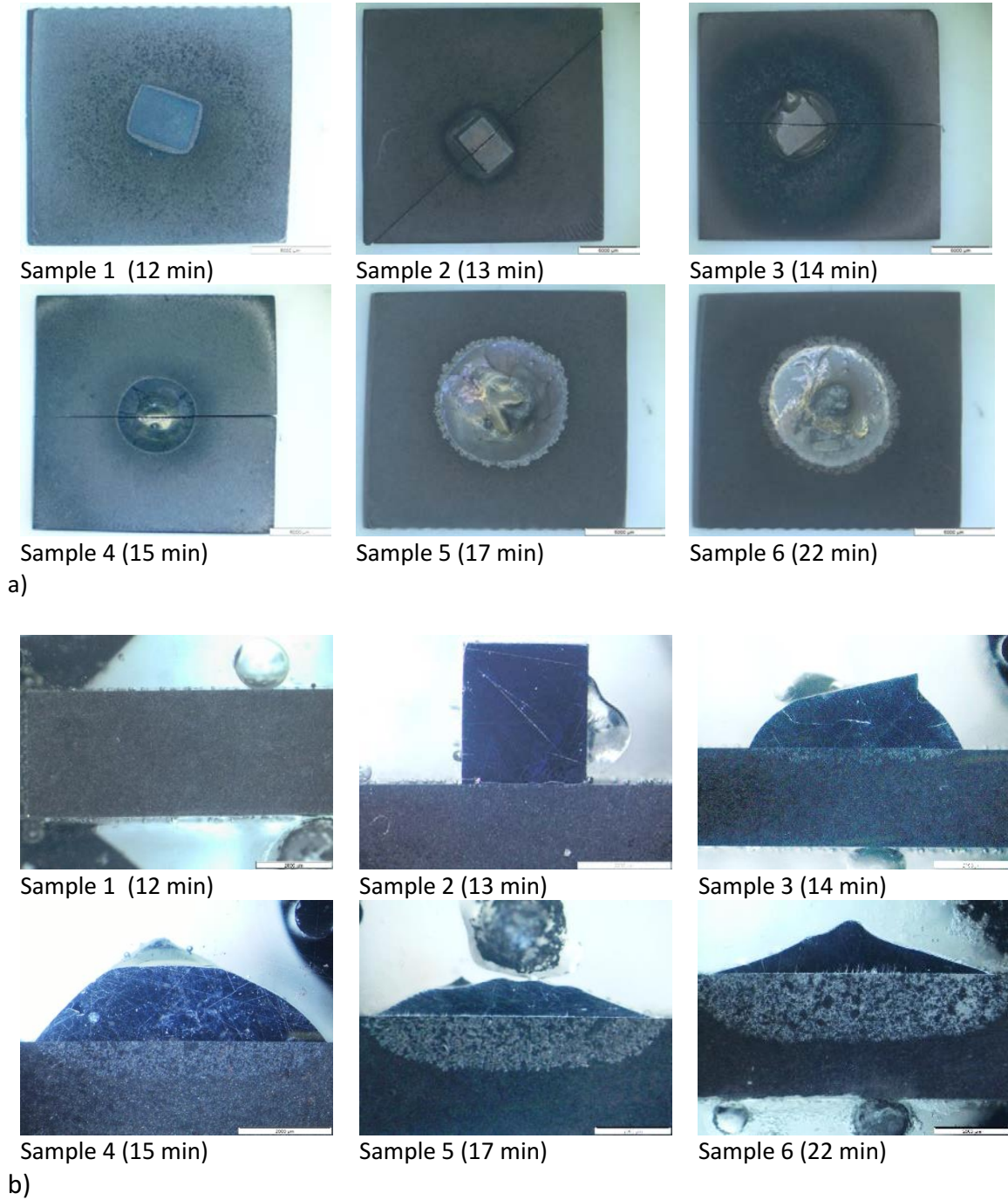


Figure 7. 1. a. Top view and b. side view images of substrates after induction furnace test.

After the induction furnace experiments, the samples were analysed by optical microscope and the images from the top view can be seen in Figure 7. 1.a, while the cross section in Figure 7. 1.b. Regarding the images, the interaction starts at 12 min, but it is not strong enough to fix the silicon sample on the sample. Then, a minute later, the silicon infiltrate and spread fixing the silicon on the substrate. The sample 3 shows while the drop is not formed yet, and the spreading and the infiltration have progressed certain distance. Once the drop is formed in the sample 4, a thin ring around the drop is seen, likely, it was the front of the triple line where the silicon and graphite are reacting and the silicon carbide is obtained boosting the spreading of the drop. When the spreading is over, the maximum diameter is obtained but the infiltration continues, so that the diameter decrease, in this case, and the ring around the drop is more visible due to the more quantity of the silicon present, as it occurs in the sample 5. Finally, the infiltration is over and the equilibrium is reached in the sample 6.

Table 7. 1. Values of maximum width spread (W_{max}) and maximum infiltrated length (h_{inf}), and the diameter of D) from the optical images.

Sample	t (min)	h_{inf} (mm)	W_{max} (mm)	Drop	D (mm)
Sample 1	12	0	0	No	-
Sample 2	13	0.08	2.76	No	-
Sample 3	14	0.47	5.86	No	-
Sample 4	15	0.85	6.45	Yes	6.36
Sample 5	17	1.56	8.39	Yes	8.06
Sample 6	22	1.85	8.72	Yes	7.89

Several interesting values from the images of the optical microscope were calculated and they are shown in Table 7. 1. The maximum width spread and the maximum infiltrated length were obtained from the cross-section and the diameter of the drop from the top view. The infiltration increases with time, not only due to the time but the increase of the temperature. During the classic sessile drop experiment, the temperature is not constant, so that in these processes the temperature is neither stable. The infiltration is boosted thanks to the fact of the decreasing of the density with the temperature. However, the diameter increases at the beginning helped by the reaction in the triple line, but once the

maximum is reached, the diameter decreases due to the infiltration. On the other hand, Figure 7. 2 shows the relation between radius maximum which is the half of maximum width spread (W_{max}), and the infiltration maximum. Once the drop is formed, there is a constant relation that agrees with the values obtained by the literature $(0.65-0.95)^{17}$.

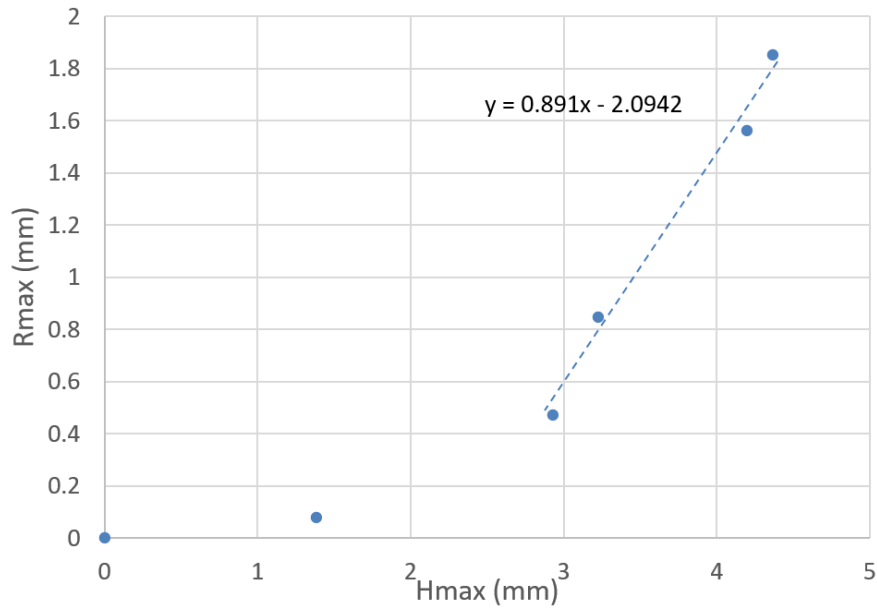
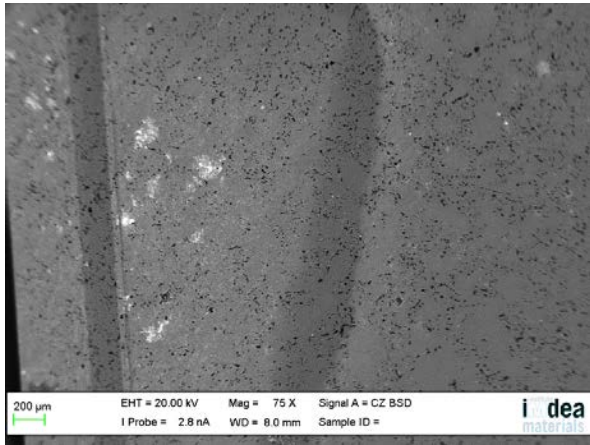
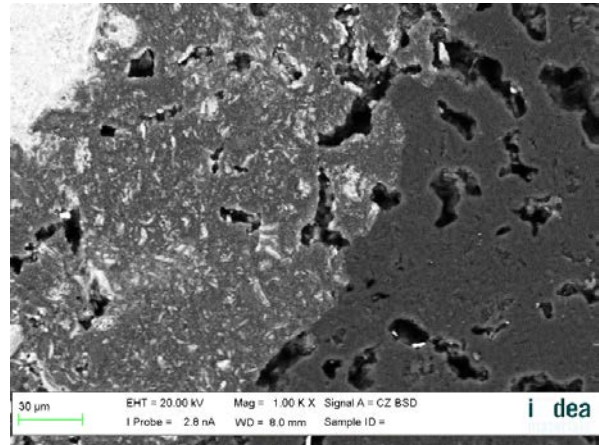


Figure 7. 2. Relation between radius maximum (Rmax) and the infiltration distance maximum (Hmax)

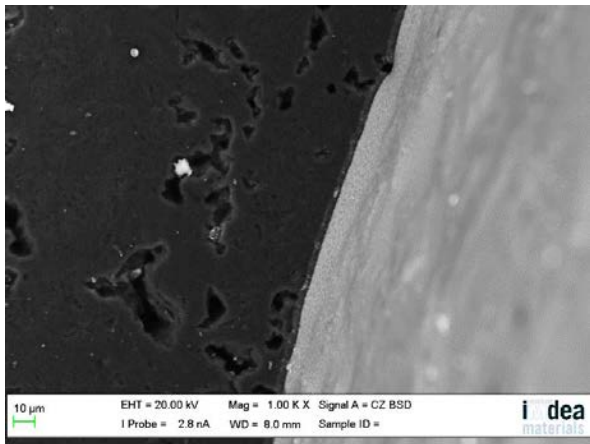
- SEM analysis of the Sessile drop samples



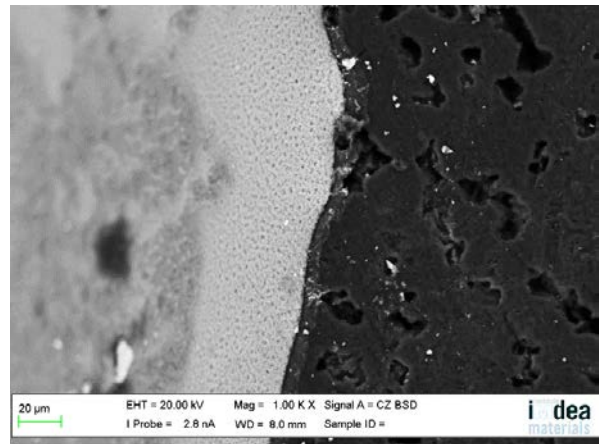
Sample 1 (12 min)



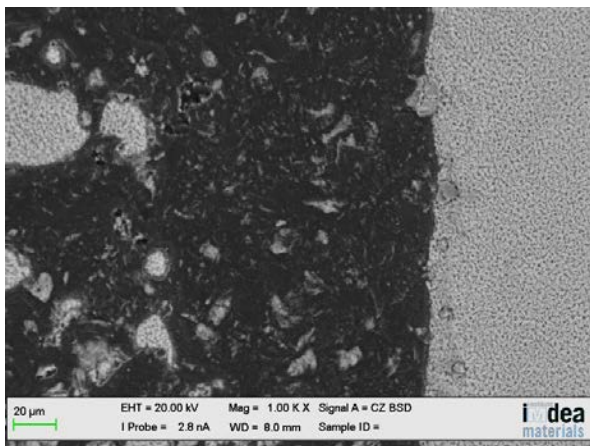
Sample 2 (13 min)



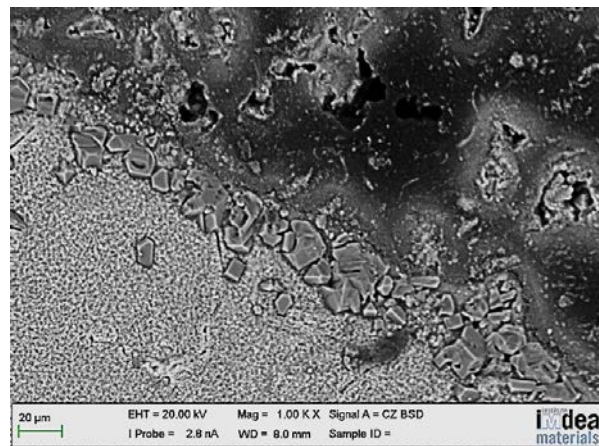
Sample 3 (14 min)



Sample 4 (15 min)

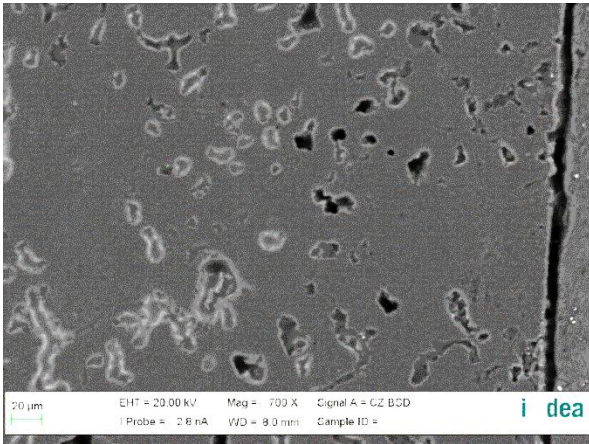


Sample 5 (17 min)

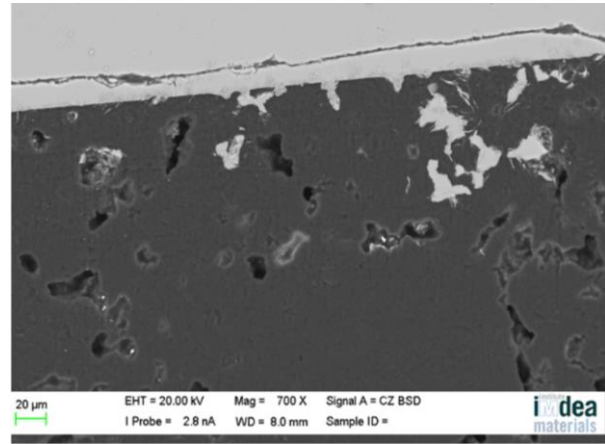


Sample 6 (22 min)

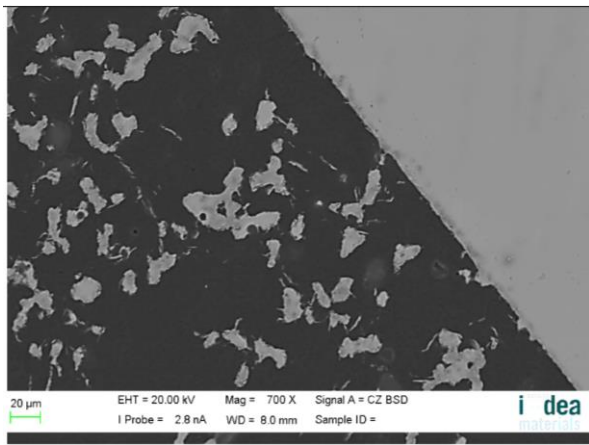
Figure 7. 3. Top view micrographs of the samples after induction furnace test.



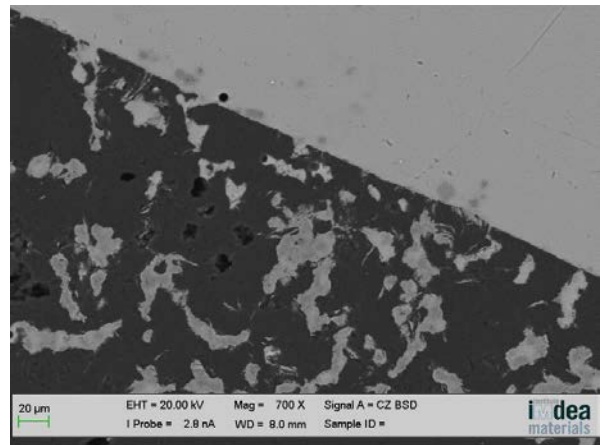
Sample 1 (12 min)



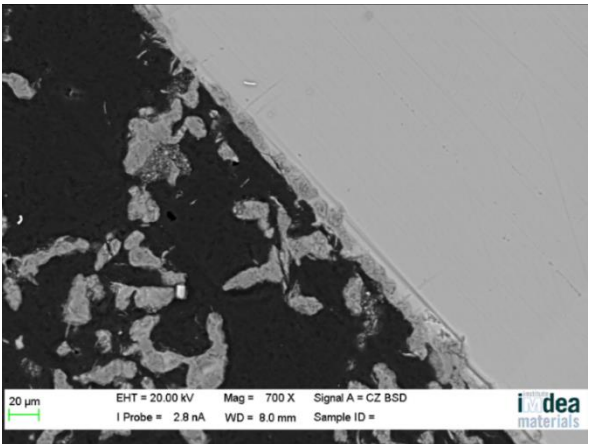
Sample 2 (13 min)



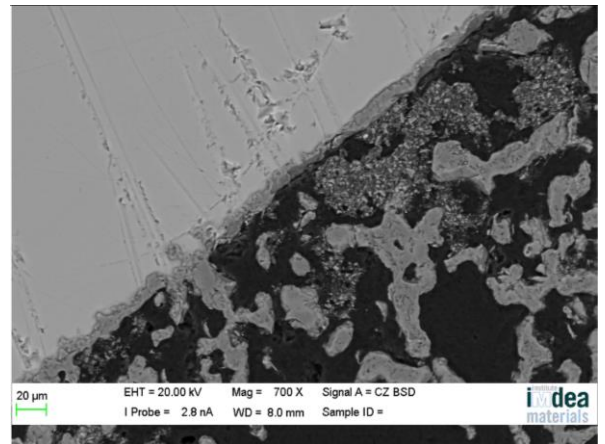
Sample 3 (14 min)



Sample 4 (15 min)



Sample 5 (17 min)



Sample 6 (22 min)

Figure 7. 4. Cross section micrographs of the samples after induction furnace test.

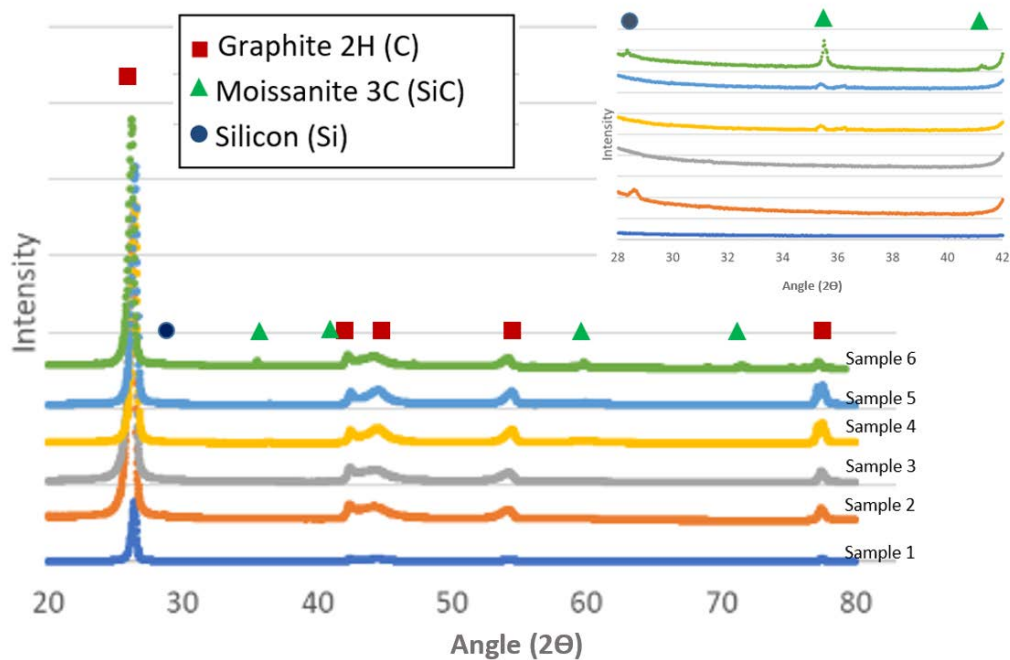
Figure 7. 3 and Figure 7. 4 show the micrographs of the surface and the cross-section after the induction furnace tests. First of all, a thin layer of silicon is deposited on the substrate, and the reaction starts. At the same time, silicon starts to infiltrate inside the substrates and the reaction, in this case, happens on the wall of the pores inside the substrate (sample 1). Then, a silicon layer spread on the graphite boosted by the reaction with the graphite substrates, in addition, the reaction is increasingly faster thanks to the increase of the temperature. Besides, the formation of the silicon improves the wettability, thus, there is an increase in the movement of the silicon, in this time the silicon starts to fill pores inside of the substrates (sample 2). Then, the silicon keeps spreading managed by the chemical reaction and the infiltration, boosted by the increase of the temperature. Silicon also dissolves the graphite because of that silicon carbide crystal starts to appear in the interface due to the saturation of the silicon (sample 3 and 4). Once the spread is over, silicon keeps infiltrating, as in the interface, silicon carbides crystals appear in the triple line due to the saturation of the silicon, and the crystal on the interface starts to grow until a stable silicon layer is formed and does not allow the progression of the infiltration (sample 5 and 6).

Our results agree with the SiC layer formed by two bilayers, a thinner layer close to graphite which was formed instantaneously over the substrate, and then there has been a growth of SiC crystals due to the saturation of the silicon. These crystals have been formed during the heating and a larger time is need to obtain a homogenous layer. There thickness of layer increase with the time (see Table 7. 2) until reaching the equilibrium around $\sim 10 \mu\text{m}$, noted these values are lower than the found ones by Voytovych¹⁰. Regarding the growth of the crystal around the droplet, the crystals were formed once the spreading was over and increased with the time.

Table 7. 2. The values of the SiC layer thickness (e) and the size of the SiC crystals formed around the silicon droplet (e_d)

	Sample 1	Sample 2	Sample 3	Sample 4	Sample 5	Sample 6
$e(\mu\text{m})$	-	-	4.33	4.54	10.19	10.23
$e_d(\mu\text{m})$	-	-	-	-	7.49	9.94

- X-Ray and Raman analysis of the Sessile drop samples

**Figure 7. 5. X-Ray results of coating graphite substrates after induction furnace test.**

The reactivity was analyzed by X-ray dispersion and the results are found in Figure 7. 5. According to the results, the silicon carbide is formed in the samples 4, 5 and 6. Although, silicon is found in previous samples. However, the SEM analysis showed that the reaction started since silicon started to melt. This is due to the small height of the silicon layer on the substrate and the signal is hindered by the carbon signal.

During the test of sample 1, the experiment was finished just at the moment when silicon started to melt, so there was not time enough to the silicon piece stayed on the substrate.

However, a little quantity of silicon remained on the substrate. Hence, the silicon layer formed on sample 1 was analyzed by Raman (Figure 7. 5Figure 7. 6). Despite the strong signal of carbon, silicon carbide is found, indicating that the reaction between silicon and graphite substrate happened almost instantaneously.

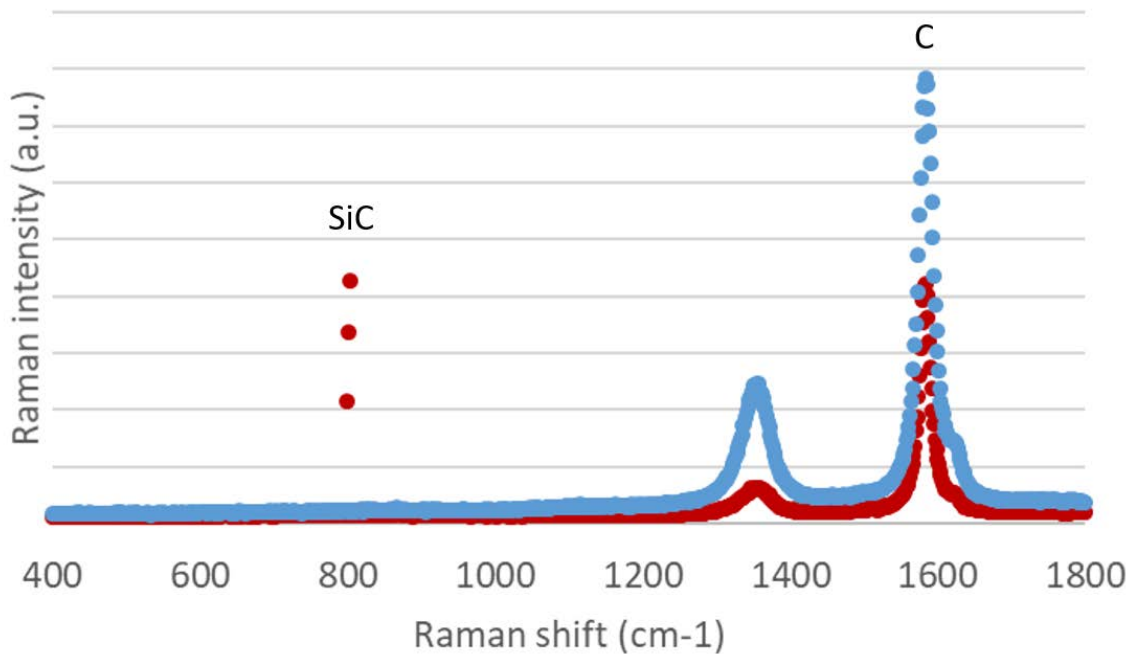


Figure 7. 6. Raman shift results of graphite substrates after induction furnace test of sample 1.

- **TEM analysis of the surface from the induction furnace test**

In order to obtain more information about the thin SiC layer on the interface of the silicon molten and graphite substrate more resolution was needed. Thanks to FIB-FEGSEM dual-beam microscope (Helios NanoLab 600i, FEI), a lamella was obtained by the Gallium ion beam in the area where the SiC layer was formed from the sample 2 (see the scheme from the Figure 7. 7) and then was analysed by FEG S/TEM microscope (Talos F200X, FEI).

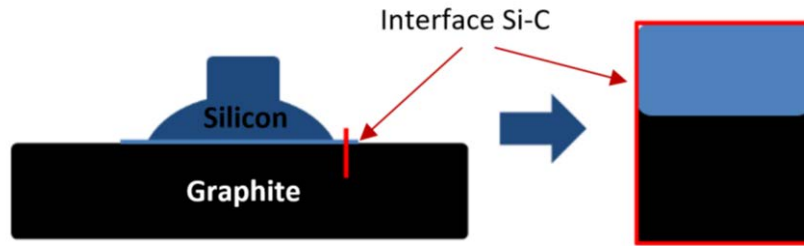


Figure 7. 7. Scheme of the lamella obtain by the Fib from the interface Silicon- Carbide

The results of TEM analyses of the lamella from the sample 2 are shown in Figure 7. 8. On one hand, micrographs and atomic map and on the other hand, lines scan of the content of silicon and carbon atoms are shown. In spite of the little time of the experiment (12 min), a silicon carbide layer under 50 nm was formed. Besides, Besides, the line scan shows that it can be found silicon in the carbon areas and carbon in the silicon areas.

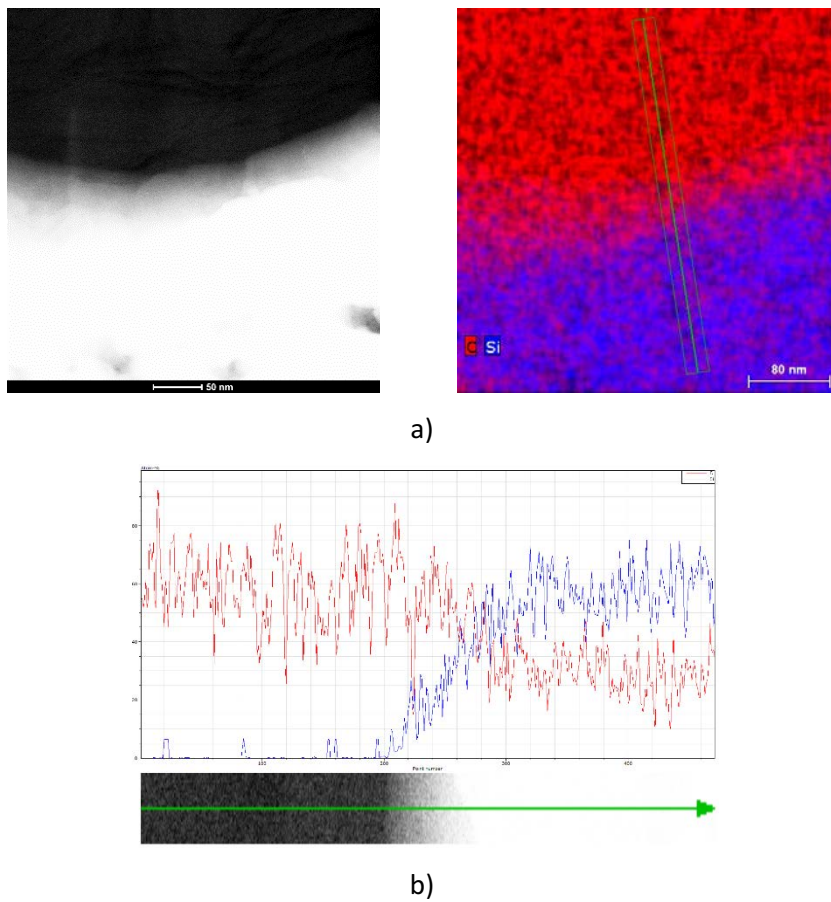


Figure 7. 8. Result of the TEM, a. micrographs and atomic map. b. Lines scan of content of silicon and carbon atoms

CONCLUSIONS

This chapter studies the reaction in the triple line between the silicon and graphite substrate due to the fact that it is a key factor on the wettability.

The piece of silicon starts to melt from the bottom, namely, the area in contact with the graphite. Spontaneously, silicon reacts with the graphite substrate, but at the same time, silicon starts to infiltrate inside of the substrate through the pores and start to dissolve the graphite. The reaction in the triple line manages the spreading and the infiltration. The reaction, and as a consequence the spreading and the infiltration is boosted by the increase of the temperature. In fact, the infiltration is also affected by the decrease of the density of the molten silicon. Due to the dissolution of carbon in silicon and subsequent silicon saturation, SiC crystals are formed on the interface and on the triple line. Once the spreading is over, silicon keeps infiltrating until these crystal grow up until a thick SiC layer is formed on the interface.

A linear relationship was found between infiltration and spreading distances and agree with the value found by other authors²¹. Besides, this study also agrees with the layer formed in the interface is, in fact, a bilayer, formed by a thin layer and faceted SiC crystal, although, with time the SiC layer finally is homogeneous. On the other hand, the thickness of the layer increase with time but a relation has been not found and the values obtained are lower than the literature¹⁰.

8. Discussion

The behaviour of molten silicon is a key factor for several applications such as photovoltaic industry, the production of refractory materials¹² or even for brazing applications²³. The previous chapters show the behaviour of several materials in contact with molten silicon in certain work conditions, in order to analyse their feasibility of being used as refractories.

Every experiment was done above 1414 °C, where the main phenomena that takes place are the reaction, the spreading and the infiltration. It was analysed the availability of different refractory materials, a specific study about Si-C system and finally the viability of two kinds of coatings. On the contrary, in this chapter, the results will be analysed according to the type of counter material used to be in contact with the molten silicon: oxides substrates, graphite substrates and covalent ceramics²⁴ in order to compare.

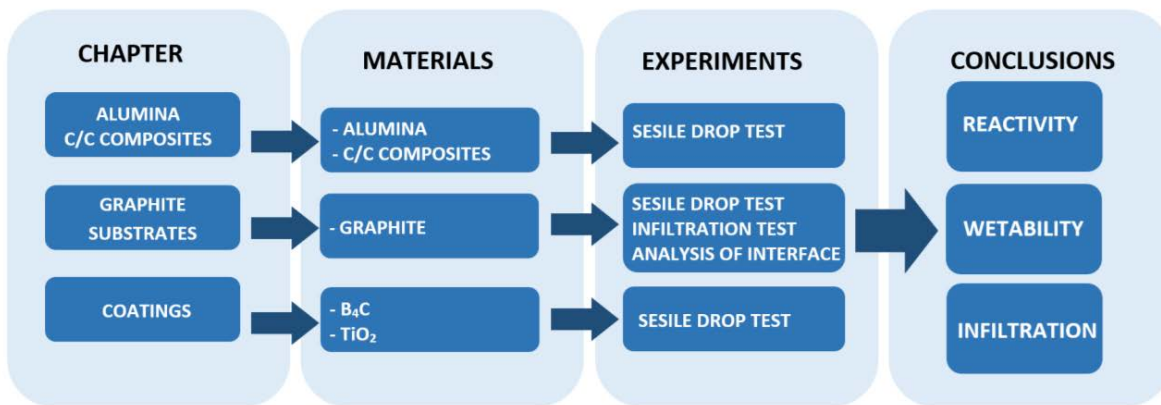


Figure 8. 1. Schema about the blocks: materials studied and techniques used.

8.1 Oxides substrates

The oxides substrates are characterized by high thermodynamic stability and high electrical resistivity. The oxides used in this dissertation are alumina as substrates and TiO₂ as the coating of graphite.

According to several authors^{27,28}, the contact angles value reported for oxides substrates are close to 90°. Although these results are usually linked to non-reactive systems, recent studies suggested that the system is reactive²¹.

8.1.1 Alumina

The behaviour of the alumina is divided into three parts: firstly, the formation of the drop, then the variation of the parameters of the drop (contact angle, width and height) with the time -highlighted slow- with a dramatical variation in these parameters at the end of the process. This process corresponds with the formation of the passive layer from the oxide of the alumina and then with the elimination of this layer through the deoxidization of the SiO₂²¹.



The spontaneous infiltration does not happen until the value of the contact angle is around 60°²¹ reaching a zero final angle. Despite the fact that it is a reactive system, oxides are not found in the micrographs.

Regarding the results, the Si/Al₂O₃ is reactive and the initial contact angle agrees with literature. However, the corrosion rings^{25,50} are not found, likely, due to the fact that the used alumina is porous and polycrystalline and the variation in the curves are hindered by the irregularities of the surfaces.

8.1.2 TiO₂

The obtained results by the substrates coated with TiO₂ corresponds with the Si/C system:

- The $U_{spr} = dR/dt$ is close to $10 \mu\text{m}\cdot\text{s}^{-1}$, as in the case of graphite substrates.
- The initial contact angle was close to 90° , but finally, the drop infiltrated totally inside of the substrate.
- The variation of the width of the drop with the time is linear.

The main difference is the presence of the oxides in the micrographs, indicating the pollution of the silicon.

To sum up, silicon likely dissolved the coatings, boosting the spreading and the infiltration so that, the equilibrium was reached faster than graphite substrate and oxides could be infiltrated inside of the substrate.

8.2 Graphite Substrates

Graphite is largely used to produce crucibles and dies for processes during the purification of solar silicon due to the good electrical and thermal properties, but especially because the effects of the carbon impurities in the efficiency of the solar cells are negligible.

On the contrary, graphite has high affinity with the silicon, so that the reactivity between Si and graphite can be a determining factor of the lifetime of graphite crucibles^{6–10}. Besides, the silicon carbide layer formed boosts the spreading and infiltration as well as the sticking of silicon on the graphite, increasing the price of the process.

In this section, the results obtained will be analysed in order to obtain accurate information about the reaction, the spreading and infiltration of the Si/C system.

8.2.1 Analysis for photovoltaic applications

Table 8. 1. The main results obtained by different substrates.

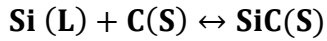
Substrate	G330	G347	G348	G530	Lorraine	R6650	R6710
Final contact angle	20.00	42.00	28.00	18.00	48.34	25.28	35.34
Spreading max (mm)	4.24	3.57	3.61	3.92	2.85	3.58	3.46
Infiltration max (mm)	1.23	1.46	1.00	0.85	1.41	0.31	0.00

The substrates needed for the photovoltaic application are those that are not wetted by silicon where, namely, the contact angle is higher than 90°, and the spreading and infiltration are negligible to enhance the detachment. Hence, several graphite substrates were analysed in order to know which one is the best option for this application. The obtained results are found in Table 8. 1

Regarding the results, the best option is the graphite grade R6710, due to the infiltration distance, which is the lowest. In addition, the contact angle is relatively high and the spreading is moderate in comparison with the other values.

8.2.2 Reaction

Previous researches⁶⁻¹⁰ have shown that Si/C is a reactive system managed by the reaction on the triple line:



Equation 19

The model most accepted is the reaction product control (RPC) where firstly, the behaviour against molten silicon corresponds to the Si/C system, but then a SiC layer is formed and finally, the behaviour is similar to the Si/SiC system¹⁴.

According to Eustathopoulos et al¹³, the systems, which are controlled by the reaction between silicon carbide in the triple line, are characterized to have a spreading rate ($U_{spr} = dR/dt$) close to $10 \mu\text{ms}^{-1}$ and a linear variation of the diameter of the drop with the time. Regarding our results, every graphite substrate showed a linear spreading with a spreading rate close to $10 \mu\text{ms}^{-1}$. Except the samples used in the dispensed sessile drop, whose values for the spreading rate were higher than those obtained in the literature. Moreover, the carbon-carbon composites did not show totally linear curves. On the other hand, the compositional analysis found SiC in all the test and the final contact angle lie between 0 to 40° .

There are differences between the classic and the dispensed drop methods. For example, although the substrates were heated until 1450° , the process in the classic sessile method started at 1414° while in the dispensed sessile method was at 1450° . On the other hand, in the classic method, the heating of the silicon took place in the same chamber, silicon can have been evaporated, condensed and reacted with the substrate. In addition, in the dispensed drop method, silicon is free of oxides. For these reasons, the properties of molten silicon during the dispensed test are different than in the classic tests. The advance of the drop could be boosted by the crush of the surface, while during the classic test was not affected. In the same way, the composites were affected due to the fact that their surface is not homogeneous because of the different directions of the fibres.

In conclusion, our results were managed by the reaction in the triple line and also agrees with the model of the reaction product control (RPC), being the final angle similar to the contact angle of Si/SiC ($\sim 40^\circ$). Although the irregularities of the surface of the sample can affect the behaviour against molten silicon as in the case of dispensed drop or composites.

- **SiC layer on the interfaces**

Table 8. 2. Values of thickness of SiC layer and size of SiC crystals around the droplet in comparison other parameters at 1450°

Substrate	Sesile drop	Rugosity	Ra (μm)	e (μm)	ed (μm)
G348	Dispensed	Polished	0.49	7.25	53.70
G347	Dispensed	Polished	0.22	7.89	22.88
G348	Classic	Polished	0.49	12.60	22.86
G330	Classic	Polished	0.48	13.30	23.70
G530	Classic	Polished	0.49	13.80	26.38
R6710	Classic	Ground	0.19	14.60	19.00
G347	Classic	Ground	0.22	15.10	21.00
Lorraine	Classic	Ground	0.34	15.90	19.40
R6650	Classic	Ground	0.32	15.90	22.60

In Chapter 7 it was analysed how the SiC layer is formed firstly by a thin SiC layer instantaneously developed and then by the formation of SiC crystals due to the saturation of the silicon, but finally with time, the layer is homogenous.

Another interesting point about this layer is the thickness, Deike et al³⁹ affirm for vitreous carbon, that the maximum thickness is reached at 10 min while for polycrystalline carbon, the thickness increases with the time. Voytovych et al¹⁰ suggest that in every graphite substrate, the thickness increases until the layer reaches a maximum value. Table 8. 2 shows the obtained values in this dissertation at 1450°C, in comparison, they are lower than literature (15-20 μm at 1600°C). This difference is likely due to the difference in the temperature. Moreover, the lowest values were obtained by the dispensed drop test, where these substrates were in contact with the silicon less time than the other samples

due to fact that the heating was done in a capillar. In addition, the results suggest that the polished samples, produce a thinner SiC layer than the unpolished ones. On the other hand, Chapter 7 suggests that the SiC crystals are formed when the spreading is over. On the contrary of the SiC layer thickness, the higher values of thickness around the droplet were obtained by the grounded samples , as can be seen in Table 8. 2

The pores of the substrates were opened by the polishing so that, the formation of the SiC was boosted.

8.2.3 Relation between spreading and infiltration rate.

Table 8. 3. Value of the tortuosity in comparison with the porosity parameters

Substrate	Technic	Uinf/Uspr	Torturoosity	%Porosity	Pore size mean (μm)
G347	Dispensed	0.22	4.45	14.00	7.48
G348	Dispensed	0.27	3.68	11.00	9.02
G530	Classic	0.27	3.67	23.00	11.69
G348	Classic	0.29	3.50	11.00	9.02
G347	Classic	0.38	2.60	14.00	7.48
G330	Classic	0.43	2.33	22.00	10.29
R6650	Classic	0.77	1.30	20.00	8.94
Lorraine	Classic	0.89	1.13	18.00	10.62
R6710	Classic	0.00	-	32.00	7.52

Einset et al²² consider that the infiltration is controlled by viscous resistance and the infiltration depth agrees with the Washburn's equation, but the results shows that the infiltration depth is linear, hence the infiltration is managed by the reaction in the triple line.

As wetting and infiltration are controlled by the reaction between silicon and graphite, Camel et al¹⁷ suggest that the kinetics rates, spreading and infiltration, should have the same order, although the value of the infiltration rate should be smaller due to the tortuosity, this relation was shown in Chapter 7.

On the other hand, Israel et al⁸ affirmed the tortuosity is inversely proportional to the porosity percentage and the pore size. In contrast, the results obtained did not show any relation with the porosity.

8.2.4 Other parameters

In spite of the fact that the systems are reactive, a scatter of results are obtained for Si/C system, and according to the literature the most relevant parameters are:

- **Influence of rugosity**

The values of the average rugosity of the polished substrates were higher than the grounded ones. This is an indication that the pores were closed thanks to the grinding of the substrates. However, deeper scratches were also found in these cases.

Table 8. 4. Analysis of the rugosity against the main results

Substrate	Rugosity	Ra (μm)	Final contact angle	Spreading max (mm)	Infiltration max (mm)
Composite 2	no	7.02	0.00	3.46	0.82
Graphite	no	4.83	0.00	3.68	0.98
Composite 1	no	4.48	0.00	4.16	0.64
G348	Polished	0.49	28.00	3.61	1.00
G530	Polished	0.49	18.00	3.92	0.85
G330	Polished	0.48	20.00	4.24	1.23
Lorraine	Ground	0.34	48.34	2.85	1.41
R6650	Ground	0.32	25.28	3.58	0.31
G347	Ground	0.22	42.00	3.57	1.46
R6710	Ground	0.19	35.34	3.46	0.00

There is not a clear relation between rugosity and parameters like the final contact angle, the spreading and the infiltration distance (see Table 8. 4). However, a perfect wetting was obtained by the samples with a high value of the average rugosity. Besides, in general terms, in the grounded samples were hindered the infiltration and boosted the spreading, although in several cases the drop was pinned because of the irregularities of the surface.

- **Influence of crystallinity**

Table 8. 5. Values of crystallinity against of main parameters of the contact angle

Substrate	Crystallinity	Final contact angle	Spreading max (mm)	Infiltration max (mm)
Lorraine	0.42	48.34	2.85	1.41
G347	0.40	42.00	3.57	1.46
G348	0.40	28.00	3.61	1.00
G330	0.40	20.00	4.24	1.23
G530	0.40	18.00	3.92	0.85
R6710	0.37	35.34	3.46	0.00
R6650	0.37	25.28	3.58	0.31

According to Eustathopoulos et al²⁰, the wettability on carbonaceous materials depends on the grade of crystallinity. Table 8. 5 shows the values of crystallinity against the main parameters for the reactivity, the spreading and the infiltration. Although a clear relationship has not been found, the highest final contact angle has been reached by the material with the highest value of the crystallinity.

- **Influence of the atmosphere**

Table 8. 6. Effect of the atmosphere in the main parameters of the reaction, the wetting and the infiltration.

Substrate	Atmosphere	Final contact angle	Spreading max (mm)	Infiltration max (mm)
G330	Argon	20.00	4.24	1.23
G330	Vacuum	0.00	7.73	0.58
G347	Argon	42.00	3.57	1.46
G347	Vacuum	0.00	8.29	0.88
G348	Argon	28.00	3.61	1.00
G348	Vacuum	0.00	8.72	0.58
G530	Argon	18.00	3.92	0.85
G530	Vacuum	0.00	8.35	0.44

The atmosphere is another highlighted parameter for the Silicon experiments, because of the silicon evaporation. Table 8. 6 show the values under vacuum and argon of the main parameters of the reaction, the wetting and the infiltration. In every case, the contact angle

and infiltration distance are higher under argon than vacuum, meanwhile, the spreading distance is larger under high vacuum than argon atmosphere.

The spreading was boosted due to the fact that part of the silicon is evaporated, and condensed on the surface of the substrate and then reacted with the graphite, forming a SiC layer and hence the spreading was boosted. The evaporation had to be as faster as the infiltration in order to avoid to be evaporated silicon, instead being infiltrated through the pores. In fact, the increase of the spreading distance is the double while the decrease of the infiltration distance is the half in comparison under argon experiments.

- **Differences between Classic and dispensed Sessile drop test**

Table 8. 7. The main results from the classic and dispensed Sessile drop test

Substrate	G347	G347	G348	G348
	classic	dispensed	classic	dispensed
Sessile drop	42.00	40.00	28.00	5.00
Final contact angle	3.57	13.11	3.61	13.46
Spreading max (mm)	1.46	0.87	1.00	0.53
Infiltration max (mm)	15.10	7.89	12.60	7.25
e (μm)	21.00	22.88	22.86	53.70
ed (μm)				

Table 8. 7 show the differences of the main results after Classic and Dispensed Sessile drop test, in every case, the value contact angle and infiltration distance decreased, while the value of spreading distance increased, as under high vacuum atmosphere likely because of the silicon evaporation.

- **Influence of the type of porosity**

Table 8. 8. Images of the distribution of pores in different graphite and parameters of the porosity in comparison with the maximum infiltration distance (hmax)

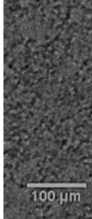
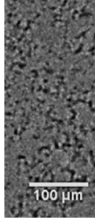
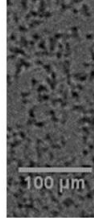
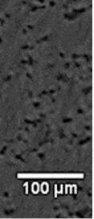
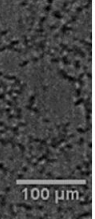
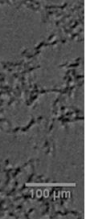
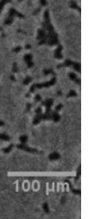
Substrate	R6710	R6650	G550	G348	G330	Lorraine	G347
H max (mm)	0.00	0.31	0.85	1.00	1.23	1.41	1.46
Pore size mean (μm)	7.52	8.94	11.69	9.02	10.29	10.62	7.48
%Porosity	32.00	20.00	23.00	11.00	22.00	18.00	14.00
Porosity							

Table 8. 8 shows the images from the tomography and the main parameters of porosity in comparison with the maximum infiltration distance obtained for several graphite substrates. The R6710 grade was not infiltrated by molten silicon and the pore size is the lowest, and on the contrary, the percentage of porosity is the highest. However, the R6710 grade is formed by small grains, leading small pores on the boundaries. This distribution hindered the interconnectivity of the pores, as well as the infiltration of molten silicon. In contrast, Lorraine and G347 substrates have big grains and there are pores on the boundaries that boosted the interconnectivity and thus, the infiltration.

- **Graphite substrates**

Table 8. 9. Main parameters obtained for carbonaceous materials.

Substrate	Graphite	Composite 1	Composite 2
Ra (μm)	4.83	4.48	7.02
Crystallinity	0.36	0.55	0.39
Final contact angle	0.00	0.00	0.00
Spreading max (mm)	3.68	4.16	3.46
Infiltration max (mm)	0.98	0.64	0.82
%Porosity	22.30	32.30	23.89
Pore size mean (μm)	9.32	26.25	11.62

Silicon has high affinity by carbides and nitrides, aluminium and boron, and these materials are considered covalent ceramics due to their chemical bonds. Besides, these materials form a stable oxide which can avoid the infiltration. Particularly, several substrates coated by B_4C with different thickness were studied in this thesis.

Regarding the results, the process was faster than using the graphite substrate, the curves of the different parameters with the time are not linear as happens with Si/C graphite, and for this reason the infiltration was hindered. On the other hand, the micrographs are similar to the graphite substrate ones as well as the chemical composition analysis. Also oxides were found in the micrographs as the TiO_2 coatings.

Everything indicates, firstly, that silicon does not react with the coating so that the process is as fast as with the non-reactive system, but then silicon can dissolve the coating and react with the graphite from the substrate. Owing to the dissolution of the coating, the molten silicon was polluted and infiltrated by the pores of the substrates.

On the other hand, the best behaviour against silicon was obtained by the sample with the thinner but more homogeneous coating.

8.3 Covalent ceramics

Table 8. 10. The main results after the sessile drop test of the G348 and the B₄C coatings.

Substrate	G348	B₄C (2μm)	B₄C (4μm)
Final contact angle	28.00	45.00	15.00
Spreading max (mm)	3.61	2.87	3.37
Infiltration max (mm)	1.00	0.67	1.07
e (μm)	12.60	13.10	12.60

Silicon has high affinity by carbides and nitrides, aluminium and boron, these materials are considered covalent ceramics due to their chemical bonds. Besides, these materials form a stable oxide which can avoid the infiltration. Particularly, several substrates coated by B₄C with different thickness was studied in this dissertation.

Regarding the results, the process was faster than the graphite substrate, the curves of the parameter with the time are not linear as Si/C graphite, and besides the infiltration was hindered. On the other hand, the micrographs are similar to the graphite substrate ones as well as the chemical composition analysis. Although oxides were found in the micrographs as the TiO₂ coatings.

Everything indicates, firstly, silicon does not react with the coating so that the process is as fast as a non-reactive system, but then silicon can dissolve the coating and react with the graphite from the substrate. Owing to the dissolution of the coating, the molten silicon was polluted and infiltrated by the pores of the substrates.

On the other hand, the best behaviour against silicon was obtained by the sample with the thinner coating but more homogeneous (see Table 8. 10.). The coating increases de contact angle and decrease the infiltration and spreading distances.

9. Conclusions

This thesis is focused on the behaviour of molten silicon on several substrates in order to satisfy the needs of the manufacturing conditions for silicon to photovoltaic applications particularly, and in general, to obtain useful information about the reaction, the wetting and the infiltration for other industrial applications such as the production of refractories¹² or brazing²³. Several experiments were carried out on oxides substrates, graphite substrates and covalent ceramics.

From this thesis, it can be summarized, as general conclusion, that properly selecting the materials to be used as refractory in the molten silicon manufacturing industry, it can be improved the efficiency of the system, optimizing the life time of the materials and reducing the interaction between the refractories and the molten silicon. The optimization for this selection have been mad studying carefully the interaction of molten silicon and the candidate materials, mainly thorough wetting experiments that allow to understand deeply this interaction. In this sense, the best studied material is R6710.

From this general conclusion of the thesis, the following partial collusions can be highlighted:

9.1 Oxides substrates

Two different oxides substrate system have been considered: Al_2O_3 and TiO_2 coatings on graphite: The Si/ Al_2O_3 is a reactive system where the formation and the posterior elimination of a passive layer manage the spreading and the infiltration of the molten silicon. Due to the reaction between silicon and oxygen, this substrate is not allowed for photovoltaic applications.

The behavior of TiO_2 coating against of molten silicon is very similar to graphite substrate although the coating boosted the spreading of the molten silicon. The dissolution of the coating was very fast and allowed the pollution of the silicon.

9.2 Graphite Substrates

Different graphite substrates have been considered. Among all the studies developed about these family of substrates, the following conditions were obtained:

- The best option, from all studied materials, is the graphite R6710 grade, due to the infiltration distance is the lowest. In addition, the contact angle is relatively high and the spreading is moderate in comparison with the other values.
- In every case of molten silicon against carbonaceous substrates, the system is reactive and controlled by the reaction in the triple line as well as it agrees with the model of the reaction product control (RPC). Although the reaction managed the behaviour against molten silicon, the scratches on the surface has remarkable effects on the cases of dispensed drop or composites.
- The initial SiC layer produced on the interface has a bilayer morphology, firstly formed by a thin SiC layer instantaneously developed and then by the formation of SiC crystals due to the saturation of the silicon. At the end of the processthe layer become homogenous. The values of the layer thickness were less than 10 μm for dispensed drop test and 10-15 μm for classic Sessile drop test.
- A linear relation between infiltration and spreading rate was found, but the obtained results did not show any relationship with the porosity.
- A perfect wetting behaviour was obtained by the samples with a high value of the average rugosity. Besides, in general terms, the grounded samples had hindered the infiltration and boosted the spreading, although in several cases the drop was pinned because of the irregularities of the surface.
- The silicon evaporation is a key factor under high vacuum, in comparison with the argon atmosphere, the spreading distance increased while the infiltration distance decrease. The velocity of the evaporation has to be of the same order of magnitude for spreading and infiltration.

- The infiltration is hindered with the use of graphite substrates with small grains and small pores on the boundaries, due to the fact that the interconnectivity of the pores is hindered.
- Regarding the results of the carbon-carbon composites, the use of these substrates could be available for photovoltaic applications because the silicon was not polluted, but it should be reduced the rugosity and the porosity.

9.3 Covalent ceramics

It was studied coatings of B_4C , and it can be highlighted that:

- B_4C coating substrates showed a non-reactive behaviour against molten silicon at the first instance, but then silicon dissolves the coating very quickly, leading the formation of the oxides, and, as a consequence, the pollution of the molten silicon.

10. Futures lines

This thesis and the obtained conclusions open several possible research lines, as is explained in the following lines:

- Regarding the oxides substrates, new coatings can be studied paying attention to the thickness and the homogeneity of the layer in order to avoid the pollution and enhancing the behaviour against molten silicon.
- The study of Carbon-Carbon composites with minimum rugosity and minimize the porosity.
- Analysis of the silicon evaporation rate, as in high vacuum experiments as in dispensed Sessile drop test.
- A tomography analysis after the experiment of the infiltration of silicon in order to obtain accurate information about infiltration.
- To determine an infiltration model that satisfy the real conditions during the melting of the silicon.
- To study the viability of the use the R6710 graphite during some purification processes at lab scale in order to check the formation of cracks as well as the detachment of the silicon or other likely problems

11. Bibliography

1. Ciftja, A., Engh, T. A. & Tangstad, M. Wetting properties of molten silicon with graphite materials. *Metall. Mater. Trans. A Phys. Metall. Mater. Sci.* **41**, 3183–3195 (2010).
2. Safarian, J., Tranell, G. & Tangstad, M. Processes for upgrading metallurgical grade silicon to solar grade silicon. *Energy Procedia* **20**, 88–97 (2012).
3. Lynch, D. Winning the global race for solar silicon. *Jom* **61**, 41–48 (2009).
4. Binetti, S. *et al.* Study of defects and impurities in multicrystalline silicon grown from metallurgical silicon feedstock. *Mater. Sci. Eng. B* **159–160**, 274–277 (2009).
5. Kraiem, J. *et al.* High performance solar cells made from 100% umg silicon obtained via the photosil process. *Conf. Rec. IEEE Photovolt. Spec. Conf.* 1427–1431 (2010). doi:10.1109/PVSC.2010.5614418
6. Safarian, J., Xakalash, B. & Tangstad, M. Vacuum Removal of the Impurities From Different Silicon Melts. *26th Eur. Photovolt. Sol. energy Conf. Exhib.* 1810–1813 (2011).
7. Flamant, G., Kurtcuoglu, V., Murray, J. & Steinfeld, A. Purification of metallurgical grade silicon by a solar process. *Sol. Energy Mater. Sol. Cells* **90**, 2099–2106 (2006).
8. Israel, R. *et al.* Capillary interactions between molten silicon and porous graphite. *J. Mater. Sci.* **45**, 2210–2217 (2010).
9. Israel, R. Etude des interactions entre silicium liquide et graphite pour application à l'élaboration du silicium photovoltaïque. (2009).
10. Voytovych, R., Israel, R., Calderon, N., Hodaj, F. & Eustathopoulos, N. Reactivity between liquid Si or Si alloys and graphite. *J. Eur. Ceram. Soc.* **32**, 3825–3835 (2012).
11. Ciftja, A., Engh, T. A. & Tangstad, M. Refining and Recycling of Silicon : A Review. *World 4*, 14–15 (2008).
12. Dezellus, O., Jacques, S., Hodaj, F. & Eustathopoulos, N. Wetting and infiltration of carbon by liquid silicon. *J. Mater. Sci.* **40**, 2307–2311 (2005).
13. Eustathopoulos, N., Israel, R., Drevet, B. & Camel, D. Reactive infiltration by Si:

- Infiltration versus wetting. *Scr. Mater.* **62**, 966–971 (2010).
14. Li, J. G. & Hausner, H. Wetting and infiltration of graphite materials by molten silicon. *Scr. Metall. Mater.* **32**, 377–382 (1995).
 15. Whalen T.J ; Anderson, A. T. Wetting of SiC, Si₃N₄ and Carbon by Si and Binary Si Alloys. **1973**, 396–399 (1975).
 16. Rubio, P. J. Y., Hong, L., Saha-Chaudhury, N., Bush, R. & Sahajwalla, V. Dynamic wetting of graphite and SiC by ferrosilicon alloys and silicon at 1550°C. *ISIJ Int.* **46**, 1570–1576 (2006).
 17. Camel, D., Drevet, B. & Eustathopoulos, N. Capillarity in the processing of photovoltaic silicon. *J. Mater. Sci.* **51**, 1722–1737 (2016).
 18. Caccia, M. *et al.* Towards optimization of SiC/CoSi₂ composite material manufacture via reactive infiltration: Wetting study of Si-Co alloys on carbon materials. *J. Eur. Ceram. Soc.* **35**, 4099–4106 (2015).
 19. Huguet, C. *et al.* Initial stages of silicon-crucible interactions in crystallisation of solar grade silicon: Kinetics of coating infiltration. *Acta Mater.* **76**, 151–167 (2014).
 20. Eustathopoulos, N., Nicholas, M. G. & Drevet, B. B. *Wettability at high temperatures. Materials Science* **3**, (1999).
 21. Drevet, B. & Eustathopoulos, N. Wetting of ceramics by molten silicon and silicon alloys: A review. *J. Mater. Sci.* **47**, 8247–8260 (2012).
 22. Einset, E. O. Capillary infiltration rates into porous media with applications to Silcomp processing. *Journal of the American Ceramic Society* **79**, 333–338 (1996).
 23. Eustathopoulos, N. The Contribution of the Grenoble Group. 350–370 (2015). doi:10.3390/met5010350
 24. Drevet, N. E. & M. G. N. & B. *Wettability at High Temperatures, 1st Edition.* (1999).
 25. KEENE, B. J., SILLWOOD, J. M., Champion, J. A., Keene, B. J. & Sillwood, J. M. Wetting of aluminium oxide by molten aluminium and other metals. *J. Mater. Sci.* **4**, 39–49 (1969).
 26. Saiz, E., Cannon, R. M. & Tomsia, A. P. Reactive spreading: Adsorption, ridging and compound formation. *Acta Mater.* **48**, 4449–4462 (2000).
 27. Yuan, Z., Huang, W. L. & Mukai, K. Wettability and reactivity of molten silicon with various substrates. *Appl. Phys. A Mater. Sci. Process.* **78**, 617–622 (2004).
-

28. YOKOYAMA, T., HIDE, I., MATSUYAMA, T., SAWAYA, K. & Maeda, Y. Releasing Material for the Growth of Shaped Silicon Crystals. *J. Electrochem. Soc.* **133**, 440–443 (1986).
29. Voytovych, R., Bougiouri, V., Calderon, N. R., Narciso, J. & Eustathopoulos, N. Reactive infiltration of porous graphite by NiSi alloys. *Acta Mater.* **56**, 2237–2246 (2008).
30. Saiz, E., Tomsia, A. P., Orlando, E., Berkeley, L. & Division, M. S. Atomic dynamics and Marangoni flows during liquid-metal spreading. **3**, 903–910 (2004).
31. Eustathopoulos, N. & Voytovych, R. The role of reactivity in wetting by liquid metals: a review. *J. Mater. Sci.* **51**, 425–437 (2016).
32. Pampuch, R., Walasek, E. & Bialoskórski, J. Reaction mechanism in carbon-liquid silicon systems at elevated temperatures. *Ceram. Int.* **12**, 99–106 (1986).
33. Schulte-Fischedick, J. *et al.* The morphology of silicon carbide in C/C-SiC composites. *Mater. Sci. Eng. A* **332**, 146–152 (2002).
34. Zollfrank, C. & Sieber, H. Microstructure and phase morphology of wood derived biomorphous SiSiC-ceramics. *J. Eur. Ceram. Soc.* **24**, 495–506 (2004).
35. Mlungwane, K., Sigalas, I., Herrmann, M. & Rodríguez, M. The wetting behaviour and reaction kinetics in diamond-silicon carbide systems. *Ceram. Int.* **35**, 2435–2441 (2009).
36. Favre, A., Fuzellier, H. & Suptil, J. An original way to investigate the siliconizing of carbon materials. *Ceram. Int.* **29**, 235–243 (2003).
37. Zhou, H. & Singh, R. N. Kinetics Model for the Growth of Silicon Carbide by the Reaction of Liquid Silicon with Carbon. *J. Am. Ceram. Soc.* **78**, 2456–2462 (1995).
38. Li, J. G. & Hausner, H. Reactive wetting in the liquid-silicon/solid-carbon system. *Journal of the American Ceramic Society* **79**, 873–880 (1996).
39. Deike, R. Reactions Between Liquid Silicon and Different Refractory Materials. *J. Electrochem. Soc.* **142**, 609 (1995).
40. GADOW, R. FIBER-REINFORCED SILICON-CARBIDE. *Am. Ceram. Soc. Bull.* **65**, 326–335 (1986).
41. Kumar, S., Kumar, A., Shukla, A., Gupta, A. K. & Devi, R. Capillary infiltration studies of liquids into 3D-stitched C-C preforms. Part A: Internal pore characterization by solvent infiltration, mercury porosimetry, and permeability studies. *J. Eur. Ceram.*

- Soc. **29**, 2643–2650 (2009).
42. MESSNER, R. P., TERWILLIGER, C. & BEHRENDT, D. R. REACTION-FORMED SILICON-CARBIDE. in *ABSTRACTS OF PAPERS OF THE AMERICAN CHEMICAL SOCIETY* **200**, 80–CHED (1990).
 43. NAIDICH, Y. V, GRIGORENKO, N. F. & PEREVERTAILO, V. M. INTERPHASE AND CAPILLARY PHENOMENA IN CRYSTAL-GROWTH AND MELTING PROCESSES. *J. Cryst. Growth* **53**, 261–272 (1981).
 44. Beyssac, O., Rouzaud, J.-N., Goffé, B., Brunet, F. & Chopin, C. Graphitization in a high-pressure, low-temperature metamorphic gradient: a Raman microspectroscopy and HRTEM study. *Contrib. to Mineral. Petrol.* **143**, 19–31 (2002).
 45. Israel, R. *et al.* Resistance to oxidation of graphite silicided by reactive infiltration. *J. Eur. Ceram. Soc.* **31**, 2167–2174 (2011).
 46. Koltsov, A., Hodaj, F. & Eustathopoulos, N. Brazing of AlN to SiC by a Pr silicide : Physicochemical aspects. **495**, 259–264 (2008).
 47. Camel, D. *et al.* The crucible/silicon interface in directional solidification of photovoltaic silicon. *Acta Mater.* **129**, 415–427 (2017).
 48. Drevet, B., Voytovych, R., Israel, R. & Eustathopoulos, N. Wetting and adhesion of Si on Si₃N₄ and BN substrates. **29**, 2363–2367 (2009).
 49. MARTIROSYAN, A. M. *et al.* Wetting of boron carbonitride by molten metals. *Powder Metall. Met. Ceram.* **28**, 961–965 (1989).
 50. Saiz, E., Tomsia, A. P. & Sukanuma, K. Wetting and strength issues at Al / a – alumina interfaces. **23**, 2787–2796 (2003).
 51. Salvo, L. *et al.* X-ray micro-tomography an attractive characterisation technique in materials science. *Nucl. Instruments Methods Phys. Res. Sect. B Beam Interact. with Mater. Atoms* **200**, 273–286 (2003).
 52. Sobczak, N., Nowak, R., Radziwill, W., Budzioch, J. & Glenz, A. Experimental complex for investigations of high temperature capillarity phenomena. *Mater. Sci. Eng. A* **495**, 43–49 (2008).
 53. Oro, R., Campos, M. & Torralba, J. M. Study of high temperature wetting and infiltration for optimising liquid phase sintering in low alloy steels. *Powder Metall.* **55**, 180–190 (2012).
 54. Novakovic, R. *et al.* Thermodynamic, surface and structural properties of liquid Co-Si

- alloys. *J. Mol. Liq.* **221**, 346–353 (2016).
55. Dezellus, O. & Eustathopoulos, N. Fundamental issues of reactive wetting by liquid metals. *J. Mater. Sci.* **45**, 4256–4264 (2010).
56. Caccia, M., Camarano, A., Sergi, D., Ortona, A. & Narciso, J. Wetting and Navier-Stokes Equation — The Manufacture of Composite Materials. *Wetting and Wettability* (2015). doi:10.5772/61167